

# **Studies on catalytic mechanism of [Fe]- hydrogenase from methanogenic archaea based on crystal structures**



## **DISSERTATION**

**zur**

**Erlangung des Doktorgrades**

**der Naturwissenschaften**

**(Dr. rer. nat.)**

dem Fachbereich Biologie

der Philipps-Universität Marburg

Vorgelegt von

**Gangfeng Huang**

aus Shaoxing, China

Marburg/Lahn, Deutschland, 2019

Die Untersuchungen zur vorliegenden Arbeit wurden in der Zeit von September 2015 bis Juni 2019 am Max-Planck-Institut für terrestrische Mikrobiologie in Marburg/Lahn unter der Leitung von Dr. Seigo Shima durchgeführt.

Vom Fachbereich Biologie der Philipps-Universität in Marburg/Lahn als Dissertation  
angenommen am:

Erstgutachter: Dr. Seigo Shima

Zweitgutachter: Prof. Dr. Johann Heider

Tag der mündlichen Prüfung:

## ERKLÄRUNG

Hiermit versichere ich, dass ich meine Dissertation mit dem Titel "Studies on catalytic mechanism of [Fe]-hydrogenase from methanogenic archaea based on crystal structures " selbständig und ohne unerlaubte Unterstützung angefertigt und mich dabei keiner anderen als der von mir ausdrücklich bezeichneten Quellen und Hilfen bedient habe. Die Dissertation wurde weder in der jetzigen noch in einer ähnlichen Form bei einer anderen Hochschule eingereicht und hat keinen sonstigen Prüfungszwecken gedient.

Marburg, den 03.2019

---

Gangfeng Huang

## Publications

### Part of this dissertation was published as below:

1. **Huang G**, Wagner T, Ermler U, Bill E, Ataka K, Shima S. Dioxygen sensitivity of [Fe]-hydrogenase in the presence of reducing substrates. *Angew. Chem. Int. Ed.* 2018, 57: 4917-4920.
2. Wagner T\*, **Huang G\***, Ermler U, Shima S. How [Fe]-hydrogenase from *Methanothermobacter* is protected against light and oxidative stress. *Angew. Chem. Int. Ed.* 2018, 57: 15056-15059.
3. **Huang G\***, Wagner T\*, Wodrich M, Ataka K, Bill E, Ermler U, Hu X, Shima S. The atomic-resolution crystal structure of activated [Fe]-hydrogenase. (A research article in revision.)

### Other Publications:

4. Bai L, Fujishiro T, **Huang G**, Koch J, Takabayashi A, Yokono M, Tanaka A, Xu T, Hu X, Ermler U, Shima S. Towards artificial methanogenesis: biosynthesis of the [Fe]-hydrogenase cofactor and characterization of the semi-synthetic hydrogenase. *Faraday Discussion* 2017, 198, 37-58.
5. Watanabe T, Wagner T, **Huang G**, Kahnt J, Ataka K, Ermler U, Shima S. The bacterial [Fe]-hydrogenase paralog uses tetrahydrofolate derivatives as substrates. *Angew. Chem. Int. Ed.* 2019, 58: 3506-3510.
6. Pan H, **Huang G**, Wodrich M, Tirani F, Ataka K, Shima S, Hu X. A catalytically active [Mn]-hydrogenase incorporating a non-native metal cofactor. *Nature Chemistry* 2019, In press.
7. **Huang G\***, Wagner T\*, Ermler U, Shima S. Multiple conformational changes involved in the catalytic cycle of methylene-tetrahydromethanopterin dehydrogenase (MtdA) (in preparation)

\* These authors contributed equally to these works.

*“To ordain conscience for Heaven and Earth, to secure life and fortune for the people,  
to continue lost teachings for past sages, to establish peace for all future generations.”*

*Zai Zhang (1020–1077), philosopher and cosmologist*

# Contents

Abbreviations.....	1
Summary .....	3
Zusammenfassung .....	4
1. Introduction.....	6
1.1 Hydrogenases .....	6
1.2 [Fe]-hydrogenase in methanogens .....	10
1.3 Current catalytic mechanism studies of [Fe]-hydrogenase .....	15
1.4 Aim of this study .....	17
2. Results .....	18
2.1 Insights into catalytic mechanism of [Fe]-hydrogenase .....	18
2.1.1 Crystal structures of [Fe]-hydrogenase in the open and closed forms .....	18
2.2.2 Mössbauer and IR spectroscopic analysis.....	26
2.2.3 Structures of the FeGP cofactor and methenyl-H <sub>4</sub> MPT <sup>+</sup> .....	29
2.1.4 A proposed catalytic mechanism of [Fe]-hydrogenase .....	31
2.2 Evidence for the presence of iron-hydride as the catalytic intermediate .....	35
2.2.1 [Fe]-hydrogenase catalyzes reduction of O <sub>2</sub> to H <sub>2</sub> O <sub>2</sub> .....	35
2.2.2 The crystal structure of O <sub>2</sub> -inactivated [Fe]-hydrogenase.....	43
2.2.3 Spectroscopic analyses of O <sub>2</sub> -inactivated [Fe]-hydrogenase.....	46
2.2.4 The proposed iron-hydride intermediate for O <sub>2</sub> reduction to H <sub>2</sub> O <sub>2</sub> .....	49
2.3 Protection-regulation mechanism of hexameric [Fe]-hydrogenase .....	51
2.3.1 The crystal structure of [Fe]-hydrogenase ( <i>M. marburgensis</i> ) in hexamer .....	51
2.3.2 Dissociation of Hexameric assembly .....	54
2.3.3 Hexameric [Fe]-hydrogenase is resistant to light and oxidative stresses .....	56
2.3.4 The strategy of [Fe]-hydrogenase against light and oxidative stresses .....	58
3. Discussion .....	60
4. Materials and methods .....	63
4.1 Materials .....	63
4.1.1 Chemicals.....	63
4.1.2 Strains .....	63
4.1.3 Media.....	63
4.2 Methods.....	63
4.2.1 Cultivation of <i>M. marburgensis</i> .....	63
4.2.2 Genes synthesis of [Fe]-hydrogenase from <i>M. aeolicus</i> .....	64

4.2.3 Heterologously production of the apoenzyme of [Fe]-hydrogenase.....	65
4.2.4 Purification of the apoenzyme of [Fe]-hydrogenase .....	65
4.2.5 Purification of [Fe]-hydrogenase from <i>M. marburgensis</i> .....	66
4.2.6 Extraction of FeGP cofactor from [Fe]-hydrogenase .....	66
4.2.7 Reconstitution of [Fe]-hydrogenase holoenzyme <i>in vitro</i> .....	67
4.2.8 [Fe]-hydrogenase enzyme activity assay .....	67
4.2.9 Crystallization .....	67
4.2.10 Structure analysis .....	69
4.2.11 Infrared spectroscopy .....	71
4.2.12 Mössbauer spectroscopy.....	72
4.2.13 QM/MM computations.....	73
4.2.14 H <sub>2</sub> O <sub>2</sub> measurement.....	73
4.2.15 O <sub>2</sub> <sup>•-</sup> measurement .....	74
4.2.16 UV-Vis spectroscopy .....	75
4.2.17 Electron paramagnetic resonance spectroscopy .....	75
4.2.18 Size-exclusion chromatography.....	75
4.2.19 Ultrafiltration to determine the oligomerization state of [Fe]-hydrogenase .....	76
4.2.20 Light-inactivation of [Fe]-hydrogenase.....	76
4.2.21 Inactivation of [Fe]-hydrogenase by oxidative stress .....	76
References .....	77
Supplementary information.....	85
Acknowledgements .....	95
Curriculum vitae.....	98

## Abbreviations

Hmd	H <sub>2</sub> -forming methylene-tetrahydromethanopterin dehydrogenase ([Fe]-hydrogenase)
mHmd	[Fe]-hydrogenase from <i>Methanothermobacter marburgensis</i>
jHmd	[Fe]-hydrogenase from <i>Methanocaldococcus jannaschii</i>
aHmd	[Fe]-hydrogenase from <i>Methanococcus aeolicus</i>
F <sub>420</sub>	Coenzyme F <sub>420</sub>
Frh	F <sub>420</sub> -reducing [NiFe]-hydrogenase
Mtd	F <sub>420</sub> -dependent methylenetetrahydromethanopterin dehydrogenase
FeGP cofactor	Iron-guanylylpyridinol cofactor
GP	Guanylylpyridinol
GMP	Guanosine monophosphate
TosMIC	Toluenesulfonylmethyl isocyanide
CHI	Cyclohexylisocyanide
H <sub>4</sub> MPT	Tetrahydromethanopterin
Methenyl-H <sub>4</sub> MPT <sup>+</sup>	Methenyl-tetrahydromethanopterin
Methylene-H <sub>4</sub> MPT	Methylene-tetrahydromethanopterin
EDTA	Ethylenediaminetetraacetic acid
DTT	Dithiothreitol
IPTG	Isopropyl β-D-1-thiogalactopyranoside
LB	Luria-Bertani medium
TP	Tryptone phosphate broth
OD	Optical density
DFT	Density functional theory
QM/MM	Quantum Mechanics/Molecular Mechanics
TS	Transition state
FTIR	Fourier-transform Infrared
XAS	X-ray absorption spectroscopy
EPR	Electron paramagnetic resonance
ESI-FT-ICR-MS	Electrospray ionization Fourier transform ion cyclotron



	resonance mass spectrometry
NRVS	Nuclear resonance vibrational spectroscopy
Å	Ångström ( $1 \text{ Å} = 10^{-10} \text{ m}$ )
MFR	Methanofuran
CHO-MFR	Formyl-MFR
CHO-H <sub>4</sub> MPT	Formyl-H <sub>4</sub> MPT
Fd	Ferredoxin
CH <sub>3</sub> -H <sub>4</sub> MPT	Methyl-H <sub>4</sub> MPT
RMSD	Root mean square deviations
MOPS	3-morpholinopropane-1-sulfonic acid
BSA	Bovine serum albumin
SOD	Superoxide dismutase

## Summary

Hydrogenases are promising templates for designing new H<sub>2</sub>-based catalysts. [Fe]-hydrogenase reversibly catalyzes H<sub>2</sub> cleavage and transfer of a hydride to the C14a of methenyl-tetrahydromethanopterin (methenyl-H<sub>4</sub>MPT<sup>+</sup>, a C1 carrier). Different from dinuclear [NiFe]- and [FeFe]-hydrogenases, [Fe]-hydrogenase harbors the iron-guanylylpyridinol (FeGP) cofactor containing a single iron. The FeGP cofactor consists of the iron site, the pyridinol ring and the guanosine monophosphate (GMP). [Fe]-hydrogenase is a dimer, in which each N-terminal domain contains one FeGP cofactor, and two C-terminal domains form the central domain. [Fe]-hydrogenase has open and closed forms. In the resting-open form, the iron site is 6-coordinated with two CO ligands, one acyl-C, one pyridinol-N, one Cys-S and a water ligand. In this work, a detailed catalytic mechanism of [Fe]-hydrogenase based on the 1.06-Å resolution structure of [Fe]-hydrogenase from *Methanococcus aeolicus* complexed with methenyl-H<sub>4</sub>MPT<sup>+</sup> in a closed-active form was studied. In the closed-active form, the iron site is changed into 5-coordinated state due to removal of the water ligand by closure of the active cleft formed by the central and the N-terminal domains, generating an empty coordination site for H<sub>2</sub>-binding and the deprotonated 2-OH of the FeGP cofactor as the catalytic base. In this situation, the Fe site of the FeGP cofactor is near the C14a (hydride acceptor) of methenyl-H<sub>4</sub>MPT<sup>+</sup> at 3.8 Å. The Quantum mechanics/molecular mechanics (QM/MM) computations based on the structure of the closed-active form indicated the nearly thermo-neutral H<sub>2</sub>-binding and smooth H<sub>2</sub>-cleavage and hydride transfer. The distorted imidazoline ring of methenyl-H<sub>4</sub>MPT<sup>+</sup> might stabilize the active state for H<sub>2</sub> binding/cleavage. Based on the results, a complete reaction cycle of [Fe]-hydrogenase was proposed. In addition, we found that [Fe]-hydrogenase catalyzes the reduction of O<sub>2</sub> to H<sub>2</sub>O<sub>2</sub> in the presence of reducing substrates (methylene-H<sub>4</sub>MPT or methenyl-H<sub>4</sub>MPT<sup>+</sup>/H<sub>2</sub>). The most possible reductant was the iron-hydride intermediate. This result provided the first evidence for the existence of the iron-hydride intermediate in the catalytic cycle. Subsequently, the crystal structure of [Fe]-hydrogenase from *Methanothermobacter marburgensis* indicated that this enzyme is a hexamer rather than a dimer, in which an aspartate ligand (Asp189) of the loop from nearby monomer binds the Fe site of the FeGP cofactor. In this case, the enzyme can protect its active center against light and oxidative stresses. When substrates bind, this enzyme dissociates into active dimers. This finding also confirmed the catalytic function of the open coordination site of the Fe site.

## Zusammenfassung

Hydrogenasen sind vielversprechende Vorlagen für das Design neuer H<sub>2</sub>-basierter Katalysatoren. Die [Fe]-Hydrogenase katalysiert die reversible H<sub>2</sub>-Spaltung und überträgt dabei ein Hydridion auf das C14a von Methenyl-Tetrahydromethanopterin (Methenyl-H<sub>4</sub>MPT<sup>+</sup>, ein C1-Träger). Anders als die zweikernigen [NiFe]- und [FeFe]-Hydrogenasen, enthält der Eisenguanylylpyridinol (FeGP) Cofaktor der [Fe]-Hydrogenase ein einzelnes Eisenatom. Der FeGP-Cofaktor besteht aus dem zentralen Eisenatom, einem Pyridinolring und einem Guanosinmonophosphat (GMP). Die [Fe]-Hydrogenase liegt als Dimer vor, in dem jede N-terminale Domäne einen FeGP-Cofaktor enthält und die zwei C-terminalen Domänen die zentrale Domäne bilden. Die [Fe]-Hydrogenase hat mehrere offene und geschlossene Zustände. Im offenen Ruhezustand wird das zentrale Eisen von zwei CO-Liganden, dem Acyl-C, dem Pyridinol-N, dem Cystein-S und einem Wassermolekül sechsfach koordiniert. In dieser Arbeit wurde ein detaillierter katalytischer Mechanismus der [Fe]-Hydrogenase basierend auf einer 1,06-Å Kristallstruktur der [Fe]-Hydrogenase aus *Methanococcus aeolicus* im Komplex mit Methenyl-H<sub>4</sub>MPT<sup>+</sup> in der geschlossenen, aktiven Form untersucht. In der geschlossenen aktiven Form ist das Eisenatom durch den Verlust des Wasserliganden fünffach koordiniert, dies geht mit dem Verschluss des aktiven Zentrums einher, welches aus der zentralen und der N-terminalen Domäne besteht, und so eine freie Koordinationsstelle für die H<sub>2</sub>-Bindung, sowie die deprotonierte Hydroxylgruppe des FeGP-Cofaktors als katalytische Base erzeugt. In diesem Zustand befindet sich das Eisenatom des FeGP-Cofaktors in einem Abstand von 3,8 Å vom C14a (Hydridakzeptor) des Methenyl-H<sub>4</sub>MPT<sup>+</sup>s. Quantenmechanik / Molekularmechanik (QM/MM) Berechnungen, basierend auf der Struktur des geschlossen, aktiven Zustands, zeigten eine nahezu thermoneutrale H<sub>2</sub>-Bindung, H<sub>2</sub>-Spaltung mit niedriger Aktivierungsenergie, sowie den Transfer des Hydridions. Der verzerrte Imidazolinring von Methenyl-H<sub>4</sub>MPT<sup>+</sup> könnte dabei den aktiven Zustand für die H<sub>2</sub>-Bindung und -Spaltung stabilisieren. Basierend auf diesen Ergebnissen wurde ein vollständiger Reaktionszyklus der [Fe]-Hydrogenase vorgeschlagen. In Gegenwart reduzierender Substrate (Methylen-H<sub>4</sub>MPT oder Methenyl-H<sub>4</sub>MPT<sup>+</sup>/H<sub>2</sub>) kann die [Fe]-Hydrogenase die Reduktion von O<sub>2</sub> zu H<sub>2</sub>O<sub>2</sub> katalysieren. Dabei ist das wahrscheinlichste Reduktionsmittel ein Eisenhydridintermediat. Dieses Ergebnis lieferte den ersten Beweis für das Vorhandensein eines Eisenhydridintermediats im Katalysezyklus. Die Kristallstruktur der [Fe]-Hydrogenase aus *Methanothermobacter*

*marburgensis* deutete an, dass es sich um einen Hexamer nicht um einen Dimer handelt, bei dem ein Aspartatligand (Asp189) aus der Schleife des nächsten Monomers das Eisenatom des FeGP-Cofaktors koordiniert. In diesem Fall kann das Enzym sein aktives Zentrum vor Licht und oxidativen Stress schützen. Wenn Substrate gebunden werden, zerfällt die [Fe]-Hydrogenase in Dimere, um aktiv zu werden. Dieser Befund bestätigte auch die katalytische Funktion der offenen Konformation des Eisenzentrums.

## 1. Introduction

### 1.1 Hydrogenases

Hydrogenases are a type of metalloenzymes (1), which can catalyze the oxidation of  $H_2$  into protons and electrons, and the reduction of protons with electrons to generate  $H_2$  (1). These enzymes are widespread in the microbial world, as a key enzyme involved in  $H_2$  metabolism (1). Based on the metals of their active center, hydrogenases were classified into three types (1-3). There are two types of di-nuclear metal hydrogenases (1), [NiFe]-hydrogenase (Fig. 1AD) and [FeFe]-hydrogenase (Fig. 1BE). The third type is [Fe]-hydrogenase, which harbors only a single iron in its active center (4-7) (Fig. 1CF). [NiFe]- and [FeFe]-hydrogenases contain the redox active center and can perform the  $H_2$  cleavage into two protons and two electrons (Fig. 2A). Different from them, [Fe]-hydrogenase can only cleave  $H_2$  into one proton and one hydride at the non-redox active site in the presence of methenyl-tetrahydromethanopterin (methenyl- $H_4MPT^+$ , a C1 carrier in methanogens) as a hydride acceptor (4, 5, 8, 9) (Fig. 2B). In addition, unlike [NiFe]- and [FeFe]-hydrogenases, having three to five iron-sulfur clusters, [Fe]-hydrogenase doesn't contain iron-sulfur clusters (10).

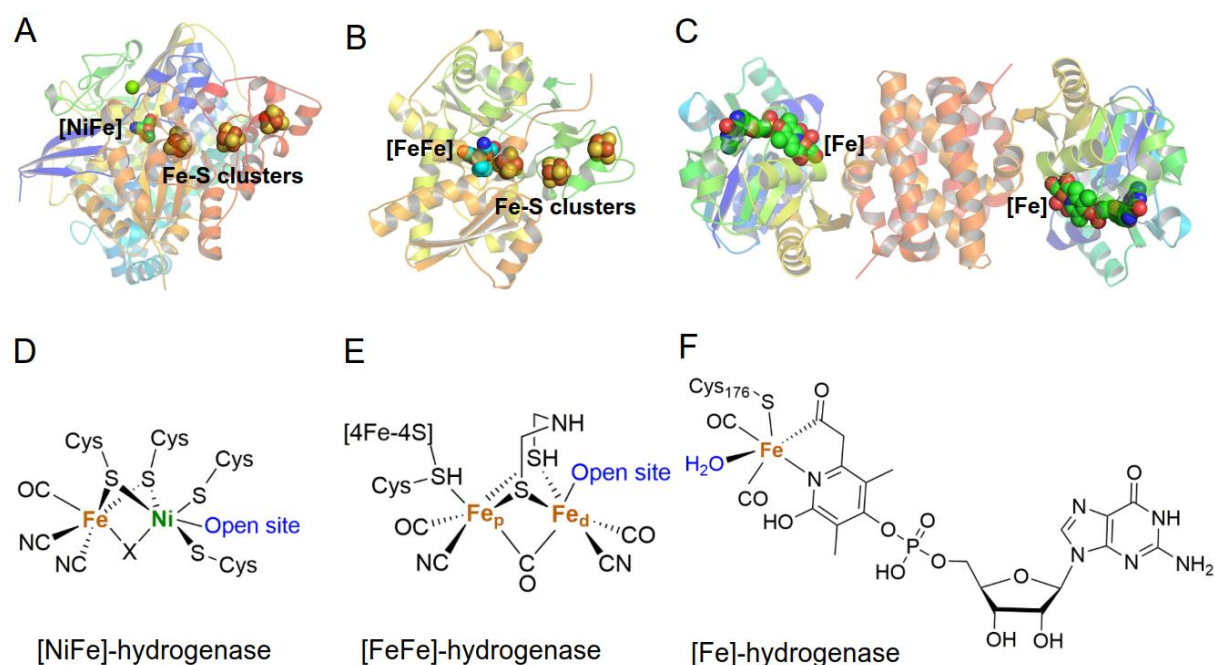


**Fig. 1. Structures of the three types of hydrogenases.** (A) The crystal structure of [NiFe]-hydrogenase (PDB code: 4U9H (11)). (B) The crystal structure of [FeFe]-hydrogenase (PDB code: 1HFE (12)). (C) The crystal structure of [Fe]-hydrogenase (PDB code: 3F47 (4)). (D) The chemical structure of [NiFe] center of the [NiFe]-

hydrogenase (1, 8, 11). (E) The chemical structure of [FeFe] center of the [Fe]-hydrogenase (1, 12-16). (F) The chemical structure of [Fe] center of the [Fe]-hydrogenase (4, 17).

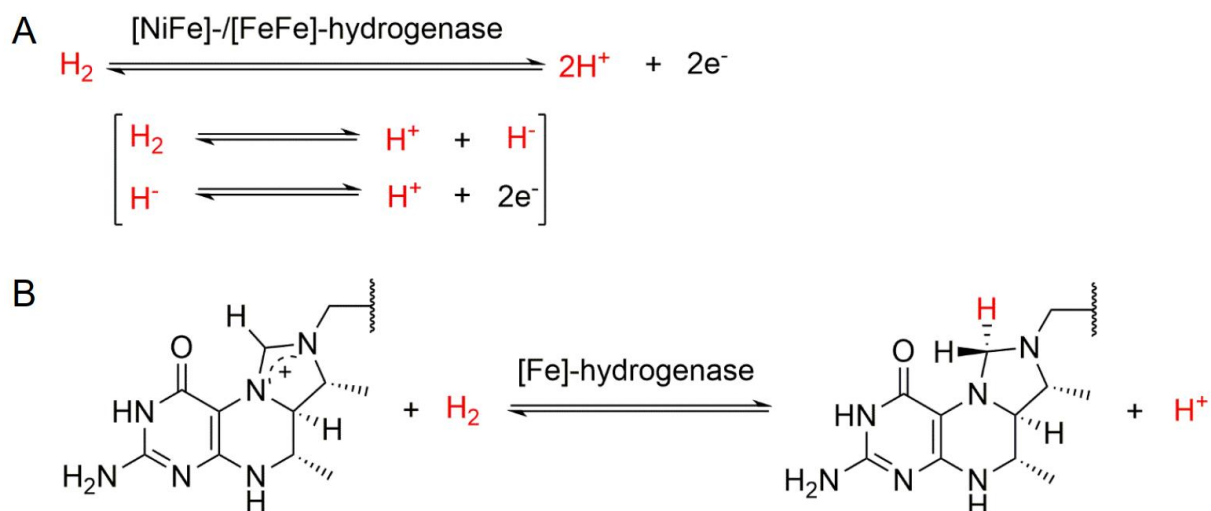


**Fig. 2. Reactions catalyzed by three types of hydrogenases. (A)** [NiFe]-/[FeFe]-hydrogenase can reversibly cleave one  $\text{H}_2$  into two protons and two electrons by two steps (1). **(B)** [Fe]-hydrogenase can reversibly cleave one  $\text{H}_2$  into one proton and one hydride, and then the hydride is transferred to methenyl- $\text{H}_4\text{MPT}^+$  (4).

Volbeda et al. reported the first structure of [NiFe]-hydrogenase (18, 19). Standard [NiFe]-hydrogenase consists of two subunits; the large subunit (~60 kDa) contains the [NiFe] active center for  $\text{H}_2$  cleavage, and the small subunit (~30 kDa) contains three Fe-S clusters for electron transfer (1). The Ni ion is anchored by four conserved cysteines, and two of them connected to the Fe ion as the bridges between these two metal ions (Fig. 1D). The Fe atom is coordinated with two CN ligands and one CO ligand (19-22) (Fig. 1D), which is confirmed by Fourier-transform infrared (FTIR) spectroscopy (23, 24). According to the physiological functions, [NiFe]-hydrogenases are classified into four groups (25): membrane-bound  $\text{H}_2$ -uptake [NiFe]-hydrogenases, cytosolic  $\text{H}_2$ -uptake [NiFe]-hydrogenases, cytosolic bidirectional [NiFe]-hydrogenases and membrane-bound  $\text{H}_2$ -evolving [NiFe]-hydrogenases. Based on crystallography, electron paramagnetic resonance (EPR) spectroscopy, Mössbauer spectroscopy, FTIR spectroscopy and density functional theory (DFT) computations, its catalytic mechanism was studied intensively and some very plausible catalytic mechanisms have been proposed (1, 26-42). A simplified catalytic cycle is drawn based on the published mechanisms (1, 26-42) (Fig. 3): (A) In the Ni-SI state, the Ni(II) ion was four-

coordinated and had one open coordination site for  $H_2$ -binding.  $H_2$  diffused to the active center through the gas channel and bound to this Ni(II) site. Afterward,  $H_2$  was polarized and cleaved into one hydride binding between Ni(II) and Fe(II) site, and a proton binding to nearby cysteine-S (Cys543 in [NiFe]-hydrogenase from *Desulfovibrio gigas* (19)). This state is named Ni-R state. (B) After releasing one proton, which bound nearby cysteine-S, one electron from Ni(II) was released, by which the Ni(II) was oxidized to Ni(III). This state is named Ni-C state. (C) One electron and one proton were released from the bridged hydride and one electron from the hydride was transferred to Ni(III) to regenerate Ni(II) and then the [NiFe] center changed to the Ni-SI state.

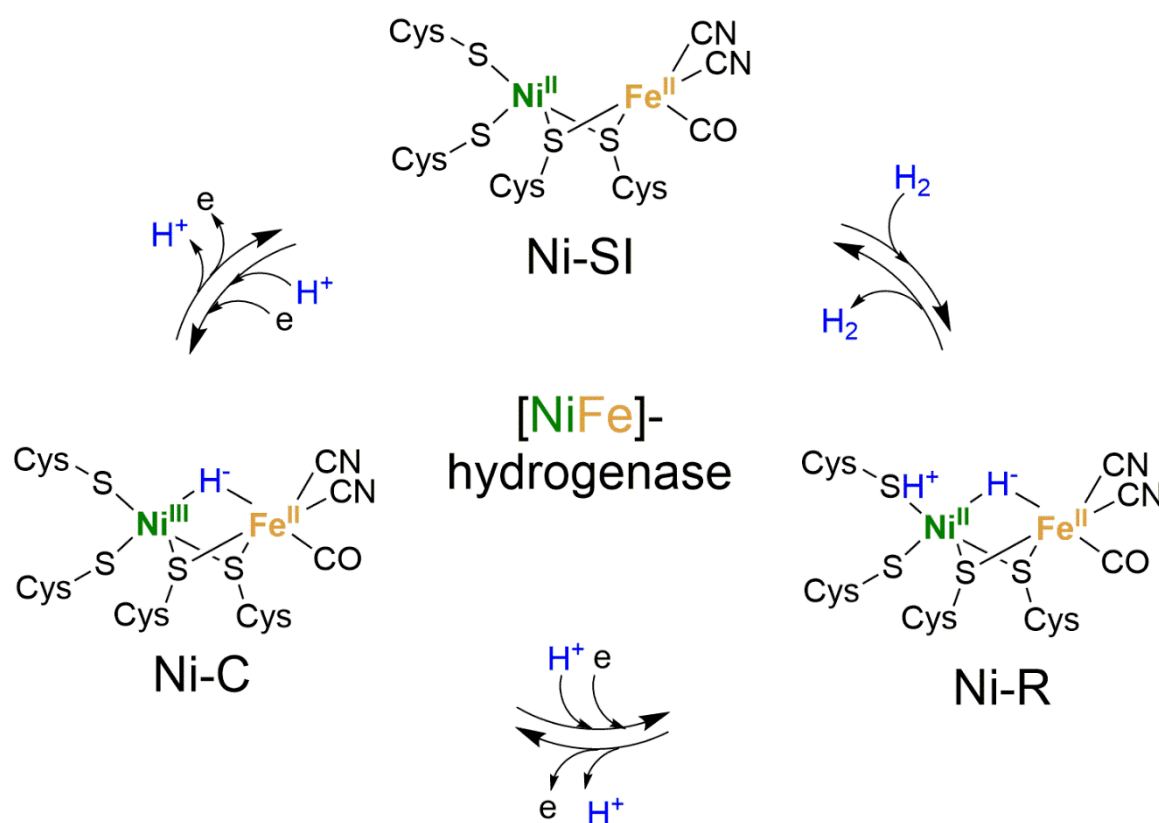


**Fig. 3. The proposal catalytic mechanism of [NiFe]-hydrogenase (1).** For the details, see text.

Although most of [NiFe]-hydrogenases are  $O_2$  sensitive, certain [NiFe]-hydrogenases are  $O_2$  tolerant due to two kinds of structural modifications (43). One is the narrow entrance of the gas channel for limiting the  $O_2$  diffusion into the active sites (44-46). The other one is the existence of two extra cysteines connecting the proximal [4Fe-3S] cluster, which can provide one more electron to the active center used for the reduction

of oxygen species bound on the NiFe sites (43, 47-54). These findings gave some hints for designing O<sub>2</sub>-insensitive hydrogenase as the alternatives for expensive metal catalysts (e.g. Pt) (47, 50, 55, 56).

In 1998, Peters et al. reported the crystal structure of [FeFe]-hydrogenase from *Clostridium pasteurianum* (Cpl) (57). Later, Nicolet et al. solved the crystal structure of [FeFe]-hydrogenase from *Desulfovibrio desulfuricans* (DdH) (12). Cpl is a 60-kDa monomeric cytoplasmic enzyme (57). DdH is a 53-kDa dimeric periplasmic enzyme (12). Both Cpl and DdH showed the unique metal active center named H-cluster, which performs the catalysis. The H-cluster includes a [4Fe-4S] cluster and a [FeFe] center (58, 59) (Fig. 1E). The [4Fe-4S] cluster connects to the proximal Fe of the [FeFe] center (Fe<sub>p</sub>) via a cysteine thiolate. Both of Fe atoms are coordinated to one CN and one CO ligand, and a bridging CO (60) (Fig. 1E). In addition, an azadithiolate group (adt, (SCH<sub>2</sub>)<sub>2</sub>NH) bridges two Fe (60) (Fig. 1E). The Fe atom distal to the [4Fe-4S] cluster (Fe<sub>d</sub>) harbors an open coordination site (Fig. 1E), which is indicated as the H<sub>2</sub>-binding site by spectroscopic analysis (IR, Mössbauer, EPR and NRVs) (15, 61, 62) and DFT computations (63). In addition, accessory Fe-S clusters are used for electrons transfer between the H-cluster and the electron donors and acceptors (64). According to the different functions, [FeFe]-hydrogenases are classified into three groups (25): prototypical/bifurcating [FeFe]-hydrogenase, ancestral [FeFe]-hydrogenase and sensory [FeFe]-hydrogenase. Using crystallography, spectroscopic analysis and DFT computations, some catalytic mechanisms of [FeFe]-hydrogenase were reported (13-16, 65-71). A proposed reaction cycle of [Fe]-hydrogenase based on current reports was described below (13-16, 65-71) (Fig. 4). (A) In the oxidized state 1 (H<sub>ox</sub>1), the open site of the Fe<sub>d</sub>(II) was empty, where could be bound with H<sub>2</sub>. (B) In the H<sub>ox</sub>2 state, a H<sub>2</sub> molecule bound to the open site of the Fe<sub>d</sub>(II). (C) Heterolytic cleavage of H<sub>2</sub> occurred on Fe<sub>d</sub>(II), in which the hydride was bound to Fe<sub>d</sub>(II) and the proton accepted by the NH group of adt group. This state is named H<sub>ox</sub>3 state. (D) Afterward, the adt group released the proton by the connecting proton transfer relay. The Fe<sub>d</sub>(II) accepted one electron from the hydride becoming Fe<sub>d</sub>(I), and the [4Fe-4S]<sup>2+</sup> also obtained one electron from the hydride becoming [4Fe-4S]<sup>+</sup>, and the left proton was nearby the active sites. This state is named super-reduced state (H<sub>sred</sub>). (E) [4Fe-4S]<sup>+</sup> released one electron becoming [4Fe-4S]<sup>2+</sup>, and the proton was obtained by the adt group. This



state is named reduced state ( $H_{red}$ ). (F) The protonated adt group released one proton, and the  $Fe_d(I)$  released one electron becoming  $Fe_d(II)$ , regenerating to the  $H_{ox1}$  state.

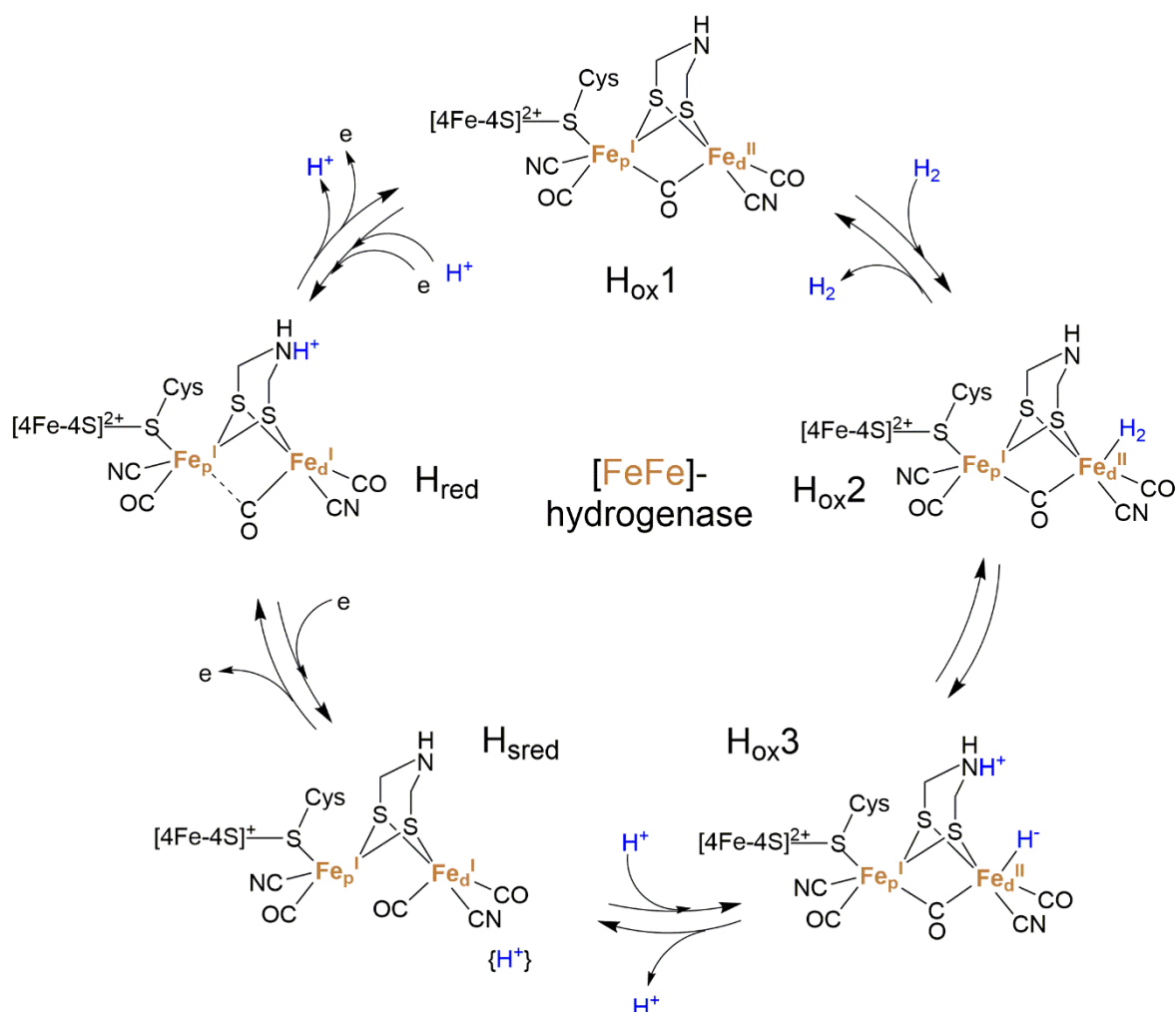


**Fig. 4. A proposed catalytic mechanism of [FeFe]-hydrogenase (1, 65).**  $H_{ox1}$ : the open site of the  $Fe_d(II)$  is empty;  $H_{ox2}$ : the open site of the  $Fe_d(II)$  is bound with  $H_2$ ;  $H_{ox3}$ : the open site of the  $Fe_d(II)$  is bound with hydride ( $H^-$ ). For details, see text.

## 1.2 [Fe]-hydrogenase in methanogens

[Fe]-hydrogenase is found in hydrogenotrophic methanogens (4, 7, 8, 10, 72, 73). The systematic name of [Fe]-hydrogenase is  $H_2$ -forming methylene-tetrahydromethanopterin (methylene- $H_4$ MPT) dehydrogenase (Hmd) (7, 10, 74, 75). This enzyme catalyzes the heterolytic cleavage of  $H_2$  and a stereo-specific hydride transfer to methenyl- $H_4$ MPT $^+$  to produce methylene- $H_4$ MPT (Fig. 2B), which is a step of hydrogenotrophic methanogenesis pathway (performing  $CO_2$  reduction with  $H_2$  to generate  $CH_4$ ) (8) (Fig. 5). In 1990, Zirngibl et al. reported the purification and characterization of Hmd from *Methanothermobacter marburgensis* (10, 76). One mole

of Hmd contains around one mole of iron, however, it does not contain iron-sulfur clusters; therefore, Hmd was named as iron-sulfur-cluster-free hydrogenase (10). At that time, Hmd was also called as the “metal-free” hydrogenase because a catalytic mechanism that did not require metal at the active site (77). Unlike [NiFe]- and [FeFe]-hydrogenases, the iron of Hmd was non-redox active (10, 75).

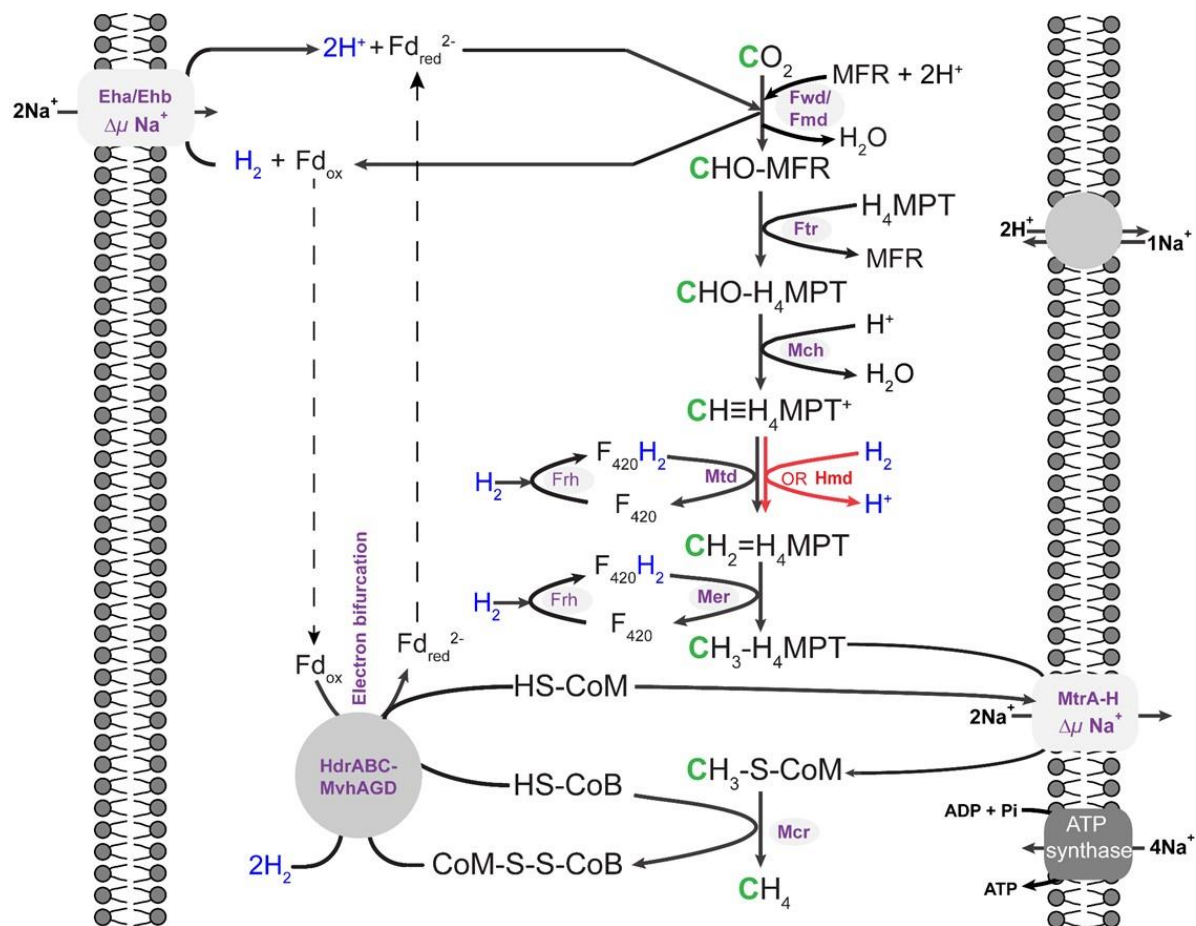


**Fig. 5. The hydrogenotrophic methanogenesis pathway (63, 78-80).** Fwd: Tungsten-dependent formyl-MFR dehydrogenase; Fmd: molybdenum-dependent formyl-MFR dehydrogenase; Ftr: formylmethanofuran:tetrahydromethanopterin formyltransferase; Mch: methenyl-H<sub>4</sub>MPT<sup>+</sup> cyclohydrolase; Frh: F<sub>420</sub>-reducing [NiFe]-hydrogenase; Mtd: F<sub>420</sub>-dependent methylene-H<sub>4</sub>MPT dehydrogenase; Hmd: [Fe]-hydrogenase; Mer: F<sub>420</sub>-dependent methylene-H<sub>4</sub>MPT reductase; Mcr: methyl-coenzyme M reductase; HdrABC-MvhAGD: heterodisulfide reductase-[NiFe]-hydrogenase complex; Eha/Ehb: energy-converting [NiFe]-hydrogenase; MtrA-H: integral membrane methyl-H<sub>4</sub>MPT:coenzymeM methyltransferase. MFR: methanofuran; H<sub>4</sub>MPT: tetrahydromethanopterin; CHO-MFR: formyl-MFR; CHO-H<sub>4</sub>MPT: formyl-H<sub>4</sub>MPT; CH≡H<sub>4</sub>MPT<sup>+</sup>, methenyl-H<sub>4</sub>MPT<sup>+</sup>; CH<sub>2</sub>=H<sub>4</sub>MPT: methylene-

H<sub>4</sub>MPT; CH<sub>3</sub>-H<sub>4</sub>MPT: methyl-H<sub>4</sub>MPT; CoB-SH: Coenzyme B; CoM-SH: Coenzyme M; CoM-S-S-CoB: heterodisulfide; Fd, Ferredoxin; F<sub>420</sub>: Coenzyme F<sub>420</sub>.

In 1998, Afting et al. reported that the production of Hmd was largely upregulated under the Ni-limiting (<0.05  $\mu$ M-Ni, compared with 5- $\mu$ M Ni in normal medium) growth conditions (7). In the Ni-limiting conditions, F<sub>420</sub>-dependent methylene-H<sub>4</sub>MPT dehydrogenase (Mtd) is also upregulated, instead F<sub>420</sub>-reducing [NiFe]-hydrogenase (Frh) is strongly down-regulated (no longer synthesized) (7). It is experimentally shown that F<sub>420</sub> is reduced by the coupled reactions of Hmd and Mtd (Fig. 6) (7). These findings indicated that in the Ni-limiting conditions, production of the Ni-dependent Frh is stopped and the function of Frh, regeneration of reduced F<sub>420</sub>, is substituted by Hmd and Mtd.

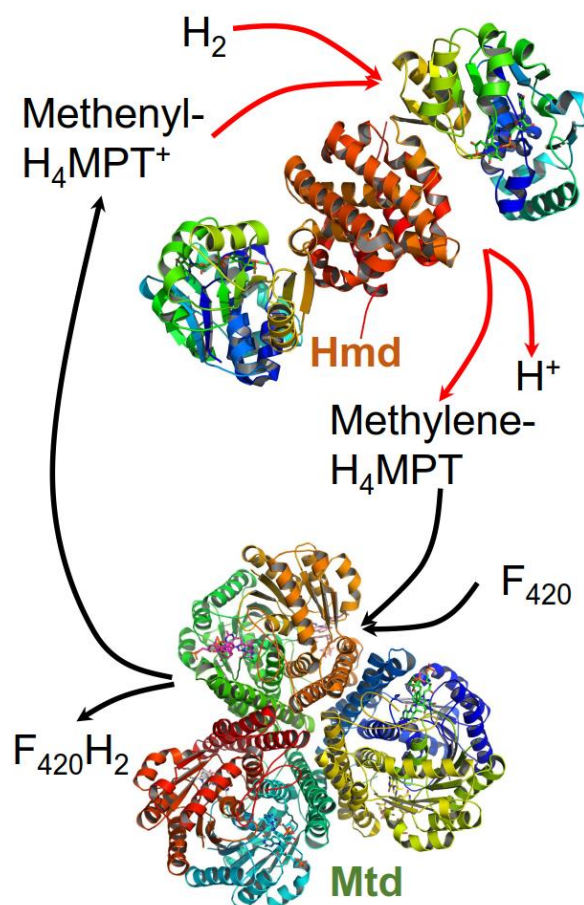


**Fig. 6. F<sub>420</sub>H<sub>2</sub> generation by the reduction of F<sub>420</sub> by the coupled reaction of Hmd and Mtd under Ni-limiting conditions (7, 80).** Hmd: [Fe]-hydrogenase (4); Mtd: F<sub>420</sub>-dependent methylene-H<sub>4</sub>MPT dehydrogenase (81).

In 2004, it was found that the redox inactive iron is a part of the iron-guanylylpyridinol (FeGP) cofactor. The FeGP cofactor can be extracted from [Fe]-hydrogenase and the active holoenzyme (protein with FeGP cofactor bound) can be reconstituted from apoenzyme (protein without FeGP cofactor bound) and the extracted FeGP cofactor (82). The iron-center structure of the FeGP cofactor in the protein-free and protein-binding forms were analyzed by FTIR (83), Mössbauer (84) and X-ray absorption (XAS) spectroscopy (9). FTIR spectrum of Hmd showed two CO bands at 2011 and 1944  $\text{cm}^{-1}$ , which was interpreted as two CO molecules bound to single iron with 90° angle (83). In addition, FTIR spectroscopy could detect extra CO or CN ligand peak when Hmd was incubated with the inhibitor CO or KCN, which suggested H<sub>2</sub>-binding site could be the same for external CO or CN (83). Lyon et al. found that the FeGP cofactor is light sensitive. UV-A/blue light decomposes the FeGP cofactor independent on binding to the protein (85). The decomposed products are Fe, CO and guanylylpyridinol (GP) (85). The Mössbauer spectra indicated that the active site contains one redox inactive iron in a low oxidation and spin state, Fe(0) or Fe(II) (84). XAS spectrum indicated that one sulfur ligand is coordinated to the iron. Mutation experiments suggested that Cys176 was the most probably ligated to the iron site (9).

In 2006, Pilak et al. reported the first crystal structure of the Hmd apoenzyme from *Methanocaldococcus jannaschii* (jHmd) (86), which opened a new window for Hmd study. The structure of the jHmd apoenzyme was solved at 1.75 Å and indicated a homodimeric oligomeric state (Fig. 7A) (86). Each monomer contains one N-terminal domain and one C-terminal domain, two C-terminal domains form the central domain (86). Possible active-site clefts are formed between the N- and central domains. In the same report, the structure of the Hmd apoenzyme from *Methanopyrus kandleri* was described. Comparison of the two Hmd apoenzyme structures revealed that the Hmd homodimer could take open and closed conformations respect to the cleft. The N-terminal domain is similar to the Rossmann fold, which is a typical structure for nucleotide binding proteins. The authors hypothesized that the mononucleotide-binding site in the N-terminal domain could function for binding of the guanosine monophosphate (GMP) moiety of the FeGP cofactor (86). In addition, in the paper, Cys176 was proposed to be a possible iron binding site (86). Two years later, Shima et al. reported the crystal structure of the Hmd holoenzyme from *M. jannaschii* at 1.75 Å (4), which was in the open conformation (Fig. 7B). In this structure, one FeGP

cofactor sits on each N-terminal domain of the dimer. It shows that the iron atom coordinated to two CO, one Cys176-S, one pyridinol-N, one solvent and one unknown ligand. Later, Hiromoto et al. reported the crystal structure of jHmd (Cys176Ala), which suggested the presence of acyl-carbon ligand at the iron site. The acyl ligand is a part of 6-acylmethyl substituent of the pyridinol ring (87). In another report in the same year, Hiromoto et al. reported the crystal structure of jHmd (Cys176Ala)/methylene-H<sub>4</sub>MPT complex in its open form at 2.15 Å (88), which provided insights about its reaction mechanism. Then, Shima et al. used electrospray ionization Fourier transform ion cyclotron resonance mass spectrometry (ESI-FT-ICR-MS) and FTIR spectroscopy to show the evidence of the presence of the acyl ligand of the iron site (17). In 2013, Tamura et al. co-crystallized Hmd from *M. marburgensis* with inhibitory isocyanides (89), which provided implications for the H<sub>2</sub>-activation site as the sixth coordination site of the iron atom trans to the acyl ligand.

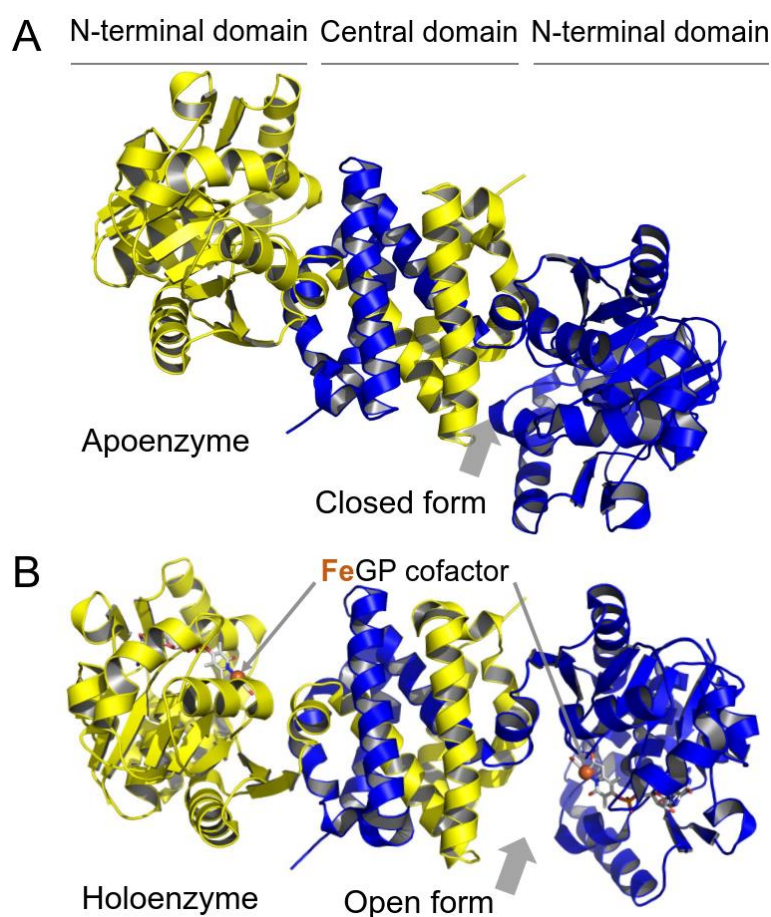
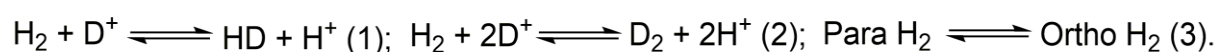


**Fig. 7. The crystal structures of the [Fe]-hydrogenase apoenzyme and holoenzyme from *M. jannaschii*.** (A) The apoenzyme was in the closed form, PDB code: 2B0J (73). (B) The holoenzyme was in the open form, PDB code: 3F47 (4). The FeGP cofactor was shown as sticks. The Fe atoms were shown as orange balls.

### 1.3 Current catalytic mechanism studies of [Fe]-hydrogenase

[Fe]-hydrogenase can catalyze reversible activation and heterolytic cleavage of H<sub>2</sub> only in the presence of methenyl-H<sub>4</sub>MPT<sup>+</sup>; hydride is directly transferred to methenyl-H<sub>4</sub>MPT<sup>+</sup> to form methylene-H<sub>4</sub>MPT. Based on the solved structures of [Fe]-hydrogenase, [Fe]-hydrogenase possibly has open and closed conformations according to the size of the active-site clefts (4, 73, 82, 88). Hiromoto et al. proposed that binding of methenyl-H<sub>4</sub>MPT<sup>+</sup> induced closing of the active site cleft and the catalytic reaction cycle proceed in the closed conformation. However, the closed conformation is not yet observed in the holoenzyme structure of [Fe]-hydrogenase (82, 88).

[NiFe]- and [FeFe]-hydrogenases can reversibly catalyze single and double exchange of proton and molecular hydrogen (Eqs. 1, 2) and para-H<sub>2</sub> to ortho-H<sub>2</sub> conversion (Eq. 3) without any other substrates (electron acceptor) (5). [Fe]-hydrogenase itself does not catalyze these exchange reactions like [NiFe]- and [FeFe]-hydrogenases. However, in the presence of methenyl-H<sub>4</sub>MPT<sup>+</sup>, [Fe]-hydrogenase can perform these reactions (Eqs. 1-3) (5, 90).



The substrate dependent proton-exchange reactions triggered researchers to probe what is the catalytic mechanism of [Fe]-hydrogenase. Olah's superacid chemistry (91) indicates isobutane can produce the carbocation under the super-acid conditions, and H<sub>2</sub> can side-on or end-on bind to the carbocation, H<sub>2</sub> is activated and cleaved, and then one hydride transferred to the carbocation, and one proton is released. Based on this knowledge, Berkessel et al. considered the structure of imidazolline ring of methenyl-H<sub>4</sub>MPT<sup>+</sup> was very similar to isobutene; the lone electron pair of the N5 and N10 of imidazolline ring could be protonated by the acidic amino acids nearby, which might convert the C14a between N5 and N10 to the carbocation like state to activate H<sub>2</sub> (77, 92). In their opinion, the substrate methenyl-H<sub>4</sub>MPT<sup>+</sup> itself plays the role of H<sub>2</sub> activation, which explained the reason that [Fe]-hydrogenase only catalyzes the exchange reactions in the presence of methenyl-H<sub>4</sub>MPT<sup>+</sup>. After proposal of this hypothesis, Vogt et al. considered the catalytic reaction was not only dependent on carbocation of methenyl-H<sub>4</sub>MPT<sup>+</sup>. The iron site might also join the activation and



cleavage of  $\text{H}_2$  (93). In the proposed mechanism, (A) methenyl- $\text{H}_4\text{MPT}^+$  triggered the conformational change of [Fe]-hydrogenase, which activated iron to catalyze  $\text{H}_2$  activation and cleavage with carbocation of methenyl- $\text{H}_4\text{MPT}^+$ . (B) The C14a of methenyl- $\text{H}_4\text{MPT}$  was juxtapositioned to the iron site, so  $\text{H}_2$  could interact with both the carbocation (C14a) of methenyl- $\text{H}_4\text{MPT}^+$  and the activated iron site. (C) The  $\text{H}_2$ -activation required both conformational changes induced by methenyl- $\text{H}_4\text{MPT}^+$  binding and juxtaposition of the C14a and the iron. Later, Hiromoto et al. solved the crystal structure of [Fe]-hydrogenase mutant Cys176Ala/methylene- $\text{H}_4\text{MPT}$  complex, which is in the open conformation (88). In this structure, the distance between the C14a of methylene- $\text{H}_4\text{MPT}$  and the Fe atom of FeGP cofactor is 9.3 Å, which was too far for the hydride transfer even  $\text{H}_2$  side-on/end-on bound into this space. Hiromoto et al. modeled a closed conformation of the binary complex based on the closed form structure of the apoenzyme; the distance between the C14a of methylene- $\text{H}_4\text{MPT}$  and the Fe atom of FeGP cofactor was  $\sim 3$  Å (88). In this closed model, C14a of methylene- $\text{H}_4\text{MPT}$  is next to one iron coordination site of FeGP cofactor, which indicated this site could be the  $\text{H}_2$ -binding site. Yang and Hall did DFT computations on the active site of [Fe]-hydrogenase using the crystal structure of [Fe]-hydrogenase mutant Cys176Ala/methylene- $\text{H}_4\text{MPT}$  complex, which supported the  $\text{H}_2$  bound to one coordination of Fe site of FeGP cofactor (94). In the mechanism, methenyl- $\text{H}_4\text{MPT}^+$  functioned as a hydride acceptor to break the hydrogen bond of  $\text{Fe}-\text{H}^\delta\cdots\text{H}^{\delta+}-\text{O}$  intermediate (94). Based on DFT computations, Dey considered  $\text{H}_2\text{O}$  could function as an inhibitor of [Fe]-hydrogenase by binding to the one coordination of Fe center, competing with  $\text{H}_2$  (95). Through quantum mechanics/molecular mechanics (QM/MM) computations using Hiromoto's closed models, Hedegård et al. indicated that Fe- $\text{H}_2$  intermediate was most stable during catalytic reaction and 2-OH of pyridinol function as the catalytic base (96). In 2015, Shima et al. also suggested 2-OH on pyridinol ring of FeGP cofactor acted as the catalytic base for  $\text{H}_2$  heterolytic-cleavage by the experiments using iron mimic compounds and DFT computations (97). Currently, all related proposal reaction mechanisms of [Fe]-hydrogenase are based on the hypothesis of the open/closed conformational changes, and these computations did not use the experimentally obtained closed form. However, for the detailed analysis of the catalytic mechanism, structures of the closed [Fe]-hydrogenase complexed methenyl- $\text{H}_4\text{MPT}^+$ /methylene- $\text{H}_4\text{MPT}^+$  is required.

#### **1.4 Aim of this study**

To reveal the precise catalytic mechanism of [Fe]-hydrogenase, structure of [Fe]-hydrogenase in the closed active form containing the substrates is important. In my PhD project, I obtained the 1.06-Å resolution structure of the target complex, which clearly indicated the atomic structure of the closed form enzyme and the substrate. Based on the structure, we proposed a catalytic mechanism including new insights using QM/MM computations. In addition, we have obtained the evidence of the presence of the Fe-hydride intermediate and the function of the open coordination site of the FeGP cofactor by biochemical and structural analyses.



## 2. Results

### 2.1 Insights into catalytic mechanism of [Fe]-hydrogenase

#### 2.1.1 Crystal structures of [Fe]-hydrogenase in the open and closed forms

Previously, our lab performed many trials to obtain the structure of the closed-form [Fe]-hydrogenase from *M. marburgensis* and *M. jannaschii* but failed. Here, I tried other [Fe]-hydrogenases from different methanogens; *Methanocaldococcus infernus*, *Methanoregula formicica*, *Methanococcus aeolicus*, *Methanotorris igneus* and *Methanolacinia paynteri*.

In this study, [Fe]-hydrogenase from the above mentioned methanogens were crystallized in the open form in the absence of substrates under gas phase 95%N<sub>2</sub>/5%H<sub>2</sub> (Fig. 8A). However, the complex with methenyl-/methylene-H<sub>4</sub>MPT was not obtained under this gas phase. One of the most possible reasons was that the presence of H<sub>2</sub> keeps the reaction cycle, which made a mixture of the proteins in different conformations bound with methenyl-H<sub>4</sub>MPT<sup>+</sup> and methylene-H<sub>4</sub>MPT, which could disturb the crystallization (Fig. 8). Therefore, I crystallized [Fe]-hydrogenase with methenyl-H<sub>4</sub>MPT<sup>+</sup> under gas phase 100% N<sub>2</sub> (Fig. 8B).

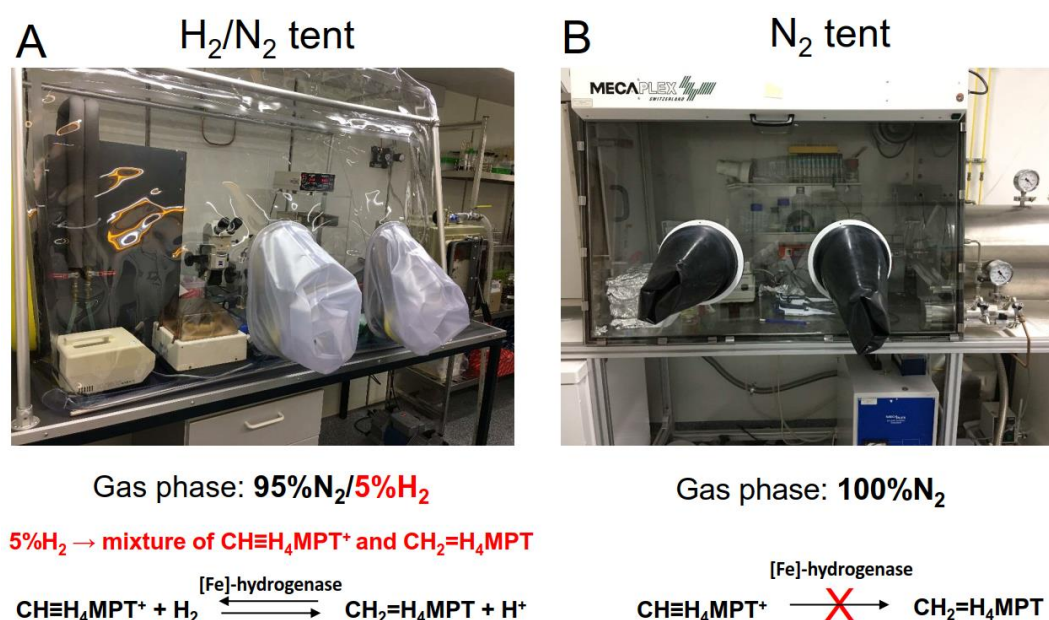


**Fig. 8. The gas phase used for the crystallization.** (A) For the growth of the crystals of [Fe]-hydrogenase (in the open form) in the absence of substrates under gas phase 95%N<sub>2</sub>/5%H<sub>2</sub>. (B) For the growth of the crystals of [Fe]-hydrogenase/methenyl-H<sub>4</sub>MPT<sup>+</sup> (in the closed form) under gas phase 100%N<sub>2</sub>.

**Table. 1. X-ray analysis statistics (*M. aeolicus*) (98).**

	[Fe]-hydrogenase <b>Open</b> conformation	[Fe]-hydrogenase/ methenyl-H <sub>4</sub> MPT <sup>+</sup> <b>Closed</b> form <b>Form A</b>	[Fe]-hydrogenase/ methenyl-H <sub>4</sub> MPT <sup>+</sup> <b>Closed</b> form <b>Form B</b>
<b>Data collection</b>			
Wavelength (Å)	0.97980	1.00001	0.99992
Space group	<i>I</i> 4 <sub>1</sub> 22	<i>C</i> 222 <sub>1</sub>	<i>P</i> 2 <sub>1</sub> 2 <sub>1</sub> 2
Resolution (Å)	50 – 2.30 (2.42 – 2.30)	47 – 1.06 (1.12 – 1.06)	45 – 1.85 (1.95 – 1.85)
Cell dimensions			
a, b, c (Å)	136.99, 136.99, 117.32	66.65, 66.25, 167.60	80.01, 156.48, 53.65
$\alpha$ , $\beta$ , $\gamma$ (°)	90.0, 90.0, 90.0	90.0, 90.0, 90.0	90.0, 90.0, 90.0
R <sub>merge</sub> (%) <sup>a</sup>	15.5 (102.3)	4.9 (98.1)	12.4 (113.3)
R <sub>pim</sub> (%) <sup>a</sup>	4.3 (28.1)	2.1 (54.2)	5.5 (62.7)
CC <sub>1/2</sub> (%) <sup>a</sup>	99.9 (60.2)	99.9 (67.2)	99.7 (32.3)
I/ $\sigma$ <sub>I</sub> <sup>a</sup>	17.9 (2.9)	15.4 (1.4)	8.6 (1.2)
Completeness (%) <sup>a</sup>	100.0 (100.0)	93.7 (74.8)	97.4 (85.0)
Redundancy <sup>a</sup>	13.7 (14.0)	6.1 (4.0)	6.0 (4.1)
Number of unique reflections <sup>a</sup>	25078 (3607)	156432 (18054)	56771 (6994)
<b>Refinement</b>			
Resolution (Å)	26.62 – 2.30	45.0 – 1.06	45.0 – 1.85
Number of reflections	25043	156000	56710
R <sub>work</sub> /R <sub>free</sub> <sup>b</sup> (%)	17.1 / 19.2	11.8 / 13.4	16.1 / 19.2
Number of atoms			
Protein	2573	2776	5173
Ligands/ions	66	136	264
Solvent	107	505	592
Mean B-value (Å <sup>2</sup> )	43.63	19.10	28.83
Molprobity clash score, all atoms	2.45 (100 <sup>th</sup> percentile)	4.38 (79 <sup>th</sup> percentile)	1.48 (100 <sup>th</sup> percentile)
Ramachandran plot			
Favoured regions (%)	326 (95.9)	326 (96.5)	656 (96.5)
Outlier regions (%)	0	0	0
rmsd <sup>c</sup> bond lengths (Å)	0.009	0.011	0.010
rmsd <sup>c</sup> bond angles (°)	1.11	1.42	1.11
<b>PDB code</b>	6HAC	6HAV	6HAE

<sup>a</sup> Values relative to the highest resolution shell are within parentheses. <sup>b</sup> R<sub>free</sub> was calculated as the R<sub>work</sub> for 5% of the reflections that were not included in the refinement.

<sup>c</sup> rmsd, root mean square deviation. This table is obtained from Ref (98).

I obtained the crystal structure of the [Fe]-hydrogenase holoenzyme from *M. aeolicus* without substrate at 2.3 Å resolution (Table. 1 and Fig. 9A) in the anaerobic tent with gas phase 95%N<sub>2</sub>/5%H<sub>2</sub>. It was crystallized in an open form, which is highly similar with that from *M. jannaschii* reported previously (4). The crystal structures of [Fe]-hydrogenase/methenyl-H<sub>4</sub>MPT<sup>+</sup> complex were crystallized in the anaerobic tent with gas phase 100%N<sub>2</sub>. The crystals diffracted to 1.06 Å (Form A) and 1.85 Å (Form B) resolution (Table. 1 and Fig. 9B). They were crystallized in the closed form.

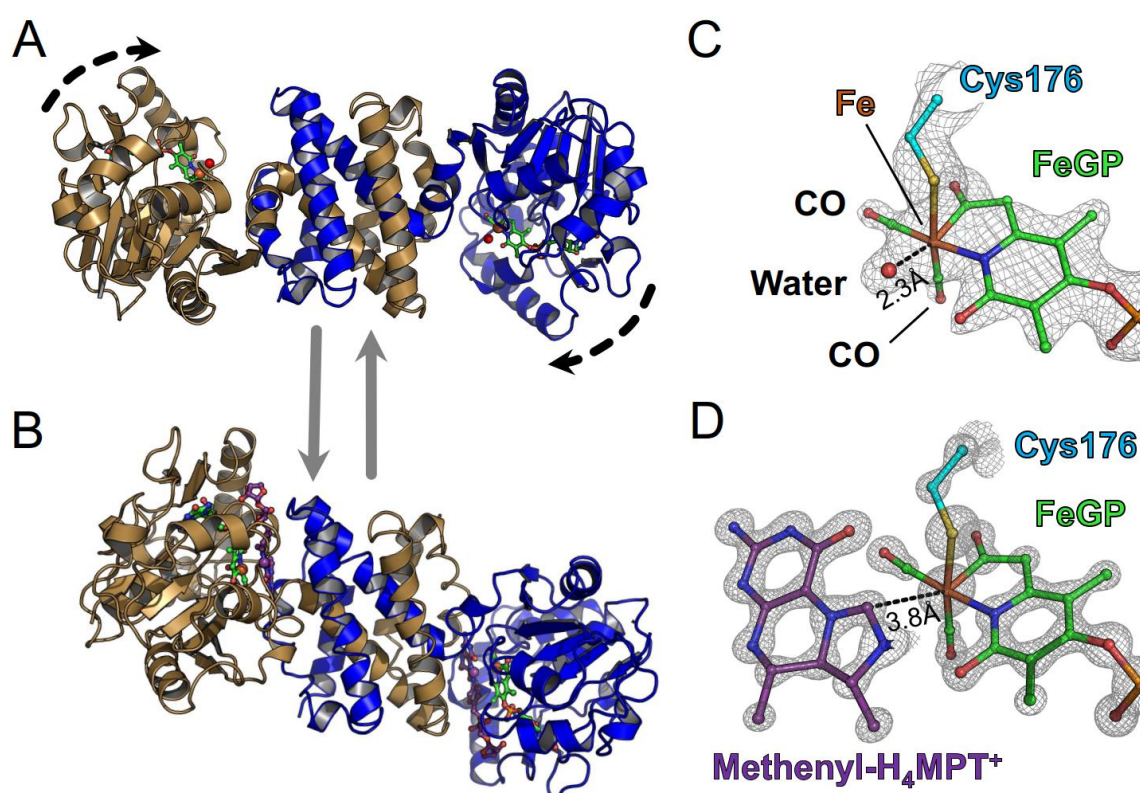


**Fig. 9. Comparison of the crystal structures of [Fe]-hydrogenase from *M. aeolicus* in the open/closed forms.** (A) The open form of [Fe]-hydrogenase diffracted at 2.3 Å resolution. The curved and dashed arrows indicate the movement of the N-terminal domains. (B) The closed form of [Fe]-hydrogenase/methenyl-H<sub>4</sub>MPT<sup>+</sup> complex diffracted at 1.06 Å resolution (Form A). (A and B) The two monomers are shown in cartoon models and colored in brown and blue. Methenyl-H<sub>4</sub>MPT<sup>+</sup> and FeGP cofactor were shown in sticks, in which carbon, nitrogen, oxygen, phosphorous, sulfur and Fe atoms were depicted in green, blue, red, orange, yellow and brown, respectively. The water molecules were shown as red balls. (C) The structure of the [Fe] center of the FeGP cofactor in the open form. (D) The structures of the [Fe] center of the FeGP cofactor and methenyl-H<sub>4</sub>MPT<sup>+</sup> at the active site of [Fe]-hydrogenase in the closed form. This figure is modified from Ref (98).

Comparison of the structures of the N-terminal and central domains indicated that the domain structures are almost identical between the open and closed [Fe]-hydrogenase holoenzymes (Fig. 9AB). This finding suggested that substrate-binding induced closing the active-site clefts; the conformational change is characterized as a rigid body movement of the N-terminal domains towards the central domain (Fig. 10).

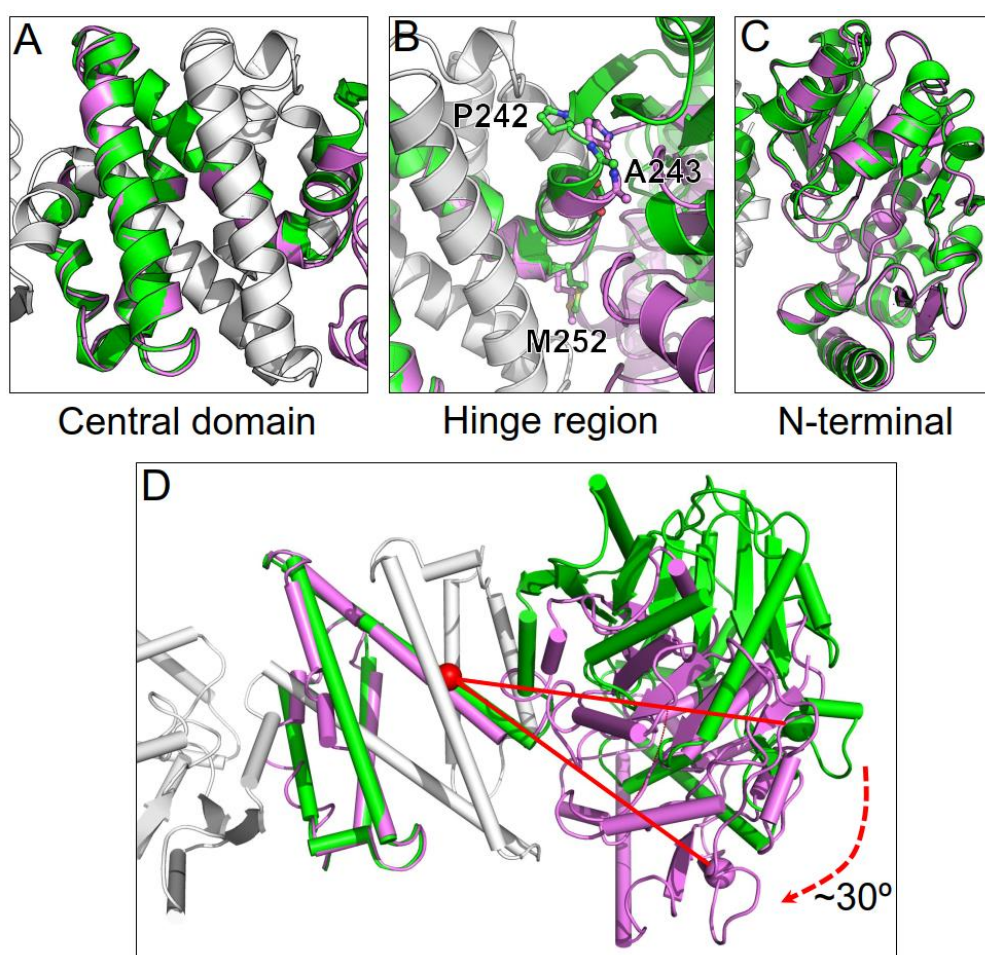


**Fig. 10. Superposition of the domains of the open and closed [Fe]-hydrogenase from *M. aeolicus*.** The structure of the open form of one monomer (green cartoon) and that of the closed form in complex with the methenyl- $\text{H}_4\text{MPT}^+$  (pink cartoon) are superposed. Another monomer of the open form is shown by white cartoon. For clarity, the FeGP cofactor and the methenyl- $\text{H}_4\text{MPT}^+$  were omitted in this figure. (A) The central domains formed with C-terminal domains, RMSD 0.34 Å for 77 C $\alpha$  residues. (B) The hinge region. (C) The N-terminal domain bound with the FeGP cofactor RMSD 0.26 Å for 191 C $\alpha$  residues. (D) The relative arrangement of the N-terminal domains by superposing the central domain (cylinder models). The rotation angle between them in the closed and open state is  $\sim 30^\circ$ . This figure is modified from Ref (98).



The crystal structures of the closed forms of [Fe]-hydrogenase showed that the FeGP cofactor and methenyl- $\text{H}_4\text{MPT}^+$  are embedded in the cleft walls of the N-terminal and central domains, respectively (Fig. 9B). In contrast to the open form, the FeGP cofactor and substrate in the closed [Fe]-hydrogenase locate nearby and form multiple contacts between them (Fig. 11). Bulky side chains of His14 (interaction with 2-OH of pyridinol of FeGP cofactor by hydrogen bond) and Trp148 (hydrophobic interaction with pyridinol ring of FeGP cofactor) oriented towards the Fe center. The side chains of Met252, Met321' and Phe281' oriented towards methenyl- $\text{H}_4\text{MPT}^+$  clamp the rings together, which may adjust ring conformations to assist in catalysis. (In this thesis, amino-acid residues in another monomer of [Fe]-hydrogenase homodimer is distinguished with the amino acid name with apostrophe.)

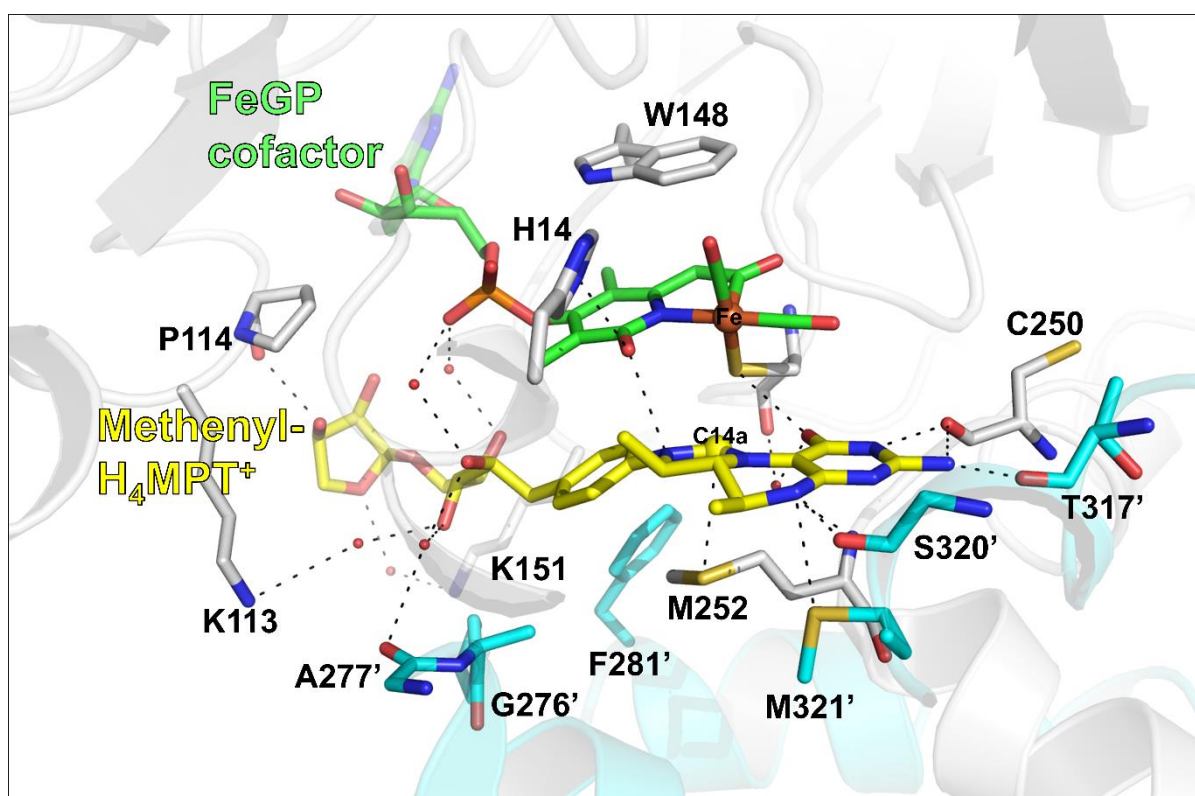


**Fig. 11. A close-up view of the active site of the closed active-form of [Fe]-hydrogenase.** The FeGP cofactor and methenyl- $\text{H}_4\text{MPT}^+$  were shown in green and yellow sticks, respectively. Two monomers were shown in white and light blue cartoon models. The waters were shown in red balls. The interactions were shown in black dash lines. The amino acid residues of the partner monomer are marked with an apostrophe. This figure is modified from Ref (98).

In addition, Met252 had van der Waals interactions between its sulfur and C14a of methenyl- $\text{H}_4\text{MPT}^+$ , and its methyl group had hydrophobic and van der Waals interactions with the phenyl ring of methenyl- $\text{H}_4\text{MPT}^+$  (Fig. 12), which both contributed to stabilize the imidazoline part facing to the Fe center of the FeGP cofactor. The Met252 is strictly conserved in all [Fe]-hydrogenases (Fig. S1). We could observe a dramatic decrease of the specific enzyme activity of the variants: Met252 to alanine (<1%), serine (<2%) and phenylalanine (<1%), which indicated the Met252 plays an important role on the enzyme catalysis.

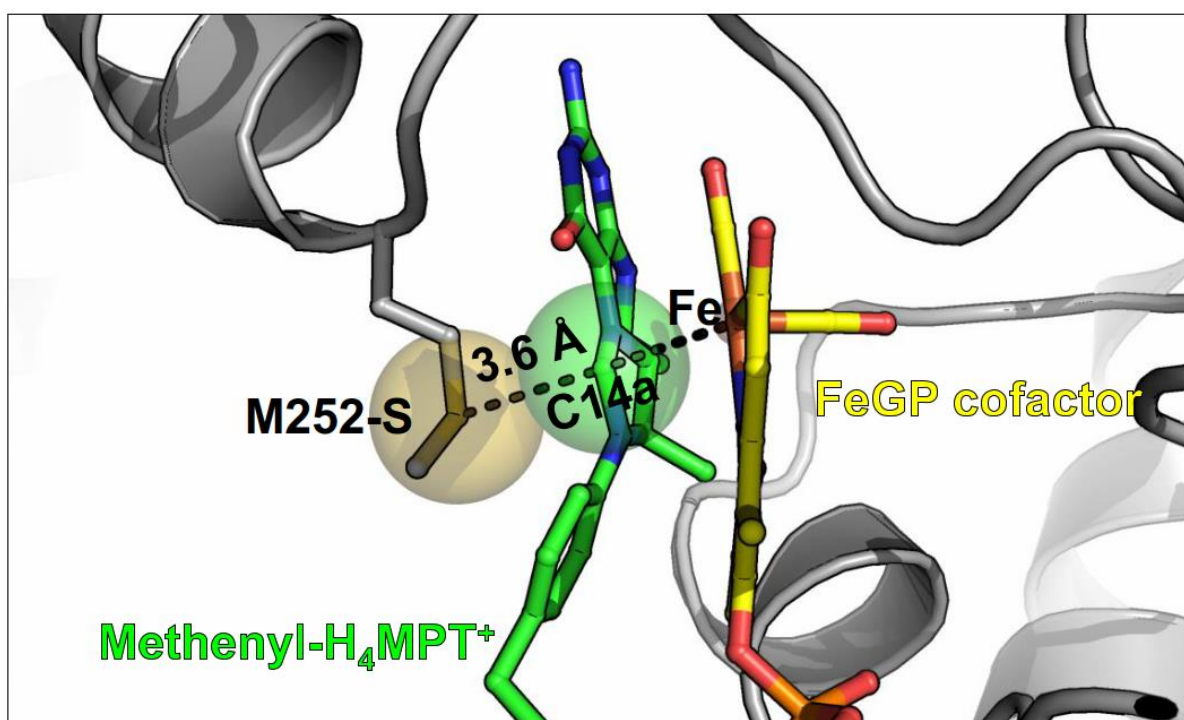


**Fig. 12. Interactions between Met252 and the imidazoline ring of methenyl- $\text{H}_4\text{MPT}^+$  in the closed active-form of [Fe]-hydrogenase.** In the closed active-form, the imidazoline part is stabilized by interactions with Met252. The van der Waals radius of S- $\text{CH}_3$  of Met252 and C14a of methenyl- $\text{H}_4\text{MPT}^+$  is illustrated with transparent balls. Met252 (carbon in grey), methenyl- $\text{H}_4\text{MPT}^+$  (carbon in green) and the FeGP cofactor (carbon in yellow) are shown in sticks and balls, in which nitrogen, oxygen, sulfur and Fe atoms were depicted in dark blue, red, dark yellow and brown, respectively.

The tight packing in the closed conformation caused a tilt of the pyridinol ring of the FeGP cofactor of  $15^\circ$  compared with that in the case of the open form. As a result, the distance between the His14 and the 2-OH of the pyridinol of the FeGP cofactor was shortened from 4.9 Å to 3.3 Å (Fig.13A). Thus, the 2-OH could become a part of a

proton transfer relay (Fig. 13B). Previous reports indicated that the mutant His14Ala has shown only less than 1% enzyme activity (4, 88). This finding also supported that the 2-OH of the pyridinol presented an enolate state in the closed form, which corresponded to its function during the catalytic reaction as the catalytic base for the H<sub>2</sub> cleavage as proposed previously (97).

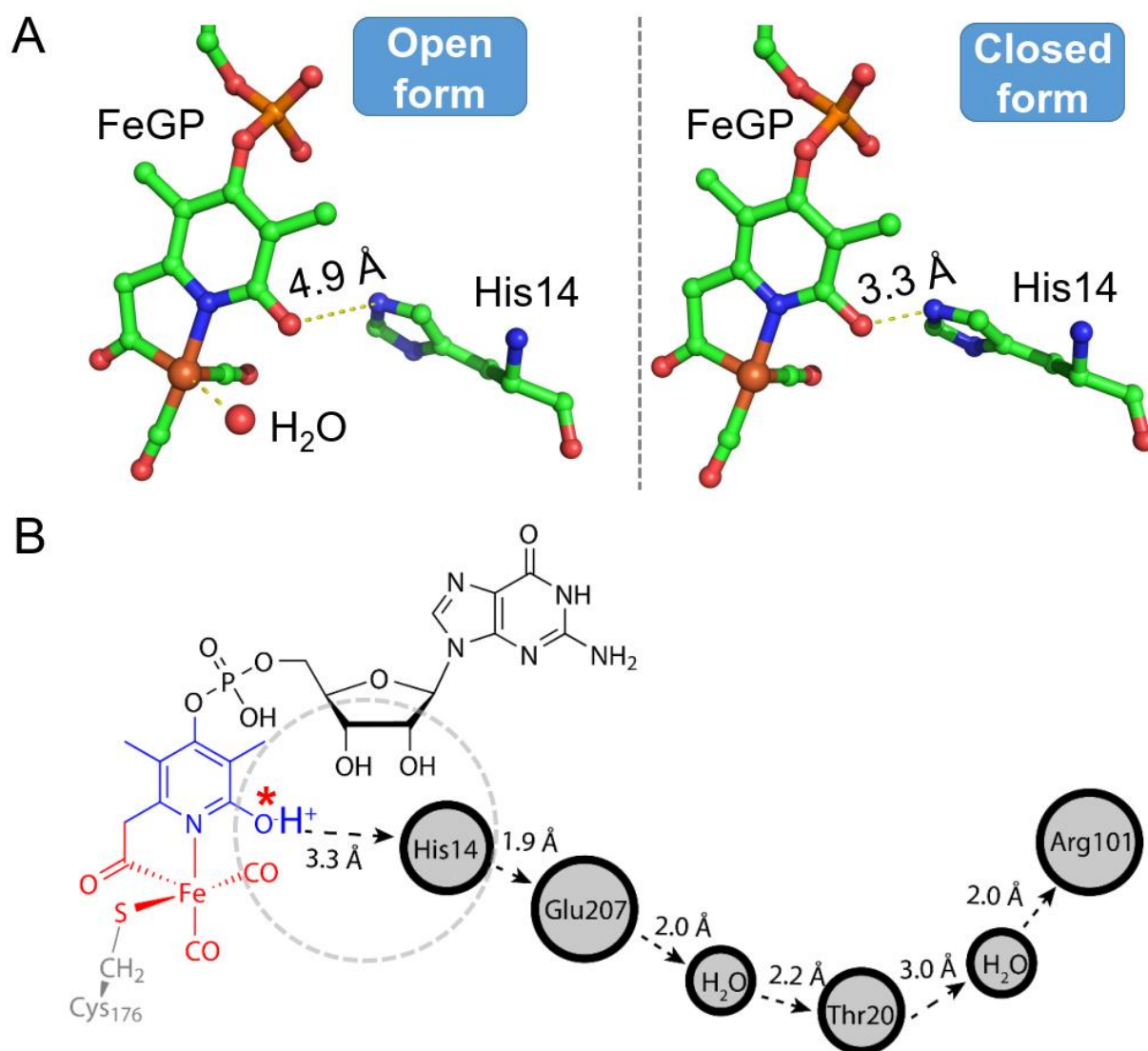


**Fig. 13. The deprotonated 2-OH of the pyridinol of the FeGP cofactor involved in catalysis and proton transfer relay in the closed active-form of [Fe]-hydrogenase. (A) The comparison of distance (yellow dash line) between the 2-OH of the FeGP cofactor and the His14 in the open and closed forms. (B) The proposed proton transfer chain in the closed active-form. The deprotonated 2-OH (enolate) of the pyridinol was marked by (\*). Black dash arrows showed the direction for proton transfer.**

Furthermore, if we compared the active sites in the open and closed form, we can observe that the water ligand on Fe site was removed upon closure of the active-site cleft (Fig. 9CD). In the Form A crystal, the occupancy of water molecules was 40-50%, and in the Form B crystal, the water molecules were not observed (Fig. S2). This finding is in agreement with the predication by Dey (95). The reason could be the limited space for a water molecule binding after embedding the methenyl- $\text{H}_4\text{MPT}^+$  nearby Fe site. After the dissociation of the water ligand, the 6-coordinated Fe (Fig. 9C) changed into an unsaturated 5-coordinated Fe (Fig. 9D) which is similar to a FeGP cofactor mimic compound (Fig. 14), thus generating an empty coordination site for  $\text{H}_2$  binding. This finding also provided the experimental evidence that [Fe]-hydrogenase had a similar open site for  $\text{H}_2$  binding like [NiFe]- and [FeFe]-hydrogenases.

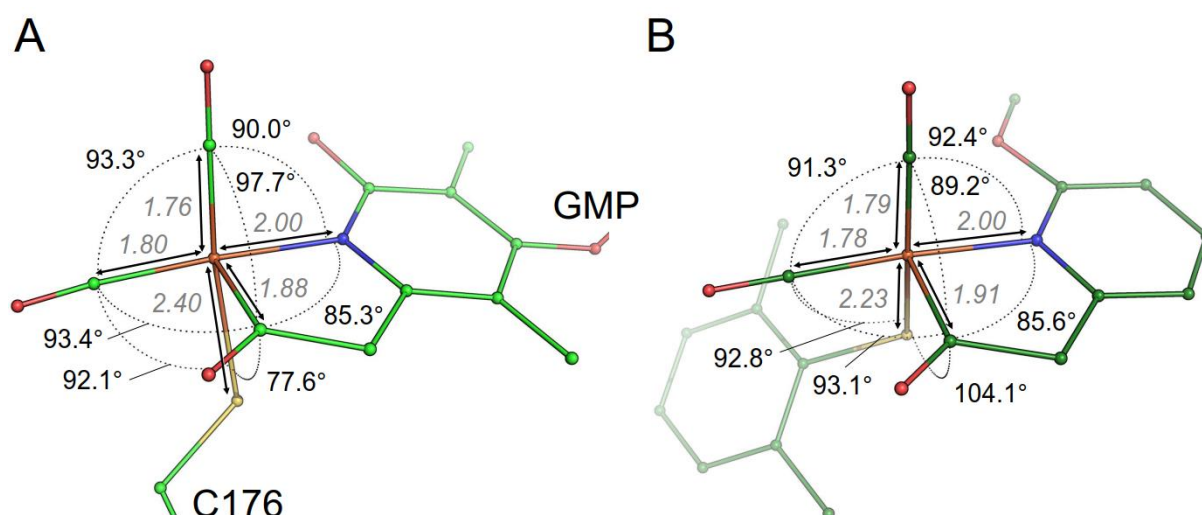


**Fig. 14. Structural comparison of 5-coordinated iron complex of closed form and a mimic iron complex.** (A) The 5-coordinated iron site of the FeGP cofactor in the closed [Fe]-hydrogenase/methenyl- $\text{H}_4\text{MPT}^+$  complex. (B) A mimic complex (2- $\text{CH}_2\text{CO}$ -6- $\text{MeOC}_5\text{H}_3\text{N}$ ) $\text{Fe}(\text{CO})_2[\text{S}-(2,6-\text{Me}_2\text{C}_6\text{H}_3)]$  (99). Structures were shown in sticks and balls, in which carbon, nitrogen, oxygen, sulfur and Fe atoms were depicted in green, blue, red, yellow and orange, respectively. This figure is obtained from Ref (98).

In the closed form,  $\text{H}_2$  could diffuse into the Fe site from the surface of the protein through a narrow hydrophobic channel (Fig.15). Val205 is strictly conserved in [Fe]-hydrogenases (Fig. S1) and makes a bottleneck just before the Fe site, which might block the entry of larger toxic solvents or gases (e.g.  $\text{O}_2$ ).



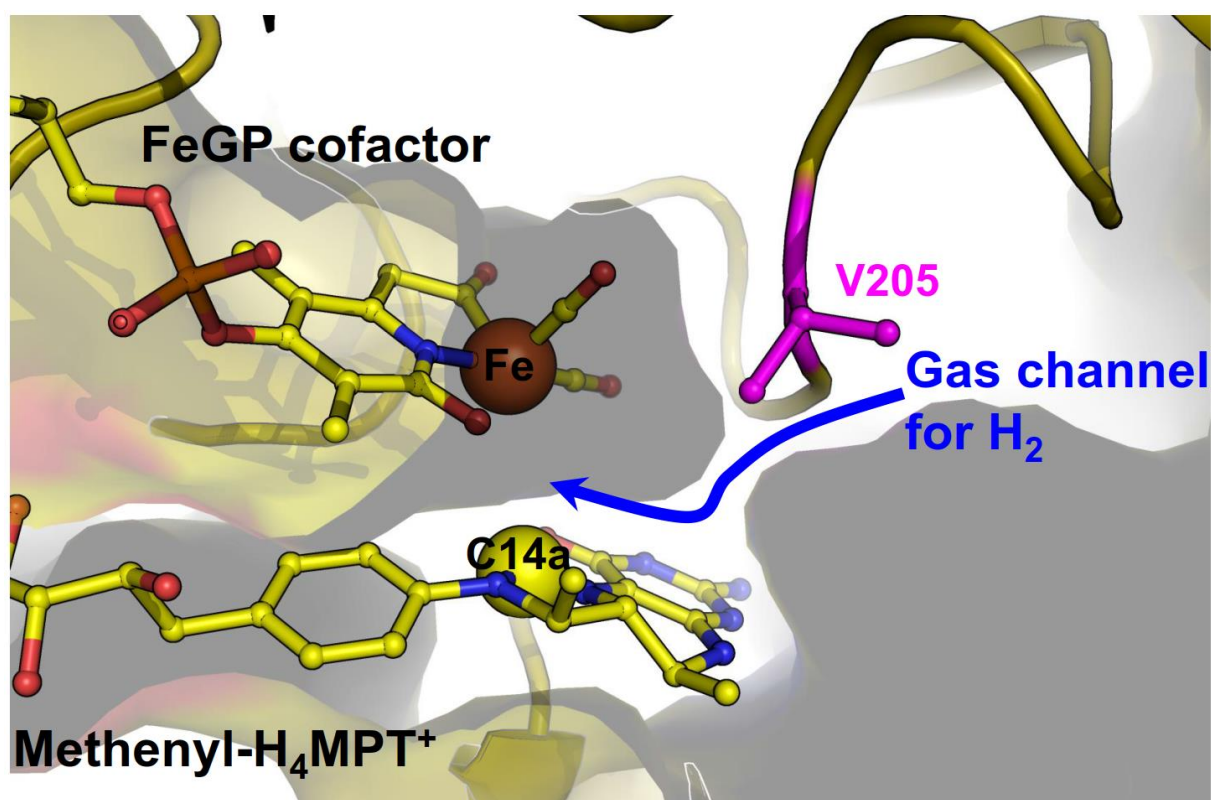


**Fig. 15. A proposed gas channel for  $H_2$  in the closed active-form of [Fe]-hydrogenase.** The [Fe]-hydrogenase was shown as dark yellow surface and the FeGP cofactor (Fe colored brown), methenyl- $H_4MPT^+$  (C14a colored light yellow) and Val205 (colored in pink) were shown as balls and sticks. A blue arrow showed the possible gas channel for  $H_2$ .

### 2.2.2 Mössbauer and IR spectroscopic analysis

We performed spectroscopic analyses to detect the open/closed conformational changes of [Fe]-hydrogenase in solution. As shown in Fig. 16A, the Mössbauer spectrum of the [Fe]-hydrogenase from *M. aeolicus* without substrates bound presented two species, which revealed that there are different two electronic structures of the Fe site. Comparison with previous Mössbauer spectroscopic data indicated that the main species, sub-spectrum 2 (80% relative intensity) was very similar to that of [Fe]-hydrogenase purified from *M. marburgensis* (84), but the new species sub-spectrum 1 (20% relative intensity) was not observed in previous measurements (9, 84). In the presence of methenyl- $H_4MPT^+$ , the relative intensity of sub-spectrum 1 increased, resulting in both species have almost the same intensity (55:45) (Fig. 16B). Two distinct Mössbauer sub-spectra 1 and 2 differ mainly by the isomer shift of 0.0 vs. 0.09 mm/s. The higher isomer shift of sub-spectrum 2 should correspond to 6-coordinated Fe site in the open form, whereas 5-coordinated Fe site in the closed form

leads, on average, to shortened bonds and, thus, lower isomer shifts (100). Therefore, the Mössbauer sub-spectra 1 and 2 presumably reflect the closed and open conformations of [Fe]-hydrogenase, respectively.

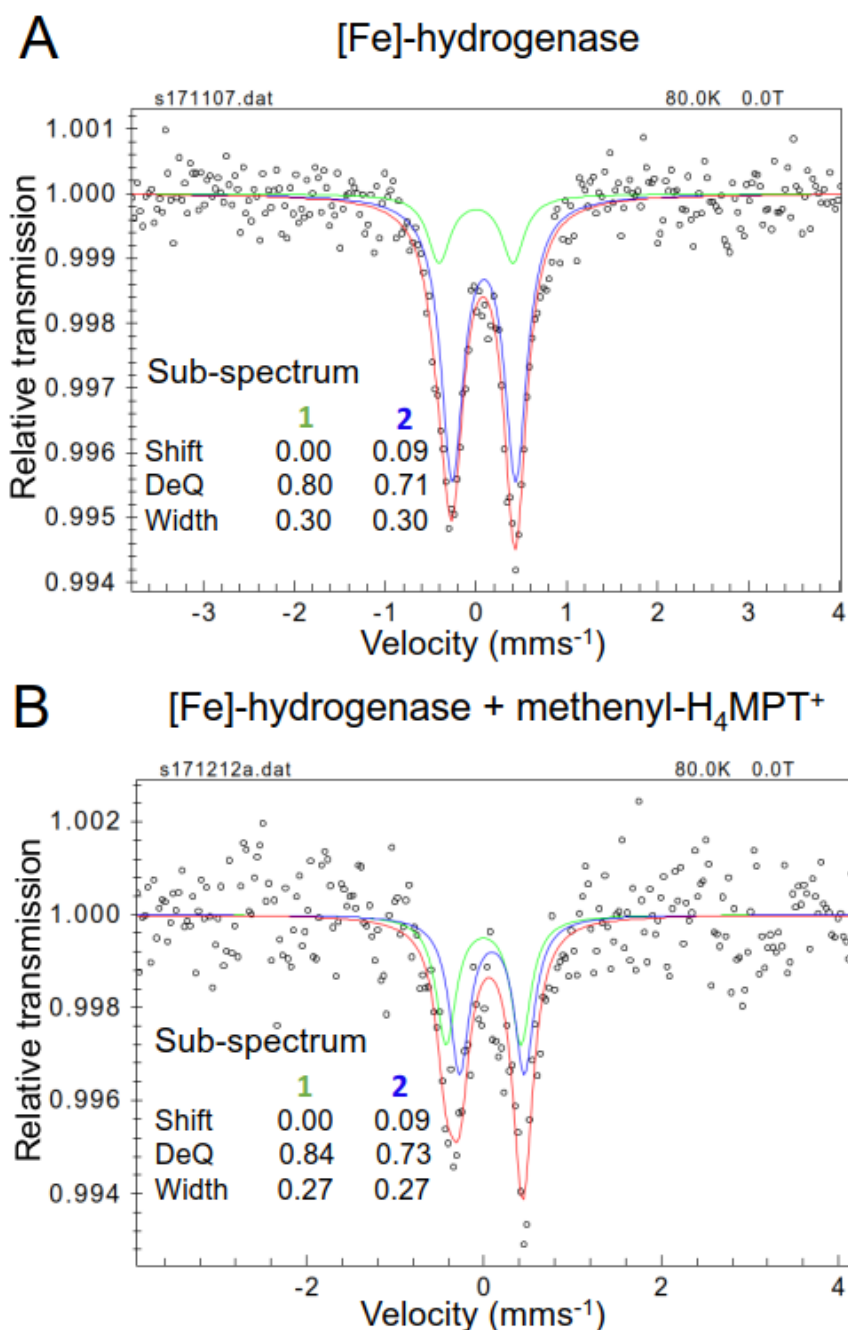


**Fig. 16. Mössbauer spectra of [Fe]-hydrogenase in the absence/presence of substrates. (A)** In the absence of substrates. **(B)** In the presence of methenyl- $\text{H}_4\text{MPT}^+$ . The Mössbauer parameters of were shown in each panel. Shift: isomer shift; Width: Line width; DeQ: Quadrupole splitting were given in mm/s; Sub-spectrum 1 (green); sub-spectrum 2 (blue); superposition of sub-spectra (red); experimental spectrum (black dots). The spectra were recorded at 80 K. This figure is obtained from Ref (98).

IR analysis indicated that the relative intensities and frequencies of the asymmetric CO ( $\sim 2000\text{ cm}^{-1}$ ) and symmetric CO ( $\sim 1940\text{ cm}^{-1}$ ) bands are only slightly changed in the absence and presence of methenyl- $\text{H}_4\text{MPT}^+$  (Fig. 17). The IR data can be interpreted that the geometry of the CO ligands and presumably of the entire Fe center appears to be largely maintained when switching from the 6-(open) to the 5-(closed)-coordinated Fe site. This conclusion is supported by the similar CO coordination structures of the Fe site of the open and closed [Fe]-hydrogenase.

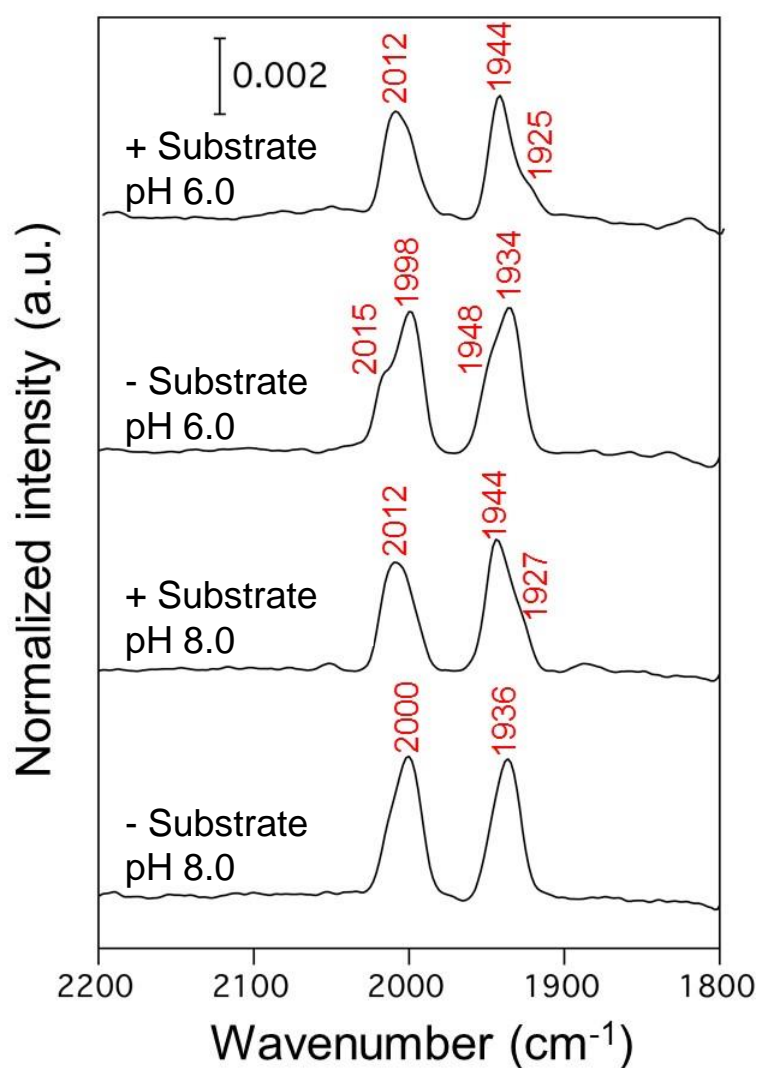


**Fig. 17. Infrared spectra of [Fe]-hydrogenase in the absence/presence of substrates.** Buffer: 50-mM MES/NaOH, pH 6.0, and 50 mM-Tricine/NaOH, pH 8.0. Gas phase: 100%  $\text{N}_2$ . This figure is modified from Ref (98).

### 2.2.3 Structures of the FeGP cofactor and methenyl-H<sub>4</sub>MPT<sup>+</sup>

Based on the 1.06-Å electron-density map of the closed [Fe]-hydrogenase/methenyl-H<sub>4</sub>MPT<sup>+</sup> complex, we can analyze the geometric parameters of the FeGP cofactor and methenyl-H<sub>4</sub>MPT<sup>+</sup> in its activated form (Fig. 18). The electron-density map clearly showed that the 5-coordinated Fe site contained two CO ligands, one pyridinol-N, one acyl-C and one Cys176-S. This is the first structural evidence of the presence of the acyl ligand (Fig. 18A). In the closed form (Form A), but not in one monomer of Form B, a weak elongated electron density is visible reaching the unoccupied Fe binding site. It might be possible for linear, rather hydrophobic, compounds like O<sub>2</sub>, N<sub>2</sub>, or HSCN to bind with a low occupancy. If two water molecules were modelled instead of the plausible compounds with a best fitting, occupancy of 40-50% can be calculated (Fig. S2).

As the 2-OH group of the pyridinol ring is assumed to act as the catalytic base for H<sub>2</sub> cleavage (97), the protonated state of 2-OH is important for the catalytic reactions. According to the references, the distance of C-O single bond in phenol is 1.36 Å and C=O double bond is 1.2 Å (101, 102). In the observed structure in the closed form, C2-O bond distance is 1.33 Å, which suggested that the 2-OH group was at least partially deprotonated. However, we cannot provide exact conclusion of the state of the 2-OH of the pyridinol ring.

The atomic-resolution crystal structure indicated that the imidazolidine ring of methenyl-H<sub>4</sub>MPT<sup>+</sup> was in a planar conformation, in which the distance between N5 and C14a (1.23 Å) (Fig.18B) was substantially shorter than that of the double bond (C=N) observed in imidazole (C2=N3, 1.313 Å) (103). The short C=N distance indicated that electron density in the imidazolidine ring are concentrated between N5 and C14a. Consistently, the distances of C-N of the imidazolidine (1.43, 1.47 and 1.48 Å) and its C-C single (1.55 Å) bonds in the imidazolidine ring were longer than those of standard imidazolidine ring (C-N, 1.364 Å and C-C, 1.460 Å) (103). The conformation of methenyl-H<sub>4</sub>MPT<sup>+</sup> bound to the closed form is substantially different from those of methylene-H<sub>4</sub>MPT obtained using NMR spectroscopy and the calculations (104, 105). The planar conformation of the imidazolidine ring does not fit to the proposed carbocationic structure (77, 92). Prerequisite of the carbocation conformation was protonation of lone-pair electrons of N5 or N10 by the carboxy group of amino-acid

residues (77, 92). However, such amino acid residues are not present in the both closed form and the open form of [Fe]-hydrogenase. The results clearly indicated the absence of the carbocationic properties of C14a of methenyl-H<sub>4</sub>MPT<sup>+</sup> in the closed form (77, 92, 106). DFT computations indicated that in contrast to the fully relaxed imidazoline ring, in the distorted imidazoline ring, the change on C14a was not change (both were +0.16), but N5 became a bit more positive (+0.13/+0.16), and N10 became a bit more negative (−0.08/−0.12) (Fig. S3). The decreased negative charge on N10 might also influence the pK<sub>a</sub> value of the 2-OH group of the FeGP cofactor (N10-2OH distance: 3.0 Å). Thus, the distorted imidazolidine structure might affect the reactivity.

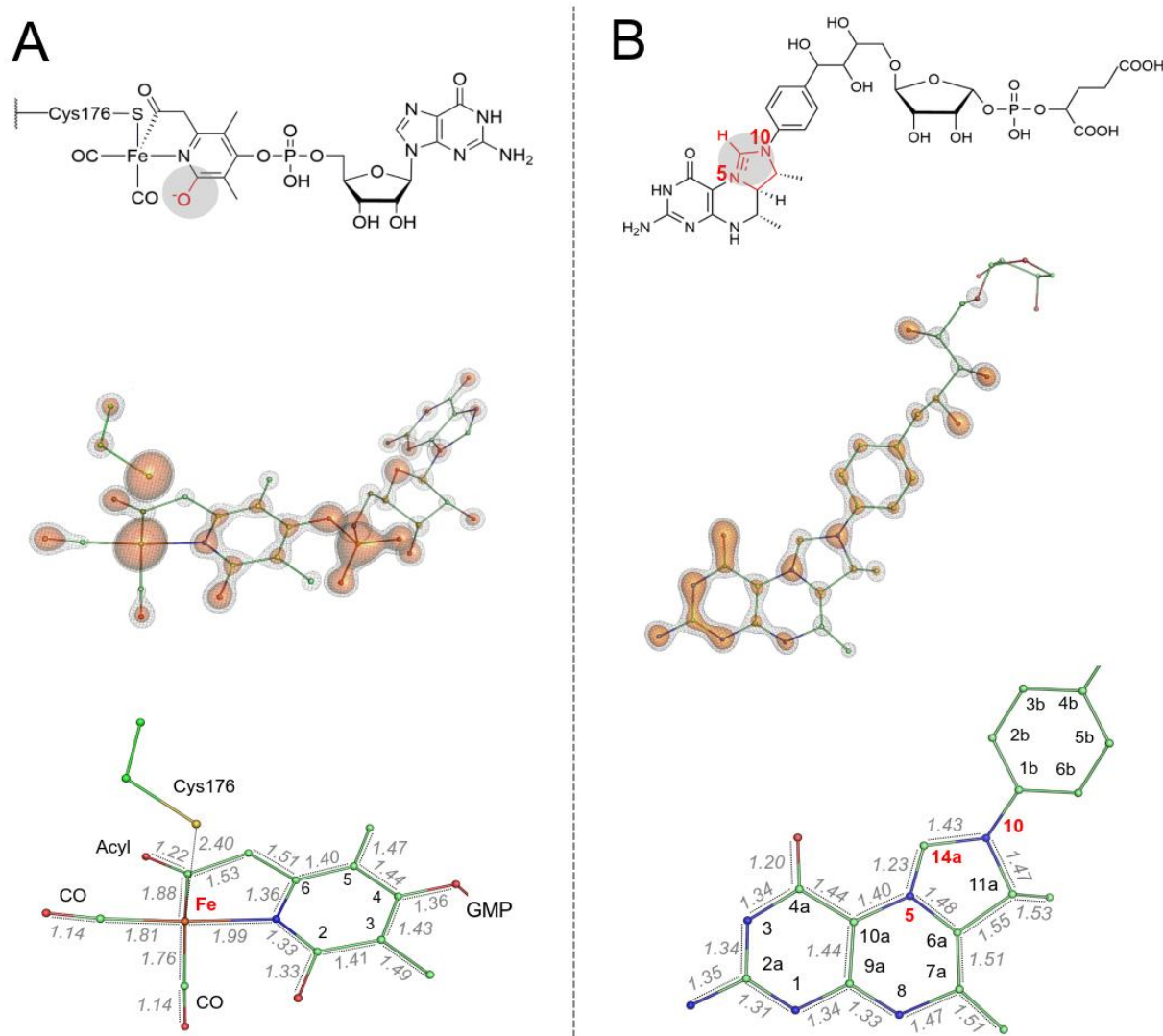


**Fig. 18. The structures of the FeGP cofactor and methenyl-H<sub>4</sub>MPT<sup>+</sup>.** The FeGP cofactor (**A**) and methenyl-H<sub>4</sub>MPT<sup>+</sup> (**B**) in the closed form of [Fe]-hydrogenase from *M. aeolicus* was at 1.06-Å resolution. (Top) Chemical structures. (Middle) The 2Fo-Fc electron-density maps shown in black mesh (contoured at 4.0 σ) and orange surface

(contoured at  $5.2 \sigma$ ). (Bottom) Ball and stick models with the bond lengths between the atoms carbon, nitrogen, oxygen, phosphorous, sulfur and iron atoms were depicted as green, dark blue, red, orange, yellow, and light brown spheres, respectively. This figure is modified from Ref (98).

#### 2.1.4 A proposed catalytic mechanism of [Fe]-hydrogenase

Base on the closed structure of [Fe]-hydrogenase/methenyl- $\text{H}_4\text{MPT}^+$  complex, QM/MM calculations were used to study the energy profiles of the catalytic cycle of [Fe]-hydrogenase (Fig. 19, Figs. S4-S5 and Table. S1). The calculations started from the 2-OH deprotonated form of the FeGP cofactor (2 in Fig. 19A). The computations results indicated that in the closed form, the binding of  $\text{H}_2$  on the sixth coordination position of Fe site is slightly exergonic ( $-0.19 \text{ kcal/mol}$ ) (Fig. 19B). The first energy barrier at  $\text{H}_2$ -activation is  $+7.6 \text{ kcal/mol}$ . After the  $\text{H}_2$ -cleavage, there was another energy barrier for hydride transfer from the Fe site to the C14a of the model substrate  $\text{MPT}^+$  (the truncated compound of methenyl- $\text{H}_4\text{MPT}^+$ ) (Fig. 19B). The computations indicated that the active site has enough space and  $\text{MPT}^+$  is flexible enough to move closer to Fe site. In this case, the distance between the Fe and C14a could decrease from  $3.73 \text{ \AA}$  (4 in Fig. 19A) to  $3.34 \text{ \AA}$  (TS4,5 in Fig. 19A) to  $3.21 \text{ \AA}$  (5 in Fig. 19A) during the reaction cycle. This behavior of  $\text{MPT}^+$  lowered the energy required for hydride transfer. This is also as an evidence for that the active site harbored enough available volume for the  $\text{MPT}^+$  to readjust itself to facilitate hydride transfer. Overall, the results of computations suggested that the catalytic process could move very fast in the closed form of [Fe]-hydrogenase.

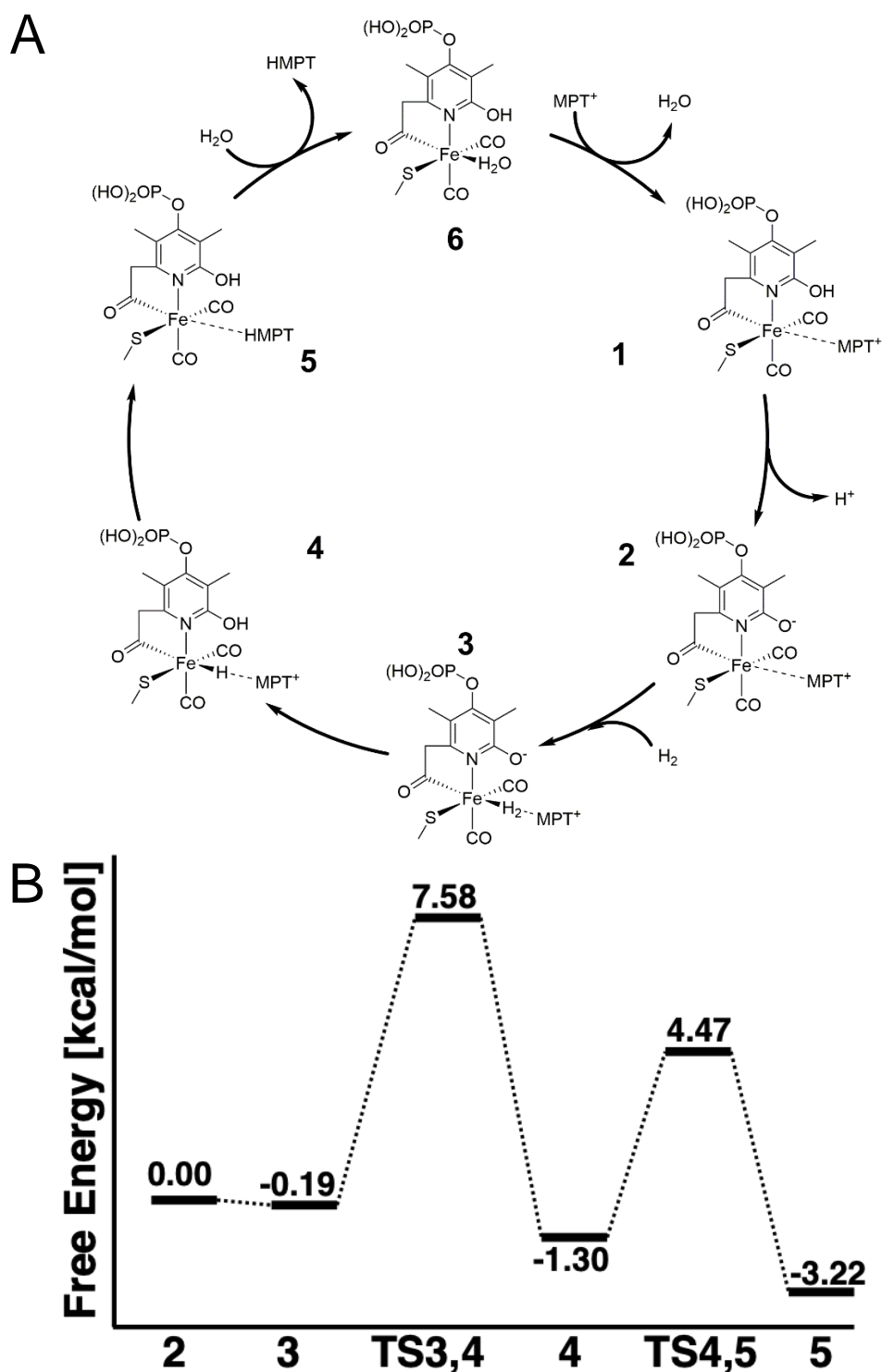


**Fig. 19.** The QM/MM computed free energy profile for the catalytic cycle of [Fe]-hydrogenase. **(A)** A proposed catalytic cycle of [Fe]-hydrogenase based on closed active-form of [Fe]-hydrogenase. The computations used the truncated forms of the FeGP cofactor and methenyl- $\text{H}_4\text{MPT}^+$  ( $\text{MPT}^+$ ) as shown in panel A. **(B)** QM/MM computed free energy profile. The methods of QM/MM computations were described in Methods. This figure is obtained from Ref (98).

Based on the crystal structures, spectroscopic measurements and QM/MM calculations, I proposed a catalytic cycle of [Fe]-hydrogenase as below (Fig. 20). (A) In the absence of methenyl- $\text{H}_4\text{MPT}^+$ , [Fe]-hydrogenase is in the open form (Step 6). The water ligand occupies one coordination position of Fe site, and the Fe is in 6-coordinated. (B) The methenyl- $\text{H}_4\text{MPT}^+$  enters the active-site cleft, which triggers a protein conformational change (from open to closed) to remove the water ligand of the Fe site (Step 1). In this state, the Fe becomes unsaturated 5-coordinated, forming an empty coordination position for  $\text{H}_2$  binding. (C) The 2-OH on the pyridinol of the FeGP cofactor is deprotonated to  $2\text{-O}^-$ , functioning as the catalytic base for the  $\text{H}_2$  heterolytic cleavage (Step 2). (D) The  $\text{H}_2$  diffuses into the active site via a hydrophobic gas channel (Fig. 15) and binds to the Fe site (Step 3). (E)  $\text{H}_2$  activation and heterolytic cleavage proceed at Fe site, which generates the iron-hydride (Fe-H) intermediate and the proton ( $\text{H}^+$ ) which is accepted by  $2\text{-O}^-$  to form 2-OH (Step 4). (F) Because of the available free space of active site as indicated by QM/MM calculations, the methenyl- $\text{H}_4\text{MPT}^+$  could readjust itself and move closer to the Fe site. With this behavior, the energy required for hydride transfer from the Fe site to C14a of methenyl- $\text{H}_4\text{MPT}^+$  could be largely reduced in the closed form. (Step 5). (G) The C14a of the methenyl- $\text{H}_4\text{MPT}^+$  accepts the hydride ( $\text{H}^-$ ) to produce methylene- $\text{H}_4\text{MPT}$ , which changes the closed form back to the open form (Step 6) and then the product methylene- $\text{H}_4\text{MPT}$  is released. Then, one water molecule occupies the one coordination site of the Fe again.



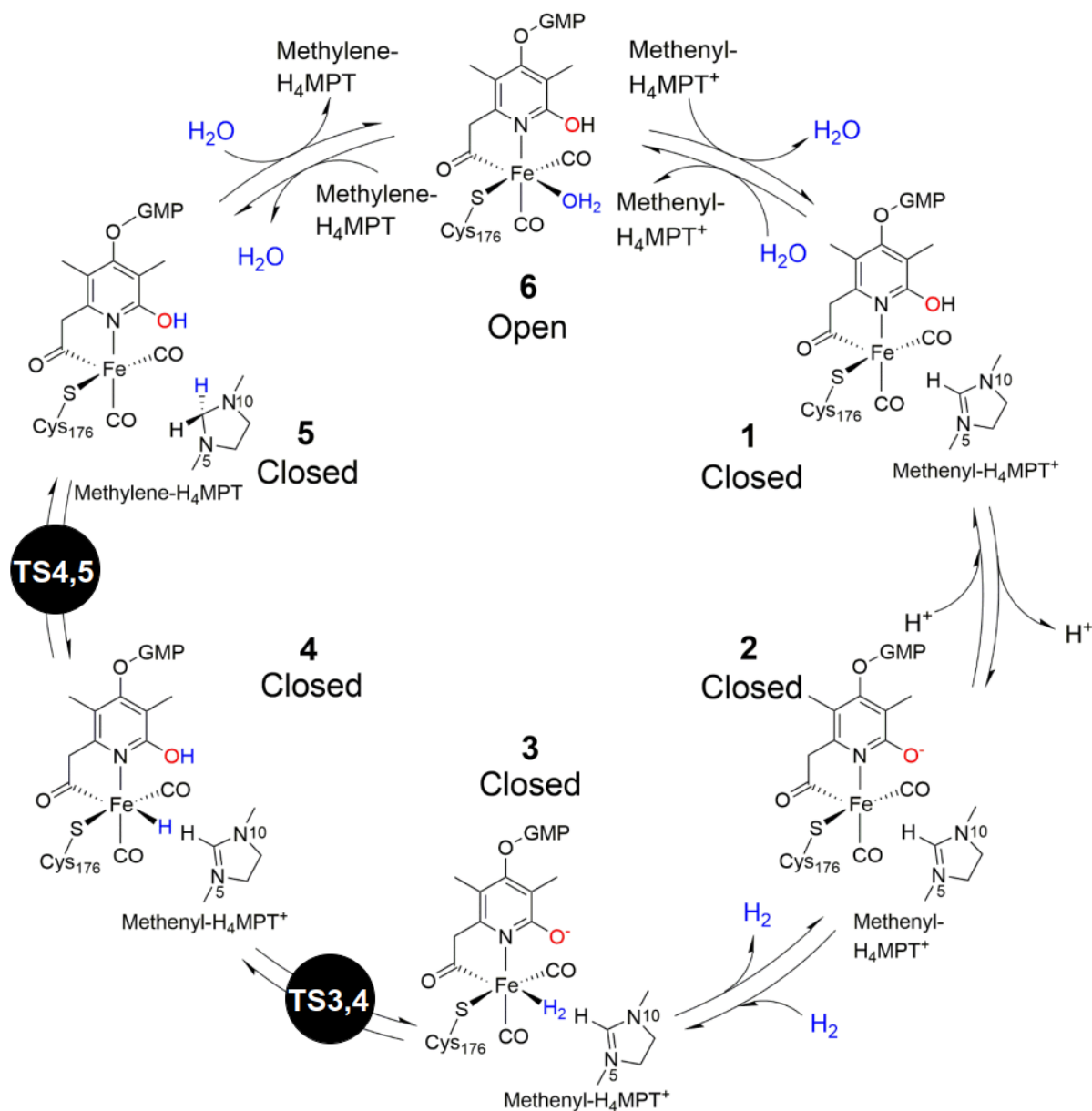


**Fig. 20. A proposed catalytic cycle of [Fe]-hydrogenase.** The presented crystal structures corresponded to step 6 and step 1 (or 2), in which the protein was in the open and closed forms, respectively. Upon binding of methenyl- $\text{H}_4\text{MPT}^+$  and closure of the active-site cleft, the water molecule on the Fe site is removed. The distorted methenyl- $\text{H}_4\text{MPT}^+$  was observed in the crystal structure of the closed form (step 2).  $\text{H}_2$  is bound to the open Fe site and then heterolytically cleaved (step 4). Subsequently the hydride ( $\text{H}^-$ ) on the Fe site is transferred to C14a of methenyl- $\text{H}_4\text{MPT}^+$  to generate methylene- $\text{H}_4\text{MPT}$  (step 5). The transient states were marked with black closed circle based on QM/MM computations (Fig. 19). This figure is modified from Ref (98).

## 2.2 Evidence for the presence of iron-hydride as the catalytic intermediate

### 2.2.1 [Fe]-hydrogenase catalyzes reduction of O<sub>2</sub> to H<sub>2</sub>O<sub>2</sub>

As previously reported, the metal sites of [NiFe]- and [FeFe]-hydrogenases were redox-active and most of these hydrogenases were O<sub>2</sub>-sensitive (47, 107, 108). Although researchers found some [NiFe]-hydrogenases from aerobic bacteria had certain O<sub>2</sub>-tolerance. The O<sub>2</sub> tolerant [NiFe]-hydrogenases could remove the oxygen species by re-reduction of the bound oxygen species with protons and electrons to water. However, the O<sub>2</sub> tolerant mechanism is not fully clarified although some hypotheses are proposed (48, 109-111). In the case of [Fe]-hydrogenase, the mono iron site was redox-inactive (84) and [Fe]-hydrogenase was believed to be O<sub>2</sub>-insensitive (85). However, one recent study reported that H<sub>2</sub>O<sub>2</sub> inactivates [Fe]-hydrogenase by decomposing the FeGP cofactor (97). We wondered whether some reductants of the [Fe]-hydrogenase reaction might produce reactive oxygen species (e.g. H<sub>2</sub>O<sub>2</sub>) by reduction of O<sub>2</sub>, which would inactivate [Fe]-hydrogenase.

[Fe]-hydrogenase utilizes H<sub>2</sub> or methylene-H<sub>4</sub>MPT as the reductant of the reactions. Firstly, we tested the effects of methylene-H<sub>4</sub>MPT and H<sub>2</sub>/methenyl-H<sub>4</sub>MPT<sup>+</sup> on the stability of [Fe]-hydrogenase against O<sub>2</sub> using the enzyme-activity-assay system. Although the initial reaction rate was unchanged in the presence of 20% O<sub>2</sub> in contrast to 100% N<sub>2</sub>, the rate of methylene-H<sub>4</sub>MPT dehydrogenation to methenyl-H<sub>4</sub>MPT<sup>+</sup> progressively decreased (Fig. 21A) and no recovery of the activity was observed by removing O<sub>2</sub> by gas exchange with N<sub>2</sub>. In the case of the hydrogenation of methenyl-H<sub>4</sub>MPT<sup>+</sup> with H<sub>2</sub>, the enzyme activity decreased with time under 20% O<sub>2</sub> containing H<sub>2</sub> gas phase compared with 100% H<sub>2</sub> (Fig. 21B). Again, no recovery activity observed after removing 20% O<sub>2</sub> by gas exchange with H<sub>2</sub>. We concluded that [Fe]-hydrogenase was inactivated rather than inhibited in the presence of the reducing-substrates and O<sub>2</sub>.

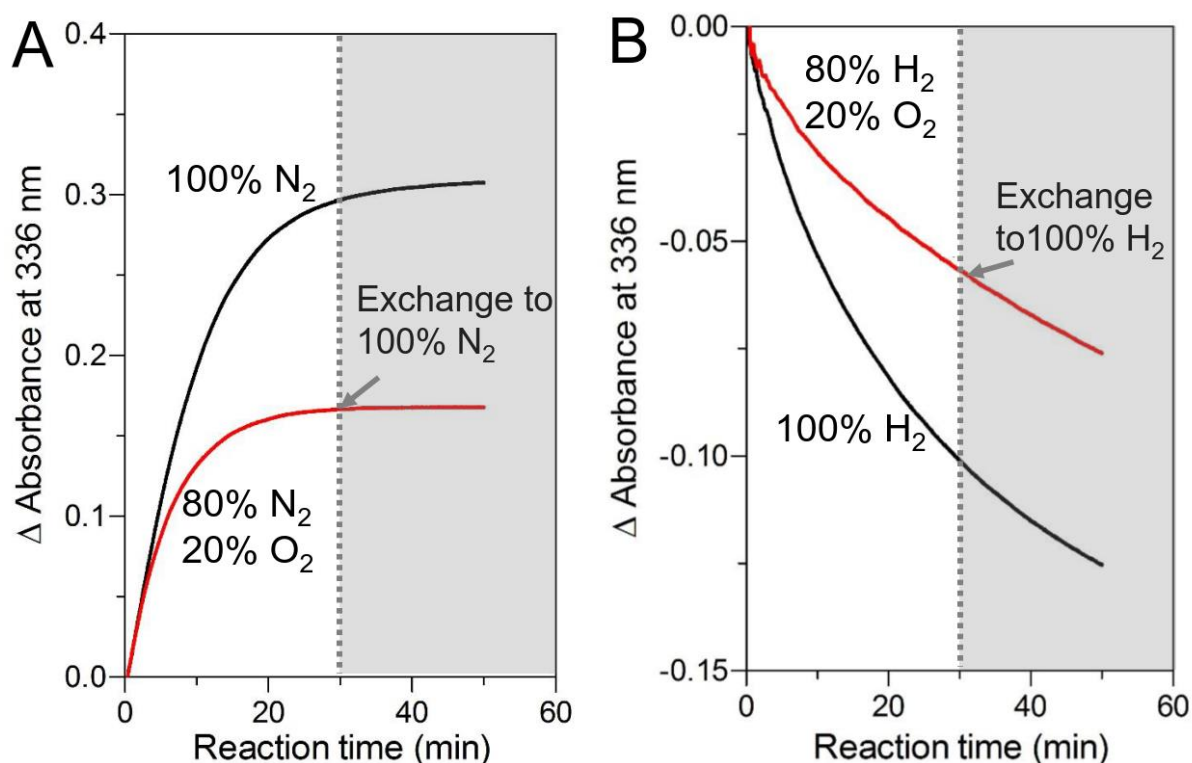


**Fig. 21. The progressing inactivation of [Fe]-hydrogenase by  $O_2$  in the presence of reducing substrates (112).** (A) Dehydrogenation of methylene- $H_4MPT$  to methenyl- $H_4MPT^+$ . (B) Hydrogenation of methenyl- $H_4MPT^+$  with  $H_2$  to methylene- $H_4MPT$ . The gas phases in the cuvettes were exchanged at the time point indicated by grey arrows. This figure is modified from Ref (112).

To further test the effect of  $O_2$  on the activity of [Fe]-hydrogenase, we tested the time-dependent decrease of the activities under the gas phase with variable  $O_2$ -concentration in the presence of methylene- $H_4MPT$  (Fig. 22). The results clearly showed that the inactivation rate of [Fe]-hydrogenase increased dependent on the concentration of  $O_2$ . The effect of  $O_2$  concentration on inactivation of [Fe]-hydrogenase could be described with the Michaelis-Menten equation. The apparent  $V_{max}$  of the inactivation rate was 5.3-nmol enzyme/min and the apparent  $K_M$  was 12.5 %  $O_2$  in the gas phase (112). This finding suggested that  $O_2$  is used as a substrate of [Fe]-hydrogenase.

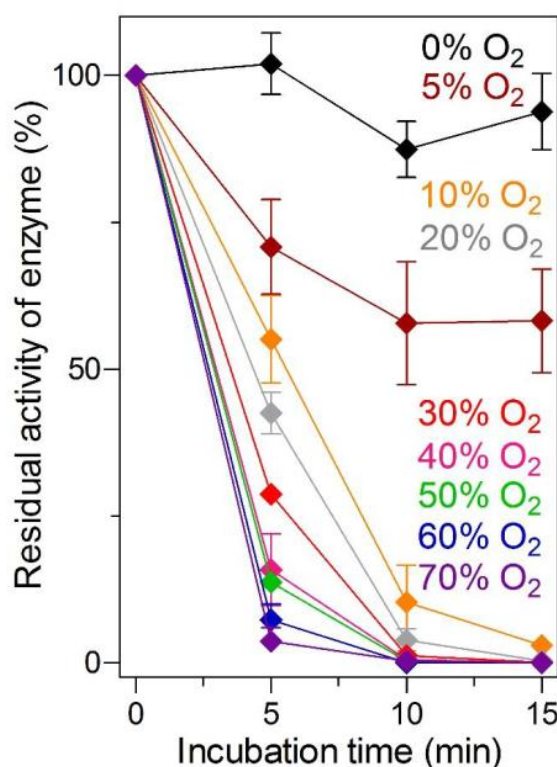


**Fig. 22. The O<sub>2</sub>-concentration dependent inactivation of [Fe]-hydrogenase in the presence of reducing substrates and O<sub>2</sub>.** This test was performed in the presence of 1-mg/ml (26- $\mu$ M) [Fe]-hydrogenase and 26- $\mu$ M methylene-H<sub>4</sub>MPT under gas phase N<sub>2</sub> containing different concentrations of O<sub>2</sub> at 40 °C. At different time points, 10- $\mu$ l aliquots from the mixture solution was taken for residual enzyme activity assay.

According to previous report, the candidates of the reactive oxygen species produced is H<sub>2</sub>O<sub>2</sub> or superoxide radical anion (O<sub>2</sub><sup>•-</sup>) (97). To detect the generated reactive oxygen species, we used higher concentrations of both [Fe]-hydrogenase (500  $\mu$ M) and methylene-H<sub>4</sub>MPT (500  $\mu$ M) together with O<sub>2</sub> (100%). As shown in Table. S2, only in the presence of both enzyme and substrate, ~3- $\mu$ M H<sub>2</sub>O<sub>2</sub> could be determined, but O<sub>2</sub><sup>•-</sup> was not detected. This data also indicated that the generation of reactive oxygen species, namely H<sub>2</sub>O<sub>2</sub>, was [Fe]-hydrogenase dependent. To test the relationship between the enzymatic activity of [Fe]-hydrogenase and H<sub>2</sub>O<sub>2</sub> production in the presence of methylene-H<sub>4</sub>MPT and O<sub>2</sub>, we performed kinetic studies. Increase of the concentrations of [Fe]-hydrogenase, methylene-H<sub>4</sub>MPT or O<sub>2</sub> resulted in the increased amount of generated H<sub>2</sub>O<sub>2</sub>, and the increased rate of inactivation of [Fe]-hydrogenase. The H<sub>2</sub>O<sub>2</sub> production stopped when [Fe]-hydrogenase was fully inactivated (Fig. 23).

These data indicated that the generation of  $\text{H}_2\text{O}_2$  needs [Fe]-hydrogenase enzyme activity and  $\text{O}_2$ .

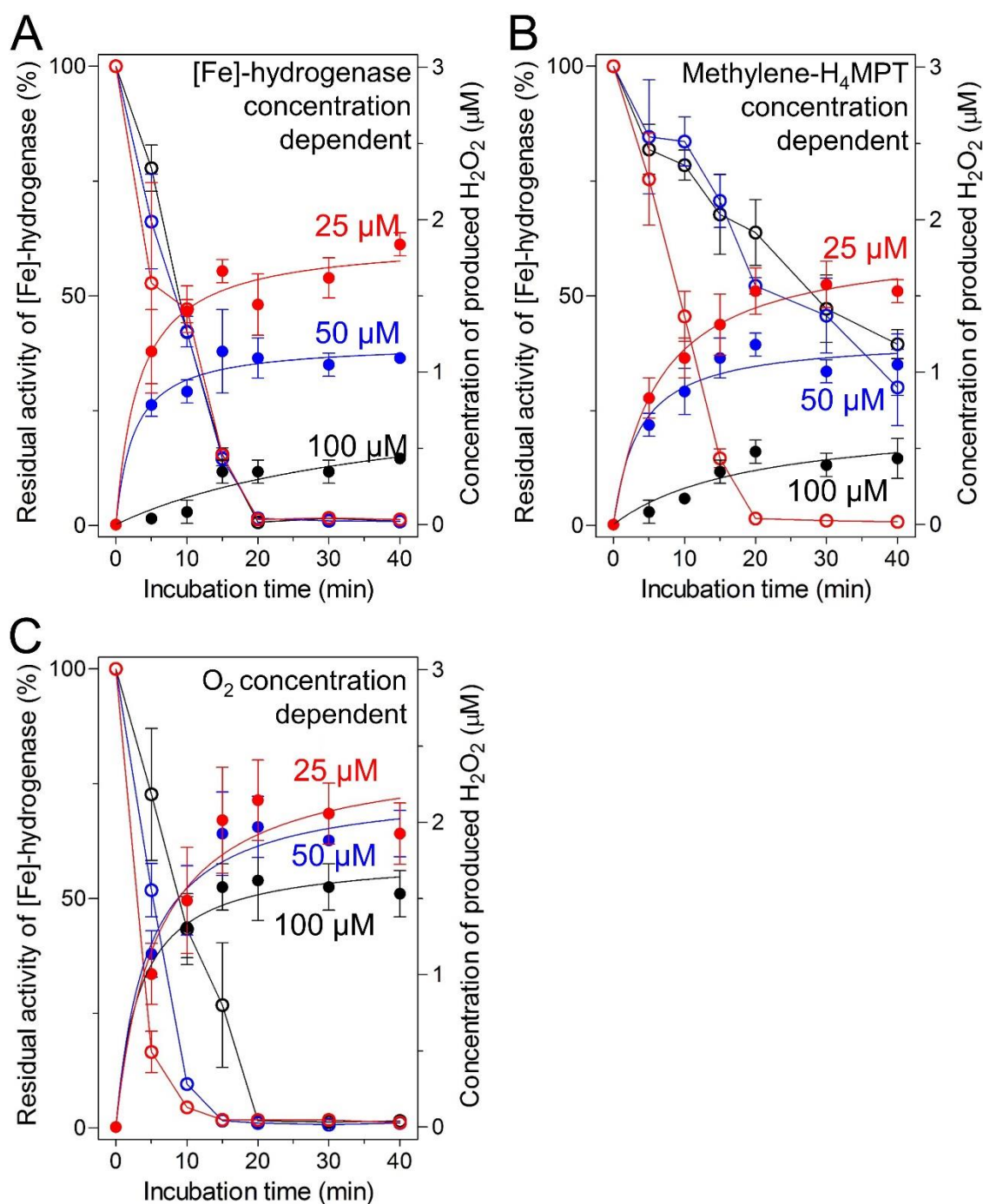


**Fig. 23. Kinetics of  $\text{O}_2$ -inactivation of [Fe]-hydrogenase and  $\text{H}_2\text{O}_2$  generation (112).** (A) The enzyme-concentration dependent  $\text{O}_2$ -inactivation of [Fe]-hydrogenase. Test conditions: 100- $\mu\text{M}$  methylene- $\text{H}_4\text{MPT}$  and different concentrations of [Fe]-hydrogenase under  $\text{N}_2/\text{O}_2$  (95%/5%). (B) The substrate-concentration dependent  $\text{O}_2$ -inactivation of [Fe]-hydrogenase. Test conditions: 100- $\mu\text{M}$  [Fe]-hydrogenase and different concentrations of methylene- $\text{H}_4\text{MPT}$  under  $\text{N}_2/\text{O}_2$  (95%/5%). (C) The  $\text{O}_2$ -

concentration dependent O<sub>2</sub>-inactivation of [Fe]-hydrogenase. Test conditions: 100-μM [Fe]-hydrogenase and 100-μM methylene-H<sub>4</sub>MPT under N<sub>2</sub> with different concentrations of O<sub>2</sub>. All mixtures contained 120-mM potassium phosphate buffer (pH 6.0) and 1-mM EDTA. The assay solutions were incubated at 40 °C and the methylene-H<sub>4</sub>MPT dehydrogenation (open circles) and the respective H<sub>2</sub>O<sub>2</sub> concentrations (closed circle) were determined. The standard error of at least three measurements was calculated. This figure is modified from Ref (112).

In order to obtain the evidence for H<sub>2</sub>O<sub>2</sub> production from the reaction of [Fe]-hydrogenase with O<sub>2</sub> and reductants, we performed an experiment shown below. According to the previous report, the compound cyclohexylisocyanide (CHI) can reversibly inhibits [Fe]-hydrogenase by occupying the open site of the Fe of the FeGP cofactor (89). As shown in Fig. 24, when the mixture containing 500-μM [Fe]-hydrogenase and 500-μM methylene-H<sub>4</sub>MPT incubated in the presence of 2-mM CHI, the enzyme activity of [Fe]-hydrogenase was completely inhibited by CHI, where even under 100% O<sub>2</sub>, no H<sub>2</sub>O<sub>2</sub> was produced. After removal of CHI from the assay solution by washing was activity-assay buffer, most of the [Fe]-hydrogenase activity was recovered. Then, treatments with 100% O<sub>2</sub> in the presence of methylene-H<sub>4</sub>MPT was performed, which resulted in total loss of the [Fe]-hydrogenase activity (Fig. 24A) and production of H<sub>2</sub>O<sub>2</sub> (Fig. 24B). However, in the case of absence of CHI, [Fe]-hydrogenase was inactivated and H<sub>2</sub>O<sub>2</sub> was produced before washing. After washing, enzyme activity and H<sub>2</sub>O<sub>2</sub> could not be observed. These findings demonstrated that H<sub>2</sub>O<sub>2</sub> only produced in the presence of O<sub>2</sub> under turnover conditions.

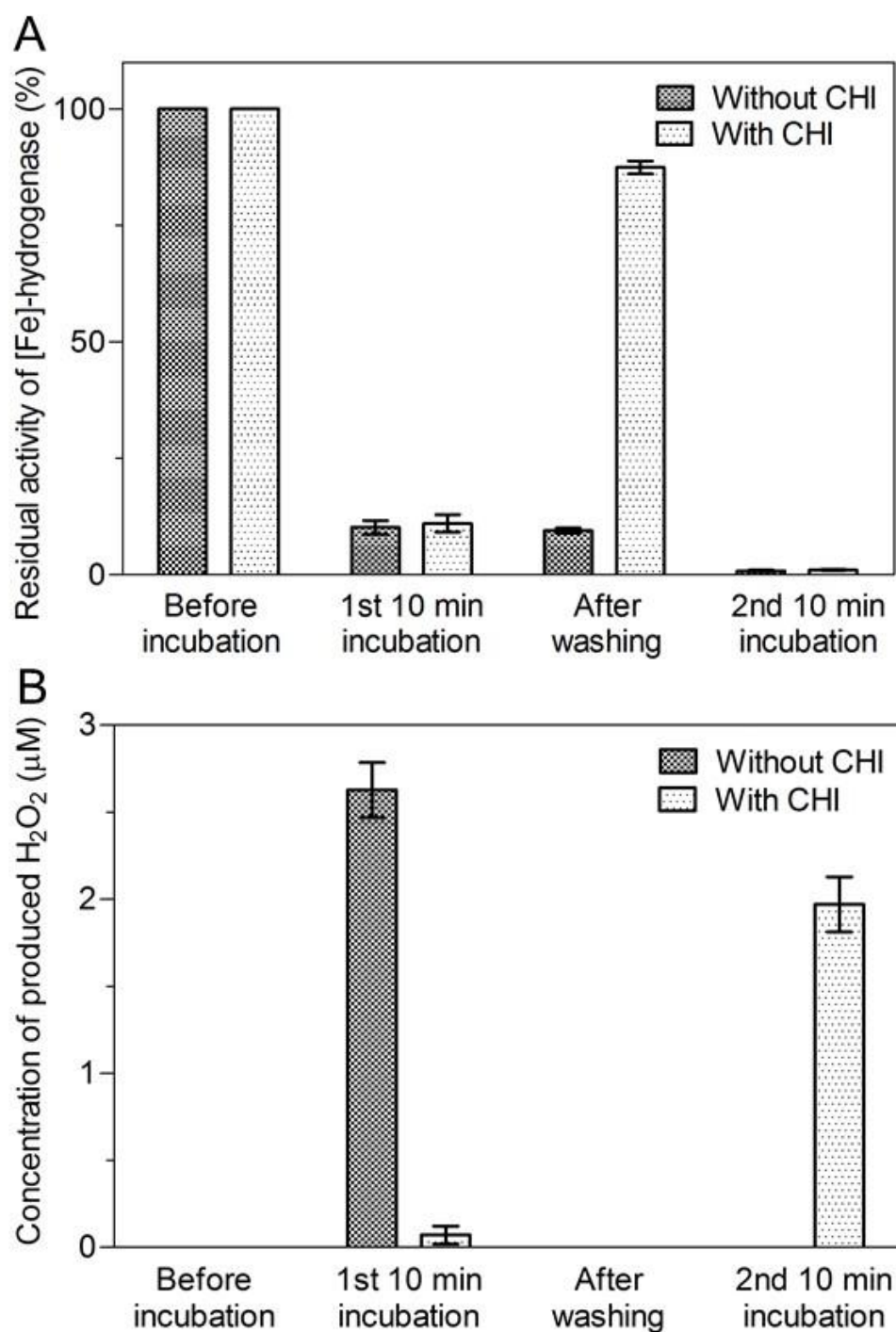


**Fig. 24. The relationship between protection of [Fe]-hydrogenase activity with CHI and  $H_2O_2$  formation.** (A) The enzyme activity of [Fe]-hydrogenase. (B) The  $H_2O_2$  production from [Fe]-hydrogenase. The 1-ml assay mixture containing 500- $\mu M$  [Fe]-hydrogenase, 500- $\mu M$  methylene- $H_4MPT$  with/without 2-mM CHI was incubated under 100%  $O_2$  at 40 °C. After incubation for 10 min, CHI was removed by ultrafiltration. Then, 500  $\mu M$  methylene- $H_4MPT$  was added to the samples and incubated at 40 °C for another 10 min under 100%  $O_2$ . The activity of “Before incubation” in panel A was measured before addition of CHI.

Since only sub-stoichiometrical concentration of  $\text{H}_2\text{O}_2$  ( $\sim 3\text{-}\mu\text{M}$ ) is generated from [Fe]-hydrogenase ( $500\text{-}\mu\text{M}$ ) and methylene- $\text{H}_4\text{MPT}$  ( $500\text{-}\mu\text{M}$ ) with  $\text{O}_2$  (100%) (Table. S2), we tested the dependency of the  $\text{H}_2\text{O}_2$  concentration on the inactivation of [Fe]-hydrogenase. As shown in Fig. 25, 0.26, 2.6 and  $26\text{-}\mu\text{M}$   $\text{H}_2\text{O}_2$  (final concentration in the assay solution) were added to  $26\text{-}\mu\text{M}$  [Fe]-hydrogenase (final concentrations). After incubation, the sample containing  $26\text{-}\mu\text{M}$   $\text{H}_2\text{O}_2$  and  $26\text{-}\mu\text{M}$  [Fe]-hydrogenase (1:1) lost full enzyme activity within 5 min, but only less than 10% of  $\text{H}_2\text{O}_2$  was lost during this process. In the case of sub-stoichiometric concentrations of  $\text{H}_2\text{O}_2$  ( $2.6\text{-}\mu\text{M}$ , 1:10 and  $0.26\text{-}\mu\text{M}$ , 1:100),  $26\text{-}\mu\text{M}$  [Fe]-hydrogenase still lost 70% and 40% activity within 10 min, respectively. These results suggested that [Fe]-hydrogenase is catalytically inactivated by sub-stoichiometric amounts of  $\text{H}_2\text{O}_2$ . It means that only a sub-stoichiometric amount of  $\text{H}_2\text{O}_2$  was produced from [Fe]-hydrogenase by reduction of  $\text{O}_2$  and this amount was already enough to fully decompose [Fe]-hydrogenase (112).



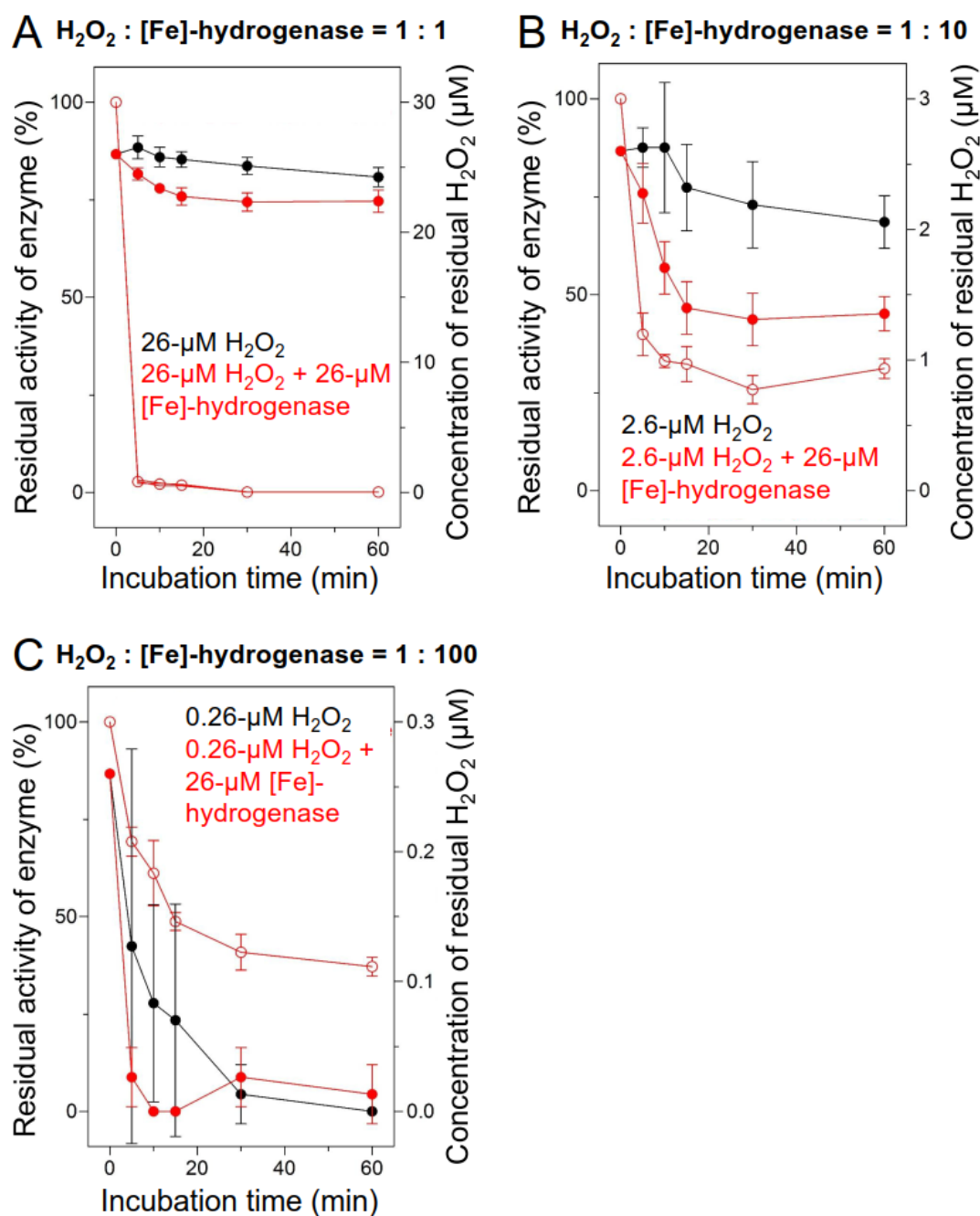


**Fig. 25. The dependency of amount of  $\text{H}_2\text{O}_2$  on inactivation of [Fe]-hydrogenase (112).** The assay solution contained 26- $\mu\text{M}$  [Fe]-hydrogenase in 120-mM potassium phosphate buffer (pH 6.0) with 1-mM EDTA with ((A) 26  $\mu\text{M}$ ; (B) 2.6  $\mu\text{M}$  and (C) 0.26  $\mu\text{M}$ )  $\text{H}_2\text{O}_2$  (red). In the control case, it only contains  $\text{H}_2\text{O}_2$  (26  $\mu\text{M}$ , 2.6  $\mu\text{M}$  and 0.26  $\mu\text{M}$ ) without [Fe]-hydrogenase (black). The 5-ml vials containing the assay solution were incubated under 100%  $\text{N}_2$  at 40 °C. The residual enzyme activity of [Fe]-hydrogenase (open circle) and the residual concentration of  $\text{H}_2\text{O}_2$  (closed circle) were measured at each time point. The determination of  $\text{H}_2\text{O}_2$  in the absence of enzyme demonstrate that a certain amount of  $\text{H}_2\text{O}_2$  gets lost in the process. This figure is obtained from Ref (112).

### 2.2.2 The crystal structure of O<sub>2</sub>-inactivated [Fe]-hydrogenase

Since O<sub>2</sub>-inactivation of [Fe]-hydrogenase occurred in the presence of substrates (mehenyl-H<sub>4</sub>MPT<sup>+</sup>/H<sub>2</sub> or methylene-H<sub>4</sub>MPT) via formation of H<sub>2</sub>O<sub>2</sub>, we crystallized O<sub>2</sub>-inactivated [Fe]-hydrogenase to analyze the O<sub>2</sub>-decomposed [Fe] center in [Fe]-hydrogenase. We prepared the protein sample as described below. The 1-ml mixture containing 26-μM (1-mg/ml) [Fe]-hydrogenase and 26-μM methylene-H<sub>4</sub>MPT was incubated under N<sub>2</sub>/O<sub>2</sub>/H<sub>2</sub> (70%/20%/10%) in 40 °C for 1 h to completely inactivate the [Fe]-hydrogenase (controlled by the enzyme activity measurement). The best crystal diffracted to 1.29-Å resolution (Table. 2).

In Fig. 26A, the structure of 2-naphthylisocyanide inhibited [Fe]-hydrogenase from *M. marburgensis* is shown (89). In this structure, the 6<sup>th</sup> water ligand of the Fe site was replaced with 2-naphthylisocyanide-C but the other Fe ligands were unchanged. In Fig. 26B, the structure of O<sub>2</sub>-inactivated [Fe]-hydrogenase from *M. marburgensis* is shown (112). The 1.29-Å resolution structure clearly indicated that the Fe center of the FeGP cofactor was decomposed and the acyl ligand was hydrolyzed to the carboxy group of guanylylpyridinol (GP) (Fig. 26B). GP has been identified as a light-inactivated product of the isolated FeGP cofactor as previously reported (85). The Fe site lost the two CO ligands, one pyridinol-N, one acyl-C; the Fe ion moved away from the original position of the FeGP cofactor but is still coordinated with Cys172-S, and interacted with GP via carboxymethyl-O of GP. The Fe ion in the decomposed structure formed new bonds with His203-N and Asp189-O from the partner monomer. Thus, the number of ligands of iron decreased from six to four by decomposition (Fig. 26).

**Table. 2. X-ray analysis statistics of O<sub>2</sub>-inactivated [Fe]-hydrogenase (112)**

O <sub>2</sub> -inactivated [Fe]-hydrogenase from <i>M. marburgensis</i>	
<b>Data collection</b>	
Wavelength (Å)	1.00005
Space group	<i>H32</i>
Resolution (Å)	47.00 – 1.29 (1.36 – 1.29)
Cell dimensions	
a, b, c (Å)	127.4, 127.4, 141.2
α, β, γ (°)	90.0, 90.0, 120.0
R <sub>merge</sub> (%) <sup>a</sup>	4.8 (112.8)
R <sub>pim</sub> (%) <sup>a</sup>	1.8 (42.3)
CC <sub>1/2</sub> <sup>a</sup>	100.0 (63.8)
I/σ <sub>I</sub> <sup>a</sup>	19.6 (1.9)
Completeness (%) <sup>a</sup>	100.0 (100.0)
Redundancy <sup>a</sup>	8.2 (8.0)
Number of unique reflections <sup>a</sup>	110077 (15981)
<b>Refinement</b>	
Resolution (Å)	43.47 – 1.29
Number of reflections	110053
R <sub>work</sub> /R <sub>free</sub> <sup>b</sup> (%)	12.7 / 14.7
Number of atoms	
Protein	2749
Ligands/ions	46
Solvent	516
Mean B-value (Å <sup>2</sup> )	21.0
Molprobability clash score, all atoms	1.79 (98 <sup>th</sup> percentile)
Ramachandran plot	
Favored regions (%)	96.5
Outlier regions (%)	0.29
rmsd <sup>c</sup> bond lengths (Å)	0.010
rmsd <sup>c</sup> bond angles (°)	1.194
<b>PDB code</b>	<b>5OK4</b>

<sup>a</sup> Values for the highest resolution shell are within parentheses. <sup>b</sup> R<sub>free</sub> was calculated as R<sub>work</sub> for 5% of the reflections that were not included in the refinement. <sup>c</sup> rmsd, root mean square deviation. This table is obtained from Ref (112).

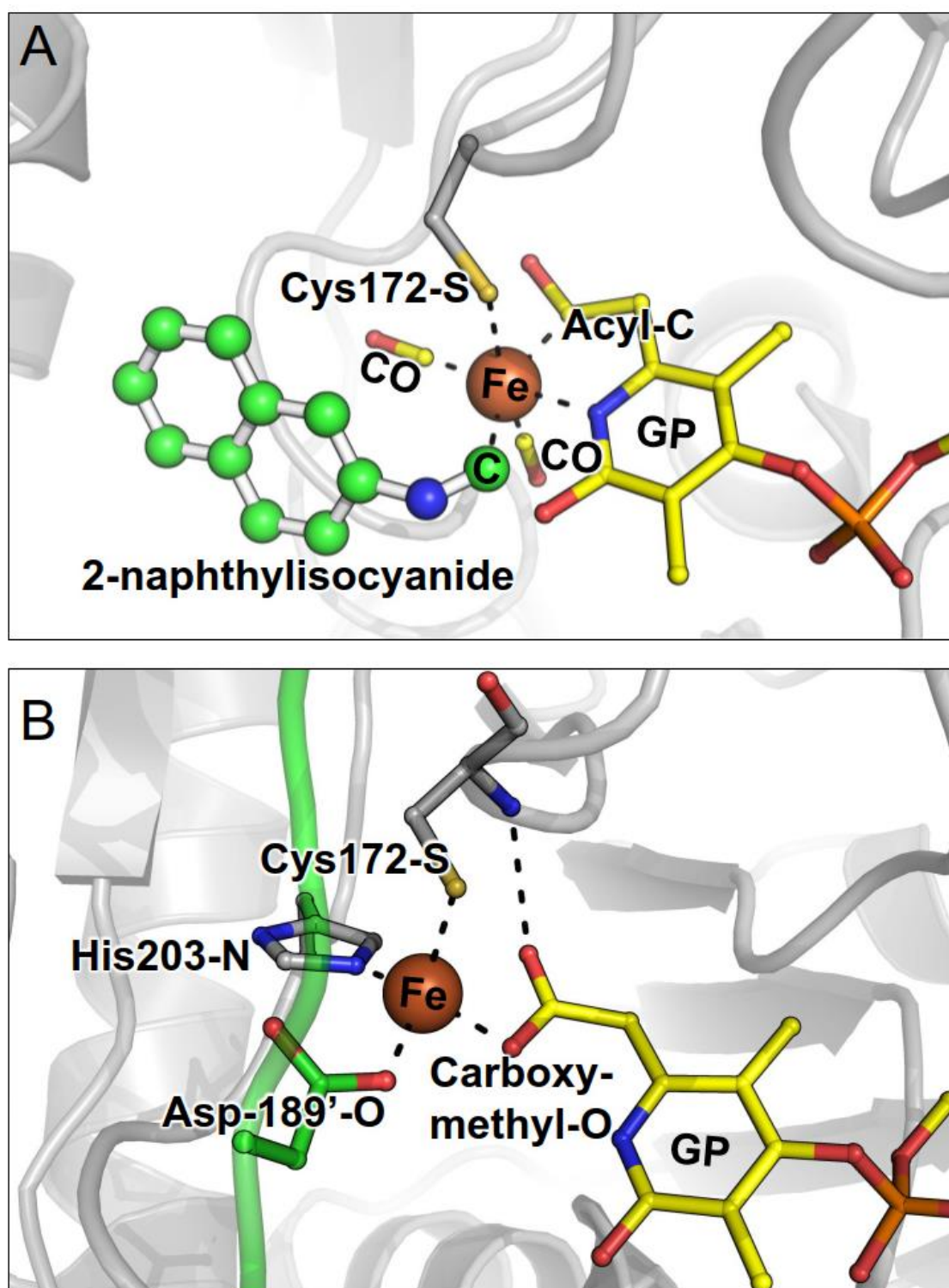


**Fig. 26. Comparison of intact and O<sub>2</sub>-inactivated [Fe]-hydrogenase (112).** (A) The active-site structure of the intact [Fe]-hydrogenase inhibited with 2-naphthylisocyanide (89). The inhibitor (2-naphthylisocyanide) was shown in sticks and balls, carbons were colored by green. (B) The active-site structure of the O<sub>2</sub>-inactivated [Fe]-hydrogenase. The loop from the partner monomer was shown as green cartoon. This figure is modified from Ref (112).

### 2.2.3 Spectroscopic analyses of O<sub>2</sub>-inactivated [Fe]-hydrogenase

Spectroscopic analyses were used to reveal the active center of O<sub>2</sub>-inactivated [Fe]-hydrogenase. The intact FeGP cofactor (enzyme bound state) has absorbance peaks at 300 nm (correspond to the pyridinol-ring) and at 360 nm (correspond to the Fe-complex) in UV-Vis spectroscopy (85). In the case of O<sub>2</sub>-inactivated [Fe]-hydrogenase, the absorbance peaks at 300 nm increased and the absorbance peaks at 360 nm decreased (Fig. 27). This phenomenon is similar to the case of light-inactivated [Fe]-hydrogenase (85). UV-Vis spectroscopy data indicated that the FeGP cofactor is decomposed by the O<sub>2</sub>-inactivation as observed in the case of light inactivation. This finding is consistent with the crystallography data (Fig. 26).

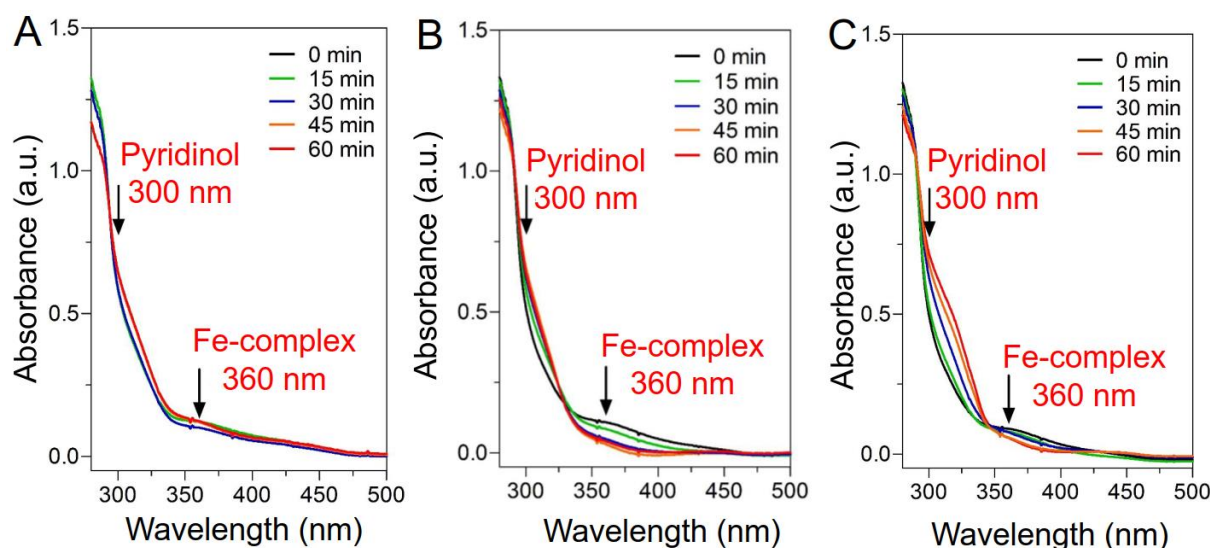


**Fig. 27. UV-Vis spectroscopic analysis O<sub>2</sub>-inactivation of [Fe]-hydrogenase (112).**

(A) In the absence of substrates. (B) In the presence of methenyl-H<sub>4</sub>MPT<sup>+</sup>. (C) In the presence of methylene-H<sub>4</sub>MPT. The assay mixture containing 120-mM potassium phosphate buffer pH 6.0, 1-mM EDTA, 130-μM (5-mg/ml) [Fe]-hydrogenase, 32.5-μM methenyl-H<sub>4</sub>MPT<sup>+</sup>/methylene-H<sub>4</sub>MPT or no substrate was incubated at 40 °C under the gas phase N<sub>2</sub>/O<sub>2</sub>/H<sub>2</sub> (70%/20%/10%). The spectrum was measured by using 3-mm light-pass quartz cuvettes. This figure is modified from Ref (112).

The intact FeGP cofactor (enzyme bound state) has two CO bands at 1938 cm<sup>-1</sup> and 2008 cm<sup>-1</sup> in the IR spectrum (83). The IR spectra of [Fe]-hydrogenase after incubation in the absence/presence of the substrates under the gas phase containing O<sub>2</sub>, N<sub>2</sub> and H<sub>2</sub> in different ratios are shown in Fig. 28. In the absence of O<sub>2</sub>, the IR spectrum of [Fe]-hydrogenase was not changed independent of the presence of the substrates. In

the presence of methylene- $\text{H}_4\text{MPT}$ , the CO ligands were almost disappeared under the gas phase containing  $\text{O}_2$ . These results indicated that  $\text{O}_2$ -treatment in the presence of methylene- $\text{H}_4\text{MPT}$  decomposed the two CO ligands of the Fe site of the FeGP cofactor.

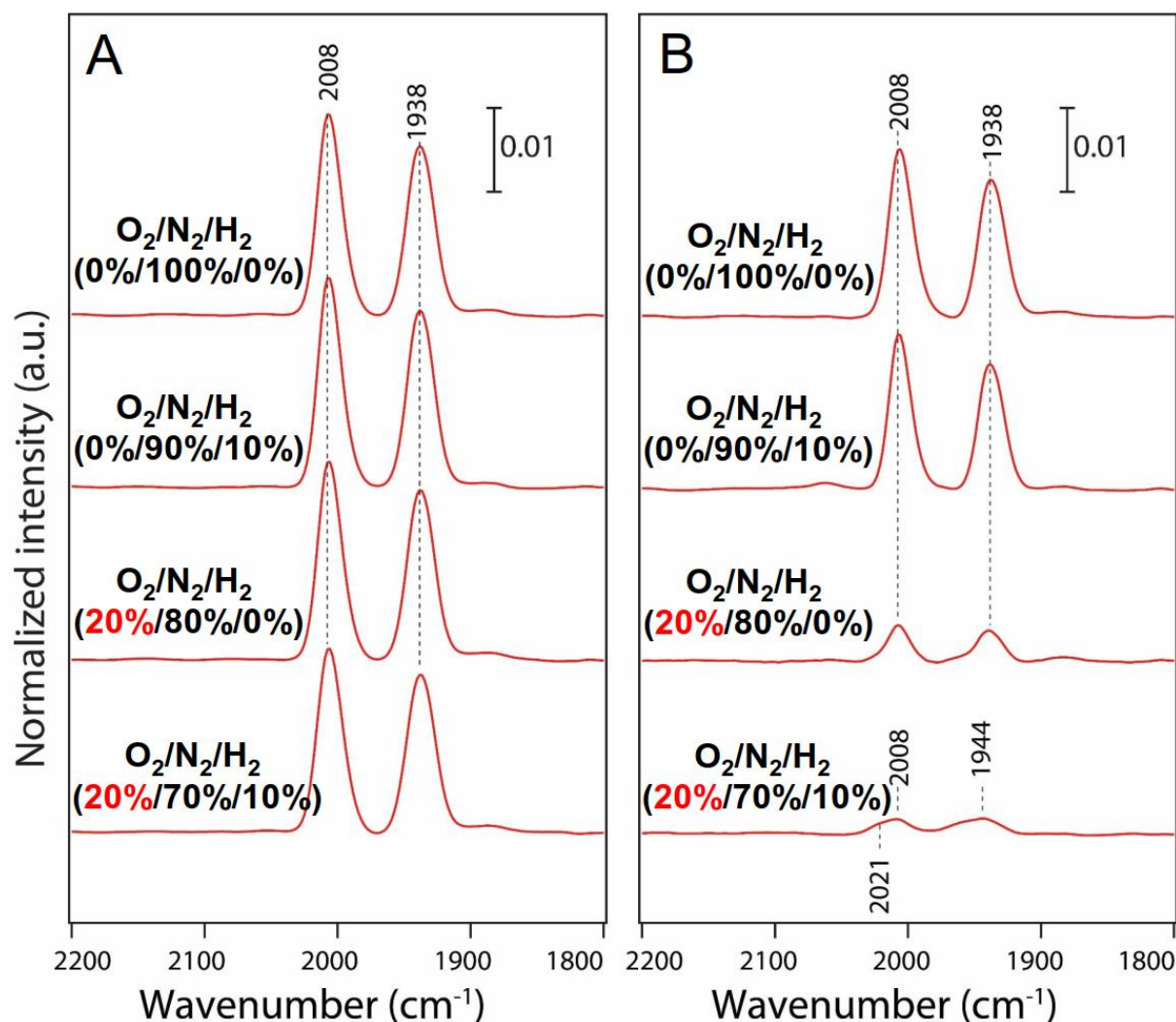


**Fig. 28. IR spectroscopic analysis of  $\text{O}_2$ -inactivation on [Fe]-hydrogenase (112).** (A) [Fe]-hydrogenase was incubated at 40 °C for 1 hour in the absence of substrates. (B) [Fe]-hydrogenase was incubated at 40 °C for 1 hour in the presence of methylene- $\text{H}_4\text{MPT}$ . The conditions of gas phase were described in the figure. This figure is modified from Ref (112).

Further, EPR spectroscopy was used to probe the Fe state after  $\text{O}_2$ -inactivation of [Fe]-hydrogenase. The low-spin Fe (II) of FeGP cofactor in [Fe]-hydrogenase is EPR silent. When we used the  $\text{O}_2$ -inactivated sample for measurements, only a weak EPR signal of high-spin Fe(III) at  $g=4.3$  could be observed. The spin concentration was less than



7% of the total [Fe]-hydrogenase (Fig. 29). Additionally, a much weaker signal of low-spin Fe(III) products could be obtained at  $g=2$ . Thus, no clear oxidation of Fe(II) to Fe(III) was observed during  $O_2$ -inactivation of [Fe]-hydrogenase, which suggested that  $O_2$  might not be reduced by direct binding on Fe site.

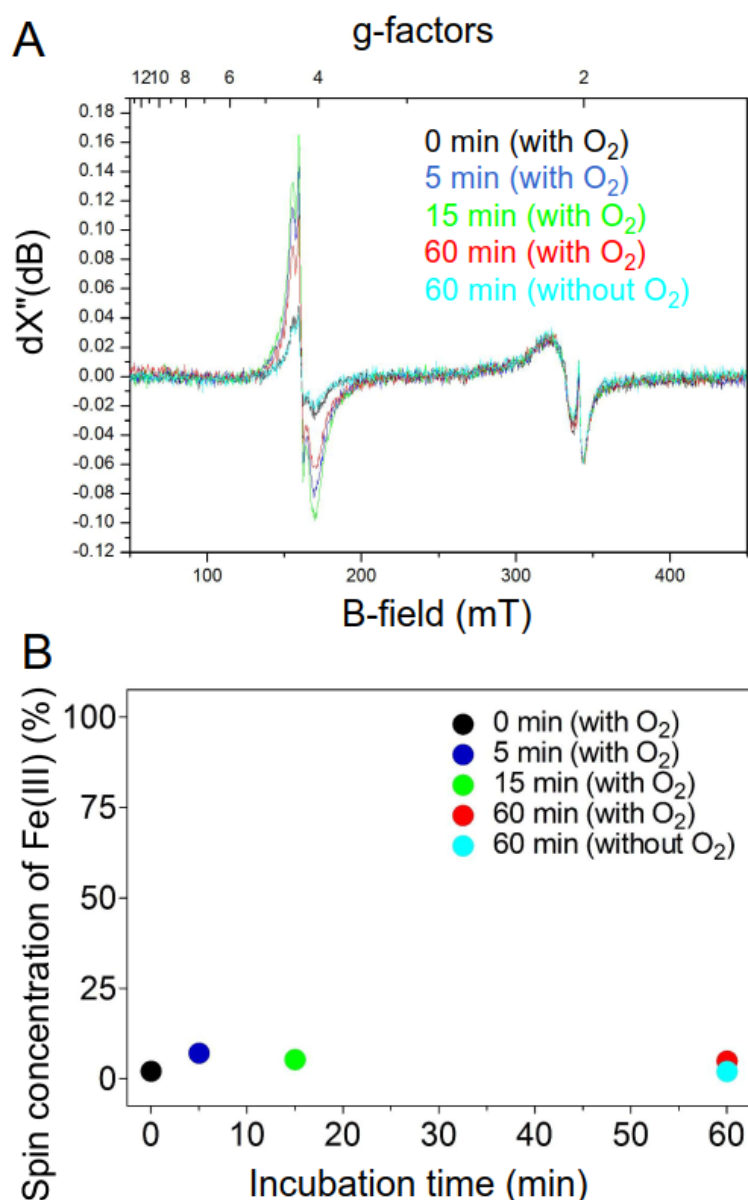


**Fig. 29. X-band EPR spectra (9.64 GHz) of  $O_2$ -inactivated [Fe]-hydrogenase (112).**

(A) X-band EPR spectra. Samples for measurements containing 0.4-mM [Fe]-hydrogenase and 0.1-mM methylene- $H_4$ MPT were incubated at 40 °C under the gas phase  $N_2/O_2/H_2$  (70%/20%/10%) for 0, 5, 15 and 60 min. All samples were dissolved in 120-mM potassium phosphate buffer pH 6.0 with 1-mM EDTA. The spectra were recorded at 10K. (B) Spin concentration of the high-spin Fe(III) species (characteristic sharp signal at  $g=4.3/160$  mT) upon  $O_2$ -inactivation of [Fe]-hydrogenase in the presence of 0.1-mM methylene- $H_4$ MPT. This figure is obtained from Ref (112).

### 2.2.4 The proposed iron-hydride intermediate for O<sub>2</sub> reduction to H<sub>2</sub>O<sub>2</sub>

As experimental data presented above, O<sub>2</sub> is reduced to H<sub>2</sub>O<sub>2</sub> only during the turn over condition of [Fe]-hydrogenase. The formation of H<sub>2</sub>O<sub>2</sub> from the O<sub>2</sub> requires two protons and two electrons. Thus, the only available reductant of the catalytic cycle is a kind of hydride-like intermediate. Based on the proposal catalytic cycle of [Fe]-hydrogenase, the most plausible one is the iron-hydride (Fe-H) intermediate (in the step 4 of Fig.20). However, we cannot exclude Fe-H<sub>2</sub> intermediate (in step 3 of Fig.20) as alternative reductant. Although the existence of iron-hydride (Fe-H) intermediate has been predicted by previous DFT calculations (94) and several experiments by using model compounds (97, 113, 114), its existence has not been experimentally proven.

Ruthenium (Ru) complexes can capture H<sub>2</sub> at the Ru site and heterolytically cleave it into one hydride and one proton (115) and can catalyze hydrogenation of polar molecules by transfer the hydride and proton (115). Based on the mechanism of the Ru-complex catalyzed reactions (Fig. 30A), reduction of O<sub>2</sub> to H<sub>2</sub>O<sub>2</sub> using Fe-H might be plausible. O<sub>2</sub> might be polarized at the active-center of the [Fe]-hydrogenase (in closed form), because the positively charged imidazolidine ring of methenyl-H<sub>4</sub>MPT<sup>+</sup> and polar residues in its surroundings might provide such conditions (92). The polarized O<sub>2</sub> molecule might be bound between the Fe-H and protonated 2-OH group on pyridinol of the FeGP cofactor, in which the Fe-H could provide the hydride and the 2-OH could provide the proton to react with O<sub>2</sub> to form H<sub>2</sub>O<sub>2</sub> (Fig. 30B). The H<sub>2</sub>O<sub>2</sub> produced could independently attack the open site of the Fe (97) and decompose the FeGP cofactor with a cascade of unknown reactions (112).



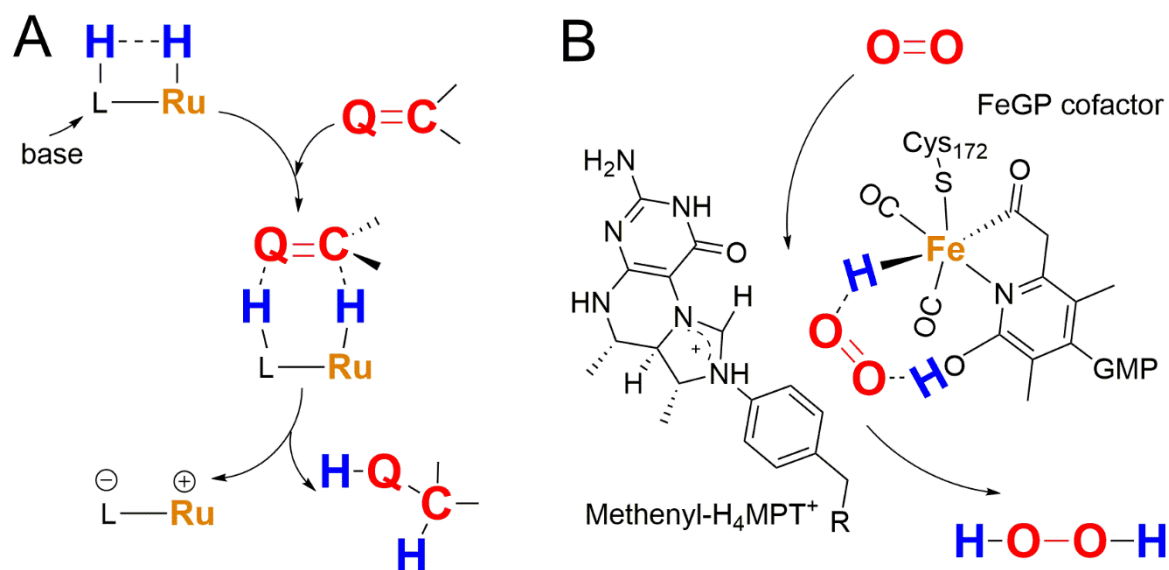


**Fig. 30. Hydrogenation of polar molecules on metal-hydride.** (A) Ru-complex catalyzing hydrogenation of the polar molecule (115) (This figure is modified from Scheme17 in Ref (115)). Q means oxygen in aldehydes or ketones. (B) The proposed mechanism of the reduction of O<sub>2</sub> to H<sub>2</sub>O<sub>2</sub> by the reaction with Fe-H intermediate during the catalytic cycle of [Fe]-hydrogenase (112). This figure is modified from Ref (112).

## 2.3 Protection-regulation mechanism of hexameric [Fe]-hydrogenase

### 2.3.1 The crystal structure of [Fe]-hydrogenase (*M. marburgensis*) in hexamer

Most of the biochemical studies of [Fe]-hydrogenase was performed using the native enzyme purified from *M. marburgensis*. However, in the previous crystallographic study of the [Fe]-hydrogenase holoenzyme, the reconstituted [Fe]-hydrogenase from *M. jannaschii* was used because the crystals of [Fe]-hydrogenase directly purified from *M. marburgensis* (mHmd) was hampered by twining of the crystals. So far, the only structure of mHmd is that inhibited by isocyanides. To study structure and function relationship of [Fe]-hydrogenase, the structure of mHmd in the native form is required. We finally obtained an untwined crystal of [Fe]-hydrogenase purified from *M. marburgensis* that diffracted at 2.6-Å resolution (Table. 3). Unlike previously reported dimeric form of reconstituted [Fe]-hydrogenase from *M. jannaschii* (jHmd) (Fig. 31A) (4, 73, 88, 89), the crystal structure of mHmd indicated a hexameric organization (116). This hexamer is consist of three indentical dimers (Fig. 31B). The hexameric mHmd is also in an open form like jHmd (4, 73, 88, 89). The N-terminal domains of mHmd (1-252) and jHmd (1-251) were superposable with a root mean square deviations (RMSD) of 0.36 Å for 202 Cα (116). Each dimer-dimer interface buries an area of ca. 2100 Å<sup>2</sup>, indicating a rather weak but biologically relevant interaction (116), which was supported by quantitative contact analysis (117). Different from the dimeric jHmd, the hexameric mHmd has a peripheral loop (183-196) located in the N-terminal domains (116), which was unfolded from the protein core and intruded to the active-site cleft of the neighboring dimer (Fig. 31BD) (116). Further comparison between the active centers in dimeric jHmd and hexameric mHmd, clearly show that the Asp189 of the loop bound to the Fe site of the FeGP cofactor via its carboxy-oxygen of the side chain. The Asp189 binding position is same as the water-binding site in dimeric jHmd at a 2.3 Å distance (Fig. 31CD). The open Fe site was occupied by Asp189, which indicates that the hexameric mHmd was in an inactive resting-form.

**Table 3. X-ray analysis statistics of intact [Fe]-hydrogenase (*M. marburgensis*) (116).**

[Fe]-hydrogenase from <i>M. marburgensis</i>	
<b>Data collection</b>	
Wavelength (Å)	0.9798
Space group	<i>P</i> 6 <sub>3</sub> 22
Resolution (Å)	47.50 – 2.60 (2.74 – 2.60)
Cell dimensions	
a, b, c (Å)	144.1, 144.1, 95.1
$\alpha$ , $\beta$ , $\gamma$ (°)	90.0, 90.0, 120.0
R <sub>merge</sub> (%) <sup>a</sup>	31.1 (91.4)
R <sub>pim</sub> (%) <sup>a</sup>	8.5 (24.4)
CC <sub>1/2</sub> <sup>a</sup>	98.9 (44.1)
I/ $\sigma$ <sub>I</sub> <sup>a</sup>	9.2 (3.4)
Completeness (%) <sup>a</sup>	99.9 (99.7)
Redundancy <sup>a</sup>	14.6 (15.0)
Number of unique reflections	18373 (2608)
<b>Refinement</b>	
Resolution (Å)	25.84 – 2.60
Number of reflections	18328
R <sub>work</sub> /R <sub>free</sub> <sup>b</sup> (%)	18.8/23.5
Number of atoms	
Protein	2644
Ligands/ions	98
Solvent	57
Mean B-value (Å <sup>2</sup> )	37.3
Molprobability clash score, all atoms	2.4 (100 <sup>th</sup> percentile)
Ramachandran plot	
Favoured regions (%)	95.3
Outlier regions (%)	0
rmsd <sup>c</sup> bond lengths (Å)	0.008
rmsd <sup>c</sup> bond angles (°)	1.03
<b>PDB code</b>	6GGU

<sup>a</sup> Values for the highest resolution shell are within parentheses. <sup>b</sup> R<sub>free</sub> was calculated as R<sub>work</sub> for 5% of the reflections that were not included in the refinement. <sup>c</sup> rmsd, root mean square deviation. This table is obtained from Ref (116).

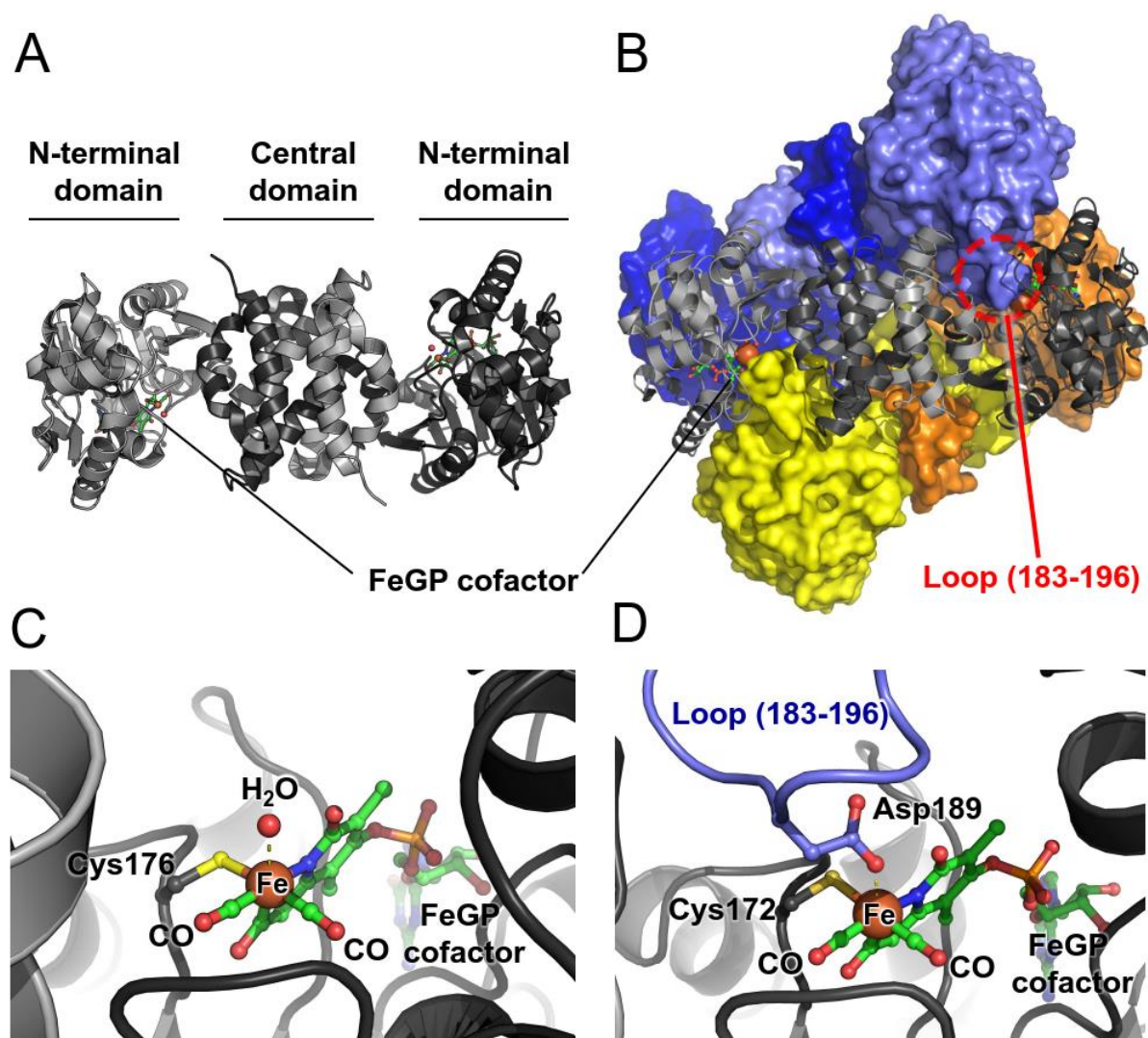


**Fig. 31. Comparison between the structures of jHmd and mHmd (116).** (A) The dimeric jHmd in the open form (PDB code: 3F47 (4)). (B) The hexameric mHmd in the open form (PDB code: 6GGU (116)). In the hexameric form, each active-site cleft of the dimer was blocked by the oligomerization loop (marked with a red dash circle) of another dimer of the hexamer. (C) The active sites of dimeric jHmd, in which a water molecule occupied the predicted H<sub>2</sub>-binding site of Fe (shown in a brown ball). (D) The active sites of hexameric mHmd, in which Asp189-O of the oligomerization loop (light blue) from another dimer of the hexamer occupied the H<sub>2</sub>-binding site of Fe like the water molecule in panel C. The FeGP cofactor was shown in sticks and balls, in which the carbon, nitrogen, oxygen, phosphorous, sulfur and Fe atoms are depicted in green, blue, red, orange, yellow and brown, respectively. In dimeric jHmd in panel C and hexameric mHmd in panel D, the distances of H<sub>2</sub>O-Fe and Asp189-O-Fe were ~ 2.3 Å. This figure is modified from Ref (116).

Since such oligomerization loop is only conserved in the genus *Methanothermobacter* (Fig. S6), we predict that jHmd and other Hmds cannot form the hexameric conformation (116).

### 2.3.2 Dissociation of Hexameric assembly

Since the loop blocked the active site of hexameric mHmd, it is in a resting state. However, under Ni-limiting conditions, the mHmd should be active *in vivo*; it means the hexameric assembly can be dissociated into active dimers in certain conditions. From the structure information, we know that isocyanides-inhibited mHmd is in dimer rather than hexamer, which indicated that isocyanides can dissociate the hexameric mHmd by binding on the Fe site, where Asp189 of the loop binds. To test the effect of isocyanides (i.e. Toluenesulfonylmethyl isocyanide, TosMIC) on the oligomeric states of mHmd in solution, we used size-exclusion chromatography. We also tested jHmd for comparison because jHmd is in dimer in the crystals and does not have the oligomerization loop as observed in mHmd. The data shown in Fig. 32A clearly showed that the elution time of mHmd shifted substantially by addition of TosMIC in contrast to the case of its absence. On the contrary, the elution time of jHmd did not change in the absence or presence of TosMIC. Although the sizes of protein at the elution times was not exactly fit to the hexameric and dimeric mHmd, the clear change of the elution time strongly supported that hexameric mHmd can be dissociated upon binding of the inhibitor.

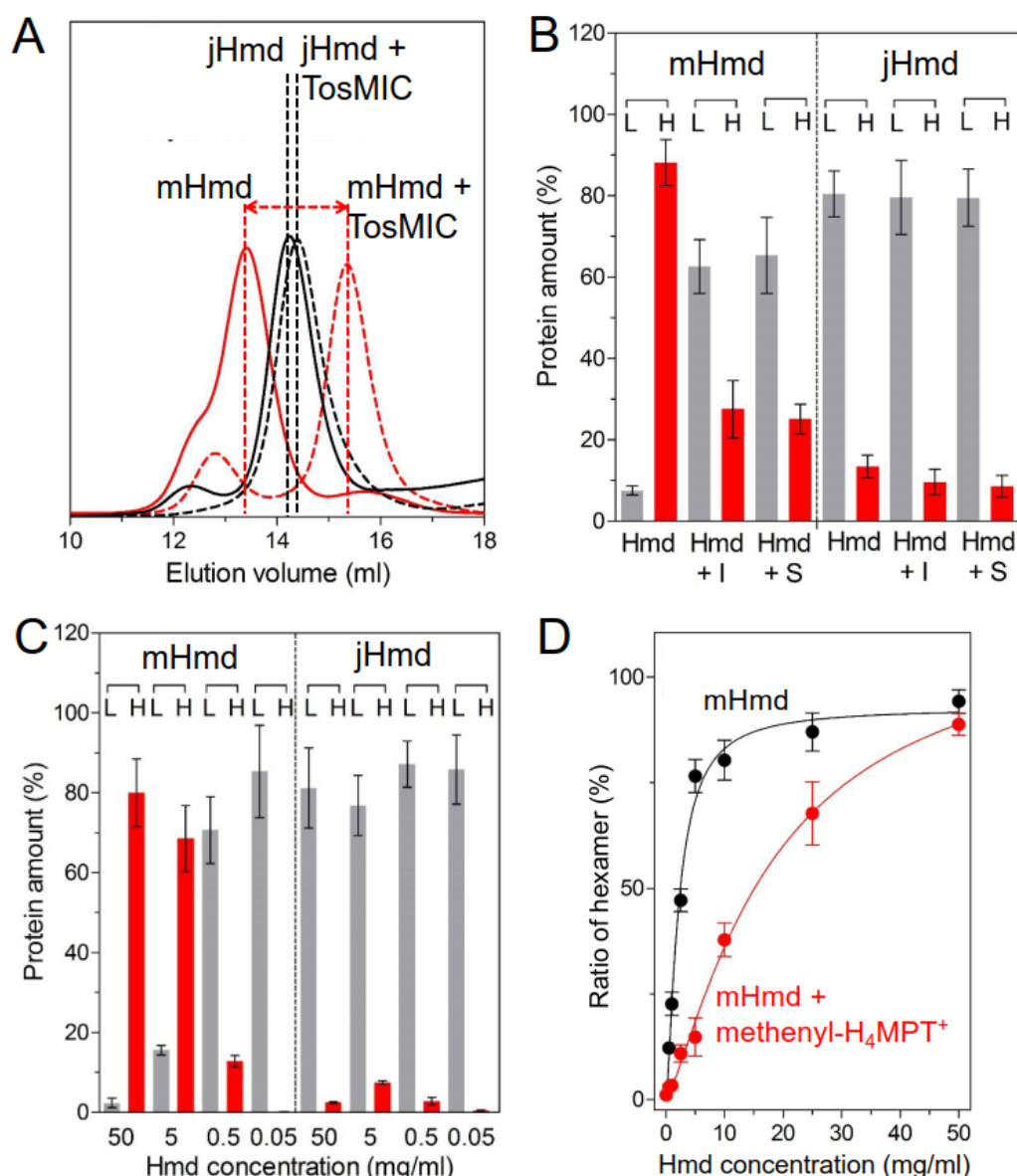


**Fig. 32. Dissociation of the hexameric assembly upon inhibitors, substrates and protein concentrations (116).** (A) Size-exclusion chromatography. Sample: 6-mg/ml mHmd or jHmd (with or without 0.5-mM TosMIC). (B) Ultrafiltration. Sample: 6-mg/ml mHmd or jHmd (with or without 0.5-mM TosMIC/methenyl-H<sub>4</sub>MPT<sup>+</sup>). I: TosMIC. S: methenyl-H<sub>4</sub>MPT<sup>+</sup>. The protein was fractionated by 100-kDa ultrafilter. L: protein size smaller than 100 kDa. H: protein size larger than 100-kDa. (C) Protein-concentration dependent hexamer-to-dimer equilibrium was determined by 100-kDa ultrafiltration. (D) The apparent  $K_d$  of hexamer-to-dimer equilibrium in the absence (black closed circle) and presence (red closed circle) of methenyl-H<sub>4</sub>MPT<sup>+</sup>. The fraction that cannot go through the 100-kDa ultrafilter considered as the hexameric form. All experiments were done under yellow light and anoxic gas phase. This figure is modified from Ref (116).

To further confirm this conclusion, we used ultrafiltration. Molecular masses of hexameric and dimeric mHmd are 228 kDa and 76 kDa, respectively. We used a 100-kDa filter to separate hexameric and dimeric mHmd. The data shown in Fig. 32B clearly indicated that mHmd in the presence of inhibitor (TosMIC) or substrate (methenyl-H<sub>4</sub>MPT<sup>+</sup>), the majority of mHmd went through the 100-kDa filter which indicated that the hexamer dissociated into protein size less than 100-kDa form, namely dimer. Additionally, we found that the protein concentration also affected the hexameric assembly. As shown in Fig. 32C, the size of mHmd decreased related to the decrease of the protein concentrations. Instead, the size of jHmd (dimer) was constant independent on the protein concentrations. This finding indicated that the size of mHmd is in a protein-concentration dependent hexamer-to-dimer equilibrium. The apparent  $K_d$  for the hexamer-to-dimer equilibrium was measured in the absence ( $2.2 \pm 0.1$  mg/ml) and presence ( $18 \pm 3$  mg/ml) of substrate (methenyl-H<sub>4</sub>MPT<sup>+</sup>) (Fig. 32D). This figure is modified from Ref (116).

### 2.3.3 Hexameric [Fe]-hydrogenase is resistant to light and oxidative stresses

Recently, Shomura et al. reported the structure of a NAD<sup>+</sup>-reducing soluble [NiFe] hydrogenase. In the oxidized enzyme structure, the carboxy group of Glu32 coordinated to Ni, which was proposed to protect the [NiFe] active site (118). In the reduced state, Glu32 dissociated from the Ni site and the enzyme is activated. In the case of hexameric mHmd, Asp189 on the oligomerization loop occupied the open site of the Fe; Asp189 blocked the Fe active site like the case of Glu32 in the NAD<sup>+</sup>-reducing soluble [NiFe] hydrogenase (118). We assumed that the Fe active site of Hmd is protected by the coordination with Asp189. To test this hypothesis, we measured the stability of hexameric mHmd under light treatments and oxidative stresses (O<sub>2</sub> and H<sub>2</sub>O<sub>2</sub>). We used the dimeric jHmd as the control. mHmd at the protein concentration of 50 mg/ml, which is mainly in the hexameric form, was stable under light treatment. At lower protein concentration of mHmd (0.05 mg/ml), which was mainly in dimeric form, almost lost full enzyme activity within 60 min (Fig. 33A). In the case of dimeric jHmd (Fig. 33B), the enzyme activity quickly lost completely within 60 min independent on the protein concentration. These data indicated that the hexameric Hmd is stabilized against the light treatments most probably by binding of Asp189 from the oligomerization loop.

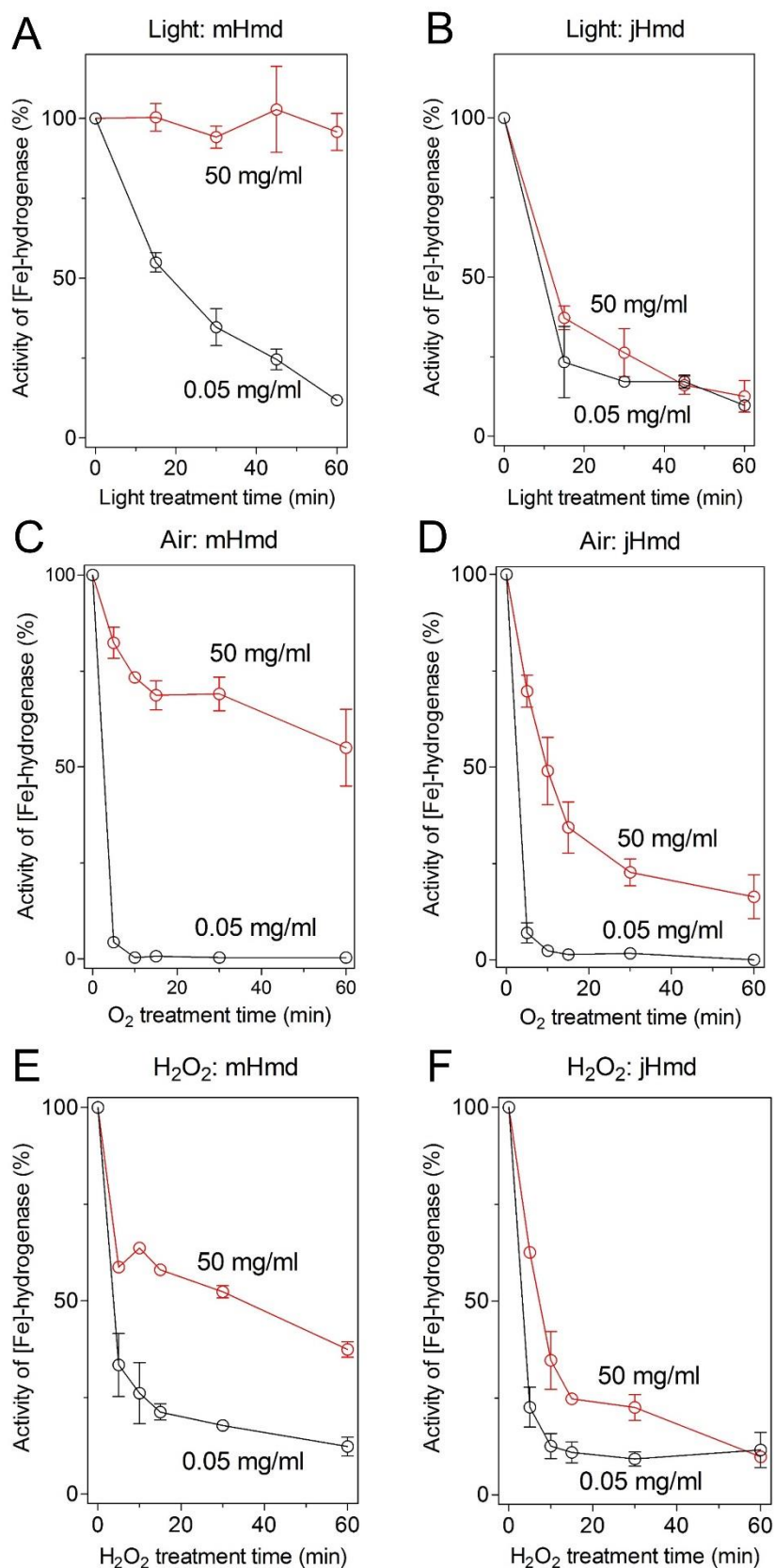


**Fig. 33. Comparison of stability between mHmd and jHmd under light and oxidative stresses (116).** Light treatments of mHmd (A) and jHmd (B) under 100% N<sub>2</sub> on ice. O<sub>2</sub> treatments of mHmd (C) and jHmd (D) at 18 °C under air in the presence of



0.5-mM methylene-H<sub>4</sub>MPT. H<sub>2</sub>O<sub>2</sub> treatments of mHmd (**E**) and jHmd (**F**) at 18 °C under 100% N<sub>2</sub>. H<sub>2</sub>O<sub>2</sub> was added to the enzyme solutions (◐, 130-μM; ○, 0.13-μM). This figure is modified from Ref (116).

We also tested the stability of mHmd under oxidative stresses. The mHmd at the protein concentration of 50 mg/ml, which was mainly in hexameric form, was more stable against air and H<sub>2</sub>O<sub>2</sub> than that of the dimeric form at 0.05 mg/ml (Fig. 33CE). The dimeric jHmd lost the enzyme activity by the oxidative stresses in both high and low protein concentrations. jHmd inactivation rate was somewhat decreased at the higher concentration of enzyme (Fig. 33DF). These results suggested that hexamerization (blocking the active site Fe) could stabilize [Fe]-hydrogenase against oxidative stresses by air and H<sub>2</sub>O<sub>2</sub>.

### 2.3.4 The strategy of [Fe]-hydrogenase against light and oxidative stresses

Data of crystallography, biophysics experiments and stability tests suggested that mHmd can have two conformations (dimeric and hexameric forms). The dimer/hexamer equilibrium is affected by protein concentrations and absence/presence of substrates and inhibitors. Under light and oxidative stresses, the hexameric form is more tolerant than the dimeric form. mHmd evolved to be protected by the hexamerization as an energetically cheap strategy to survive under toxic natural environments. Under Ni-limiting conditions, in the cell, where the concentration of mHmd is estimated to ~ 4mg/ml (116), where mHmd is in the equilibrium between dimer and hexamer. The increase of available substrates makes the conformations towards the unprotected but active dimer. In the case of facing to environmental stresses, where presumably lower concentration of the substrate, mHmd takes the protected but inactive hexamer to survive in nature (Fig. 34). *In vivo*, the activity and the stability could be regulated by such kind of conformational changes. Thus, we considered that reversible dimer-to-hexamer exchange is a regulation and protection mechanism of [Fe]-hydrogenase as a repose to the toxic outside conditions.

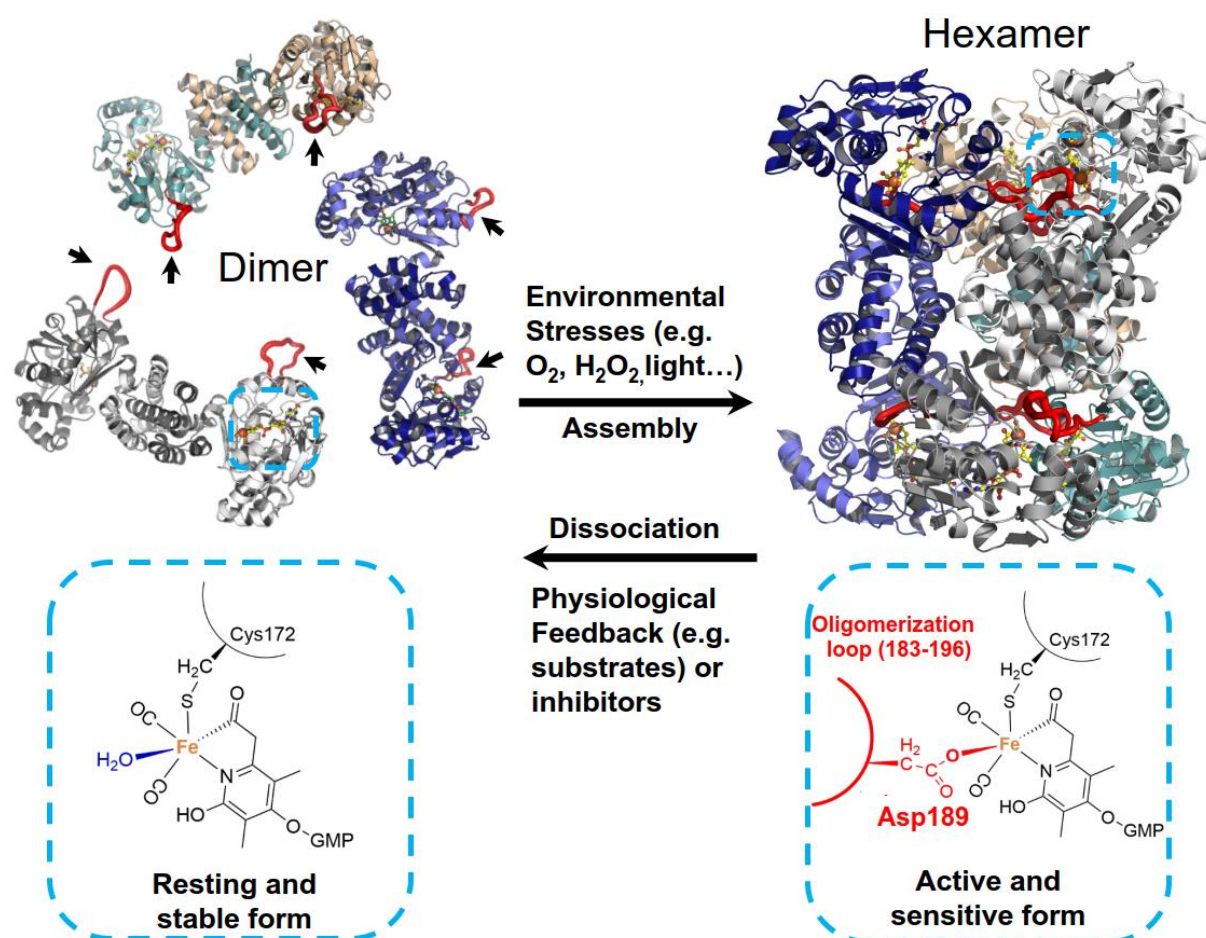


**Fig. 34. A proposed dimer-to-hexamer based protection-regulation mechanism of mHmd (116).** In the presence of higher concentration substrates, mHmd shifts to the dimeric form to conduct physiological functions. When the organism faces environmental stresses, the substrate concentration decreases and mHmd shifts to hexameric form for protection of the Fe center. The oligomerization loop (183-196) is indicated by black arrow and highlighted by red color.

### 3. Discussion

Specific discussion of the studies was already described in each chapter. Here, I would like to provide an overall discussion. In this study, I focused on the catalytic mechanism of [Fe]-hydrogenase. We used crystallography, spectroscopic analyses and QM/MM computations to propose the steps of the catalytic cycle. Additionally, I analyzed the sensitivity of [Fe]-hydrogenase against  $O_2$ . From the results, we found that  $O_2$  could be reduced to  $H_2O_2$  most probably with the iron-hydride intermediate during the [Fe]-hydrogenase catalyzed reaction (112), which provided the experimental evidence that the existence of iron-hydride intermediate in the reaction cycle as predicted by computations (94, 96). Furthermore, based on the crystal structure and biophysical analyses of [Fe]-hydrogenase from *M. marburgensis*, this enzyme is in an equilibrium of dimer and hexamer. In the hexameric form, the Fe active site is protected by coordination of the Asp189 carboxy oxygen. This finding strongly supported that the open coordination site of the Fe site is crucial for the enzymatic activity as shown by the crystal structure of the closed active-form of [Fe]-hydrogenase/methenyl- $H_4MPT^+$  complex.

For a long time in the past, we could not understand why the proton exchange (H/D) of [Fe]-hydrogenase could not be observed in the absence of methenyl- $H_4MPT^+$ . To explain this interesting feature of [Fe]-hydrogenase, it was proposed that the carbocationic C14a of methenyl- $H_4MPT^+$  functioned as the  $H_2$ -activation site (77, 92). In this work, we revealed the structures of [Fe]-hydrogenase in complex with methenyl- $H_4MPT^+$ . The binding of the substrate to the enzyme induced the closed form, which uncovered the mystery that methenyl- $H_4MPT$  dependent proton-exchange (H/D) reactions. In the absence of methenyl- $H_4MPT^+$ , the Fe site of FeGP cofactor was a saturated hexa-coordination in the open form, where a water molecule occupied the  $H_2$ -binding position of the Fe site, which could inhibit the exchange activity. The presence of methenyl- $H_4MPT^+$  triggered the closure of the active-site cleft, which resulted in the removal of the water ligand on the Fe site due to the limited space of the closed active sites. The generated unsaturated penta-coordinated Fe site harbors one empty coordination site for  $H_2$  binding. In the closed form, as QM/MM computations shown in Fig.19,  $H_2$  could be captured, activated and cleaved by the Fe site easily. Thus, proton exchange (H/D) could be observed in the presence of methenyl- $H_4MPT^+$ . The closed structure of [Fe]-hydrogenase clearly indicated that

C14a of methenyl-H<sub>4</sub>MPT<sup>+</sup> is not carbocationic in this structure. This structural work suggested that methenyl-H<sub>4</sub>MPT<sup>+</sup> should have other functions rather than just acted as the hydride acceptor. For example, methenyl-H<sub>4</sub>MPT<sup>+</sup> might tune the Fe site by some interactions between the FeGP cofactor, which makes the FeGP cofactor more favorable for H<sub>2</sub> binding/activation. The distorted imidazoline of methenyl-H<sub>4</sub>MPT<sup>+</sup> might have some effect although I cannot provide any evidence in this moment.

Moreover, the 1.06 Å-resolution atomic structure of closed [Fe]-hydrogenase provided the first high-resolution picture of the FeGP cofactor bound on protein in its activated state. Now, we confidently say that Fe site was coordinated with two CO ligand, one acyl-C, one pyridinol-N and one Cys-S. As many mimic compounds of FeGP cofactor is reported (99, 114), the exact structure of the activated FeGP cofactor should be of important for chemists. We are also collaborating with the group of Prof. Dr. Xile Hu (EPFL) on metal-containing mimic cofactor for the semi-synthesized enzymes. We have recently established the semisynthetic [Mn]-hydrogenase using Mn-containing mimics and the jHmd apoenzyme (unpublished data). The semisynthetic [Mn]-hydrogenase showed the potential of higher H<sub>2</sub>-activation activity than the semisynthetic [Fe]-hydrogenase.

QM/MM computations based on the crystal structure of closed-active [Fe]-hydrogenase/methenyl-H<sub>4</sub>MPT<sup>+</sup> complex could provide more accurate predictions on possible steps in its catalytic cycle rather than basing on previous open-resting [Fe]-hydrogenase structure. This gave us important hints to more detailed and more deep understand of the reaction mechanism of [Fe]-hydrogenase. For example, the states of Fe-H<sub>2</sub>/Fe-H state could help to understand the action of H<sub>2</sub>-activation on the metal. The study using new mimic compounds might provide further evidence of new catalytic intermediates involved in the catalytic cycle of [Fe]-hydrogenase as shown in Fig. 20. Now, we are collaborating with the group of Dr. Ingo Zebger (Technische Universität Berlin) and Dr. Sven Stripp (Freie Universität Berlin) to probe the Fe-H<sub>2</sub>/Fe-H intermediates using resonance Raman and ATR-FTIR spectroscopy.

This study indicated that O<sub>2</sub> could react with the reductant like Fe-H at the active center to produce H<sub>2</sub>O<sub>2</sub>. The experimental data (Fig. 23-24 and Table. S2) showed that “O” and “H” of H<sub>2</sub>O<sub>2</sub> originated from O<sub>2</sub> gas and reducing substrates (methylene-H<sub>4</sub>MPT

and methenyl- $\text{H}_4\text{MPT}^+/\text{H}_2$ ) during the turnover process of [Fe]-hydrogenase, respectively. As proposed in Fig. 28, in the system of [Fe]-hydrogenase/reducing substrates,  $\text{O}_2$  could be polarized and obtained  $\text{H}^-$  from Fe-H intermediate and  $\text{H}^+$  from the 2-OH on pyridinol of the FeGP cofactor to be reduced to  $\text{H}_2\text{O}_2$ . Based on this finding, I am tending to speculate similar hydride-transfer reactions to some unsaturated compounds, e.g. formaldehyde ( $\text{HCHO}$ ), ethylene ( $\text{C}_2\text{H}_4$ ), acetylene ( $\text{C}_2\text{H}_2$ ) etc. In the case of  $\text{HCHO}$ , methanol ( $\text{CH}_3\text{OH}$ ) will be produced by the [Fe]-hydrogenase/reducing-substrates system. This would be quite interesting that the [Fe]-hydrogenase/reducing-substrates system could work as the “hydrogenation factory”.

The finding of the hexameric structure of [Fe]-hydrogenase from *M. marburgensis* gave us another interesting hint (116). We found that in the hexameric form, the oligomerization loop (183-196) of one dimer of the hexamer inserted into the active-site cleft of nearby dimer, Asp189 on this loop blocked the  $\text{H}_2$ -binding site of the Fe site via Asp-O-Fe interaction (116). As the experimental data shown in Fig. 30, [Fe]-hydrogenase from *M. marburgensis* could perform the assembly and dissociation of hexamer depended on available concentrations of enzyme and reaction substrates. Moreover, the hexameric form could protect the [Fe]-hydrogenase against the light and oxidative stresses from the outside environments (Fig. 34). This finding not only supported that FeGP cofactor was the catalytic center of the [Fe]-hydrogenase, but also exhibited a new protection-regulation mechanism of [Fe]-hydrogenase for it to survive in nature. This finding also provided the example of a result of the structure-to-function strategy.

In conclusions, all findings of this study contributed to the catalytic mechanism of [Fe]-hydrogenase. I believe that the detailed study of  $\text{H}_2$ -based hydrogenation reaction will provide a strong basis for design new synthetic and plastic catalysts used for hydrogenation of new substrates with  $\text{H}_2$ .

## 4. Materials and methods

### 4.1 Materials

#### 4.1.1 Chemicals

Tetrahydromethanopterin (H<sub>4</sub>MPT) and methenyl-H<sub>4</sub>MPT<sup>+</sup> were purified from *M. marburgensis* cells in the lab as described previously (72). Methylene-H<sub>4</sub>MPT was synthesized from H<sub>4</sub>MPT by reaction with formaldehyde (72). The Amplex® Red Hydrogen Peroxide/Peroxidase Assay Kit was purchased from Thermo Fisher Scientific (Dreieich, Germany). Catalase, superoxide dismutase and other chemicals were purchased from Sigma-Aldrich (Taufkirchen, Germany).

#### 4.1.2 Strains

*M. marburgensis* (DSM 2133) was purchased from the Deutsche Sammlung von Mikroorganismen und Zellkulturen (DSMZ). *Escherichia coli* BL21(DE3) was kept in AG Shima (Max Planck Institute for Terrestrial Microbiology, Marburg, Germany).

#### 4.1.3 Media

LB-medium: 10-g/L tryptone, 5-g/L yeast extract and 10-g/L NaCl. TP-medium: 20-g/L tryptone, 15-g/L yeast extract, 8-g/L NaCl, 2-g/L Na<sub>2</sub>HPO<sub>4</sub> and 1-g KH<sub>2</sub>PO<sub>4</sub>. The media were autoclaved at 121 °C for 20 mins.

The growth medium for *M. marburgensis*: 2.12-g/L NH<sub>4</sub>Cl, 6.8-g/L KH<sub>2</sub>PO<sub>4</sub>, 2.544-g/L Na<sub>2</sub>CO<sub>3</sub>, 1-ml trace element solution (1000X) and 0.3-mL resazurin (0.2%).

Trace element solution (1000X) for *M. marburgensis*: 90-g Nitrilotriacetic acid, 40-g MgCl<sub>2</sub>·6H<sub>2</sub>O, 10-g FeCl<sub>2</sub>·6H<sub>2</sub>O, 0.2-g CoCl<sub>2</sub>·6H<sub>2</sub>O, 1.2-g NiCl<sub>2</sub>·6H<sub>2</sub>O and 0.2-g Na<sub>2</sub>MoO<sub>4</sub>·2H<sub>2</sub>O.

### 4.2 Methods

#### 4.2.1 Cultivation of *M. marburgensis*

*M. marburgensis* was cultivated with continuous gas flow (1.5 L/min) of H<sub>2</sub>/CO<sub>2</sub>/H<sub>2</sub>S (80%/20%/0.1%) using a synthetic medium as described previously (119). In the pre-cultivation (2-L fermenter), the concentration of Ni was 0.65 µM (the final concentration). Using cells (around 100 to 200 ml) from the pre-cultivation to inoculate to 10-L fermenter in which no more Ni was added in the medium. When OD<sub>600</sub> reached

~7 to 7.5 within ~20 to 24 h, the cells were harvested using the continuous-flow centrifugation. Normally, yield of the cells was ~90 to 110 g in each 10-L fermenter. Cells were frozen in liquid N<sub>2</sub> and stored at -75 °C under 100% N<sub>2</sub>.

#### 4.2.2 Genes synthesis of [Fe]-hydrogenase from *M. aeolicus*

The [Fe]-hydrogenase gene sequence from *M. aeolicus* (NCBI Reference Sequence: WP\_011973735.1) is described below; the codon usage was optimized and synthesized by GenScript (New Jersey, America).

5'-

CATATGAAAGTAGCAATACTAGGAGCTGGGTGTTATAGGTCACACGCTGCATGT  
GGGATTACCAACTTTAGCCGTGCGGCGGAAGTGGCGAACAAAGTGGGCATTCC  
GGAAATCACCATGACCCACAGCACCATTACCATGGGTGCGGAGCTGCTGCACC  
TGGTTGACGAGATCGATGAAGTGGTTGTGAGCGACCCGTGCTTTGCGGAGGAA  
CCGGGTCTGATCATTATCGACGAATTTGATTGCAAAGAGGTGATGGAAGCGCAT  
CTGGCGGGCAAGGCGGAGGATGTGATGCCGGCGATTCTGTATGCGGTTAAGG  
CGAAAGCGAAGGATAGCCCGAAACCGCCGAAGGGCTGCATCCACTTTGTGAAC  
CCGGAAAAAGTTGGTCTGAAGGTGACCAGCGACGATCGTGAGGCGATCGAAGG  
CGCGGACATTGTTATCACCTGGCTGCCGAAGGGTGGCAGCCAGCCGGCGATTA  
TCGAGAAATTCGTGGATGCGATTAAGGAAGGCGCGATCGTTACCCACGCGTGC  
ACCATTCCGACCCCGAAATTCGCGAAGATCTTTAAAGACCTGGGTCTGTGAGGAT  
CTGAACATTGTTAGCTTTACCCGGGTTGCGTGCCGGAGATGAAAGGCCAAGTT  
TACCTGAGCGAAGGTTATGCGAGCGAGGAAGCGGTTGAGAAGCTGTACAAAAT  
TGCGAAGATCAGCCGTGGCACCGCGTTCAAGATGCCGGCGAACCTGATCAGCC  
CGGTGTGCGACATGGGTAGCGCGGTTACCGCGCCGGTGTATGCGGCGATTCT  
GAGCTATCGTGATGCGGTTACCAACATTCTGGGTGCGCCGGCGGACTTTGCGC  
AGATGATGGCGGATGAAGCGATTACCCAAATGCTGGAGCTGATGCGTAACGAA  
GGTATCCAGAACATGGAGAACAACCTGAACCCGGGTGCGCTGACCGGTACCGC  
GGACAGCATGTGCTTCGGTCCGCTGAGCGAACTGCTGCCGGCGAGCCTGAAG  
GTTCTGGAGGAACATAAAAAGTAAGTCGAC-3'

The pET-24b(+) was used as the expression vector, and the gene was inserted into the vector at the *Nde*I and *Sal*I sites. Genes of the mutants (M252A, M252F and M252S) were synthesized using the template of the wild-type [Fe]-hydrogenase gene.

#### 4.2.3 Heterologously production of the apoenzyme of [Fe]-hydrogenase

The apoenzymes of [Fe]-hydrogenase (wild type and mutants) were produced in *E. coli* BL21(DE3). The recombinant *E. coli* was cultivated in the TP medium with 50 µg/mL kanamycin at 37 °C (4, 73). The gene expression was induced by addition of 1-mM isopropyl β-D-thiogalactopyranoside (IPTG) when the optical density at 600 nm was 0.6-0.8. After 4-hours expression, the cells were harvested by centrifugation using Avanti JXN-26 centrifuge with JLA-10.500 rotor (Beckman-Coulter) at 8,000 rpm for 30 min at 4 °C. The cells were stored at -20 °C.

#### 4.2.4 Purification of the apoenzyme of [Fe]-hydrogenase

The cells (~10 g) were re-suspended in 50-mM MOPS/KOH pH 7.0 containing 1-mM Dithiothreitol (DTT). The cells were disrupted by sonication using SONOPULS GM200 (Bandelin) with KE76 tip using 80% power and 50 cycles. Removing the cell debris and the unbroken cells by centrifugation using an Avanti JXN-26 centrifuge with a JA-25.50 rotor (Beckman-Coulter) at 15,000 rpm for 30 min at 4 °C. The proteins were precipitated by adding 2-M (the final concentration) (NH<sub>4</sub>)<sub>2</sub>SO<sub>4</sub> powder to the supernatant followed by incubation on ice for 10 min. The precipitated proteins were removed by centrifugation using an Avanti JXN-26 centrifuge with JA-25.50 rotor (Beckman-Coulter) at 15,000 rpm for 30 min at 4 °C. The supernatant was applied to a Phenyl Sepharose High Performance column (75 ml, GE Healthcare Life Sciences) and eluted with a linear gradient of (NH<sub>4</sub>)<sub>2</sub>SO<sub>4</sub> elution from 2 M to 0 M in 50-mM MOPS/KOH buffer pH 7.0 containing 1-mM DTT (4, 73). Fractions containing the apoenzyme of [Fe]-hydrogenase were pooled and concentrated by using a centrifugation filter (30-kDa) (Millipore). Then the concentrated apoenzyme sample was applied to a HiPrep 16/60 Sephacryl S-200 HR size-exclusion column (120 ml, GE Healthcare Life Sciences) equilibrated with 25-mM Tris/HCl buffer pH 7.5 containing 150-mM NaCl, 5%-glycerol and 2-mM DTT. The size-exclusion chromatography was repeated totally 2 times to increase the purity of the protein. Finally, the purified apoenzyme was concentrated to ~50 mg/mL and stored at -75 °C. Protein concentration determination was performed using Bradford method using the assay solution from Bio-Rad Laboratories and bovine serum albumin (BSA) as the standard.



#### 4.2.5 Purification of [Fe]-hydrogenase from *M. marburgensis*

All purification procedures were performed under strictly anoxic conditions using a Coy Chamber filled with N<sub>2</sub>/H<sub>2</sub> (95%/5%) or in glass vials with rubber stoppers. The *M. marburgensis* cells were disrupted by sonication using SONOPULS GM200 (Bandelin) with VS-70-T tip using 90% power and 50 cycles for 1.5 h (8-min sonication with 7-min pause, repeat 6 times) (119). The samples were centrifuged at 40,000 rpm for 30 min at 4 °C to remove unbroken cells, cell debris and particulate fraction. Taking the supernatant for ammonium sulfate precipitation (60% saturation) and centrifuged at 20,000 rpm for 20 min at 4°C. Taking the supernatant for ammonium sulfate precipitation (90% saturation) and centrifuged at 20,000 rpm for 20 min at 4 °C. The precipitated fraction was dissolved in 50-mM MOPS/KOH buffer pH 7.0 and dialyzed in 50-mM citric acid/NaOH buffer pH 5.0 at 8 °C for 24 h to remove ammonium sulfate. Taking dialyzed sample solution for centrifugation (20,000 rpm for 20 min at 4 °C). Kept the supernatant and applied to Source 30Q column as described previously (119). The protein of [Fe]-hydrogenase was eluted when the conductivity of the elution buffer reached from 33% to 37%. Pooling all [Fe]-hydrogenase fractions and adjusting the pH of the protein solution to 7 using 1-M NaOH and 1-M MOPS/KOH buffer pH 7 quickly to avoid the precipitation of [Fe]-hydrogenase. Then, removing the salts of protein solution using a HiTrap 26/10 desalting column with water as the elution solvent. Finally, the purified protein was concentrated to ~100 mg/ml using a centrifugation filter (30-kDa) and quickly frozen in liquid N<sub>2</sub> and stored at -75 °C.

#### 4.2.6 Extraction of FeGP cofactor from [Fe]-hydrogenase

The FeGP cofactor was extracted from the purified [Fe]-hydrogenase from *M. marburgensis* as previously described (119). The solution used for extraction contains 60% methanol, 1% NH<sub>3</sub>, 1 mM 2-mercaptoethanol and [Fe]-hydrogenase (the final concentration should be less than 5 mg/ml). Incubating the mixture at 40 °C water bath for 15 min. The extraction solution was centrifuged under anoxic gas phase at 4 °C via 10-kDa filter to remove protein fraction. The filtrate containing the extracted cofactor was concentrated by evaporation at 4 °C. When the sample was totally dried, which made thin film; 10 mM (NH<sub>4</sub>)<sub>2</sub>CO<sub>3</sub> buffer pH 9.0 containing 1-mM 2-mercaptoethanol was added to dissolve the FeGP cofactor. The extracted FeGP cofactor solution was frozen in liquid N<sub>2</sub> and stored in liquid N<sub>2</sub>.

#### 4.2.7 Reconstitution of [Fe]-hydrogenase holoenzyme *in vitro*

The [Fe]-hydrogenase holoenzyme was reconstituted under anoxic conditions and low temperature as previously described (4, 119). The mixture containing [Fe]-hydrogenase apoenzyme (57 mg/ml, 1.5 mM) (the final concentration) and the FeGP cofactor (2-mM) (the final concentration) in 50-mM Tris/HCl buffer pH 8.5 was incubated under anoxic gas phase at 8 °C for 15 min. The ratio of [Fe]-hydrogenase apoenzyme and FeGP cofactor was 0.75:1. To remove the unbound FeGP cofactor, the reconstituted solution was washed with the 30-kDa filter using 10-mM MOPS/KOH pH 7.0. The reconstituted [Fe]-hydrogenase holoenzyme was concentrated to ~ 50 mg/ml by the 30-kDa filter. The quality of reconstitution was controlled by enzyme-activity assay and UV-Vis spectroscopy. The samples were frozen in liquid N<sub>2</sub> and stored at -75 °C.

#### 4.2.8 [Fe]-hydrogenase enzyme activity assay

The enzyme activity of [Fe]-hydrogenase was measured as previously described (119). For the hydrogenation of methenyl-H<sub>4</sub>MPT<sup>+</sup> with H<sub>2</sub>, the 1-cm light-pass quartz cuvette containing 680-μl reaction buffer (120-mM potassium phosphate pH 7.5, 1-mM EDTA) was firstly incubated at 40 °C water bath for at least 5 min. The gas phase in the cuvette was 100% H<sub>2</sub>. The concentration of methenyl-H<sub>4</sub>MPT<sup>+</sup> for reaction was 20 μM (final concentration) in the cuvette. The assay was started by injecting 10-μl [Fe]-hydrogenase. The enzyme solution was diluted with the assay buffer before measurement. The change of absorbance from methenyl-H<sub>4</sub>MPT<sup>+</sup> at 336 nm was recorded. For the dehydrogenation of methylene-H<sub>4</sub>MPT, 120-mM potassium phosphate buffer pH 6.0 containing 1-mM EDTA was used. The gas phase in the cuvette was 100% N<sub>2</sub>. The other conditions were the same as the case of the hydrogenation of methenyl-H<sub>4</sub>MPT<sup>+</sup>. The methylene-H<sub>4</sub>MPT concentration for reaction was 20 μM (final concentration) in the cuvette. The specific activity of [Fe]-hydrogenase was calculated using the extinction coefficient of methenyl-H<sub>4</sub>MPT<sup>+</sup> ( $\epsilon_{336 \text{ nm}} = 21.6 \text{ mM}^{-1}\text{cm}^{-1}$ ).

#### 4.2.9 Crystallization

##### (A) [Fe]-hydrogenase from *M. aeolicus* (98)

[Fe]-hydrogenase alone and [Fe]-hydrogenase/methenyl-H<sub>4</sub>MPT<sup>+</sup> complex were crystallized in different conditions. [Fe]-hydrogenase was crystallized on 96-well 2-drop

MRC crystallization plates (Molecular Dimensions, Suffolk, UK) under gas phase 95% $\text{N}_2$ /5% $\text{H}_2$  at 8 °C. The sitting drop vapour diffusion method was used. The crystallization solutions (90  $\mu\text{l}$ ) were filled into the wells of the MRC crystal plates with multi-pipet. The plates were covered by PARAFILM-M (PECINEY PLASTI PACKING, Chicago) and transferred into the anoxic tents. The plates were incubated in the tent without cover film for 1 h and then the plates were covered by the sticky plastic tape (Jena Bioscience). To make them anaerobic states, the plates were further incubated for one week. After removal of the plastic tape, 0.7  $\mu\text{l}$  of 24-mg/ml protein and 0.7  $\mu\text{l}$  of reservoir solution were mixed in the crystallization stages in the plate under yellow light, and incubated under the dark condition. The best crystal in a diamond shape came out within one month. The crystallization reservoir solution is 20% w/v polyethylene glycol 3350, 100-mM tri-sodium citrate pH 4.0 and 200-mM tri-sodium citrate (JBScreen Wizard 3&4 HTS, Jena Bioscience).

Crystallization of [Fe]-hydrogenase/methenyl- $\text{H}_4\text{MPT}^+$  complex was done under gas phase 100% $\text{N}_2$  at room temperature. [Fe]-hydrogenase (50-mg/ml) and 10-mM methenyl- $\text{H}_4\text{MPT}^+$  were mixed in 10-mM MOPS/KOH pH 7.0. The final concentrations of [Fe]-hydrogenase and methenyl- $\text{H}_4\text{MPT}^+$  were 24 mg/ml and 3 mM, respectively. The enzyme/substrate mixture was incubated for 5 min under dark condition and centrifuged using centrifugal filters (0.45  $\mu\text{m}$ ) at 8,000 rpm for 5 min to remove the aggregated proteins and dusts. The crystallization plate with the buffer solutions were prepared as described above. In the initial screen, 0.7- $\mu\text{l}$  of the enzyme/substrate solution was mixed with 0.7  $\mu\text{l}$  of reservoir solution in the crystallization stages on 96-well MRC crystallization plates. The initial small rod shape crystals were obtained from the condition containing 20% w/v polyethylene glycol 3350 and 200-mM sodium thiocyanate (JBScreen Wizard 3&4 HTS, Jena Bioscience). Then, we reproduced the crystals using the same solution purchased from the company. Notably, we cannot reproduce the crystals using the crystallization solution prepared by ourselves. We obtained larger crystals using 24-well Junior Clover plates (Jena Bioscience). The best crystals of the long-rod-shape (Form A) came out within two weeks (sample: reservoir = 2  $\mu\text{l}$ : 2  $\mu\text{l}$ ). Supplementation of 10- $\mu\text{l}$  of 3% w/v 1,5-diaminopentane dihydrochloride to 90- $\mu\text{l}$  reservoir solution, which is the same as the form A, yielded the new shape of the crystals (plate-shape) (Form B) in 10 days (sample: reservoir = 0.7  $\mu\text{l}$ : 0.7  $\mu\text{l}$ ; 96 well-plates).

**(B) O<sub>2</sub>-inactivated [Fe]-hydrogenase from *M. marburgensis* (112)**

To prepare the O<sub>2</sub>-inactivated [Fe]-hydrogenase sample, the mixture containing 120-mM potassium phosphate pH 6.0, 1-mM EDTA, 26-μM (1-mg/ml) [Fe]-hydrogenase and 26-μM methylene-H<sub>4</sub>MPT was incubated under N<sub>2</sub>/O<sub>2</sub>/H<sub>2</sub> (70%/20%/10%) at 40 °C for 1 h under dark condition. The complete inactivation of [Fe]-hydrogenase was confirmed by the enzyme activity assay. The 10 preparations are pooled and concentrated to ~30 mg/ml using a 30-kDa centrifugal filter (Millipore). The O<sub>2</sub>-inactivated [Fe]-hydrogenase was crystallized under 95%/N<sub>2</sub>/5%H<sub>2</sub> at 8 °C using sitting drop vapor diffusion method. In the crystallization stages in the 96-well 2-drop MRC crystallization plates, 0.7 μl of 25-mg/ml protein and 0.7 μl of reservoir are mixed under yellow light and then incubated under dark condition. The best crystal presenting in long-rod shape came out within one month in the crystallization reservoir containing 2-M (NH<sub>4</sub>)<sub>2</sub>SO<sub>4</sub>, 100-mM Tris/HCl pH 7.0 and 200-mM Li<sub>2</sub>SO<sub>4</sub> (JBScreen Wizard 1&2 HTS, Jena Bioscience) under dark condition.

**(C) Intact [Fe]-hydrogenase from *M. marburgensis* (116)**

The [Fe]-hydrogenase from *M. marburgensis* was crystallized under the gas phase 100% N<sub>2</sub> at 20 °C using the sitting drop vapor diffusion method. The 0.7 μl sample containing 30 mg/ml [Fe]-hydrogenase and 2-mM methenyl-H<sub>4</sub>MPT<sup>+</sup> in water was mixed with 0.7-μl reservoir solution on 96-well 2-drop MRC crystallization plates (Molecular Dimensions, Suffolk, UK). The best crystal presenting in long-hexagonal shape came out in the reservoir solution containing 0.1-M MES pH 6.0 and 0.8-M (NH<sub>4</sub>)<sub>2</sub>SO<sub>4</sub> (JCSG Core Suite III, QIAGEN) within 2.5 months under dark condition.

**4.2.10 Structure analysis****(A) [Fe]-hydrogenase from *M. aeolicus* (98)**

The crystals of reconstituted [Fe]-hydrogenase holoenzyme alone (open form) from *M. aeolicus* were put into the cryo-protection solution, which is composed of 20% w/v polyethylene glycol 3350, 100-mM tri-sodium citrate pH 4.0, 200-mM tri-sodium citrate and 10% v/v glycerol (cryo-protectant) at 8 °C in the anaerobic condition (95%N<sub>2</sub>/5%H<sub>2</sub>). After 3-5 seconds, the crystal was picked up and frozen in liquid N<sub>2</sub>. Crystals of Form A and Form B of reconstituted [Fe]-hydrogenase complexed with methylene-H<sub>4</sub>MPT<sup>+</sup> were put into each crystallization reservoir solutions, in which the buffers were supplemented with 20% v/v glycerol. The crystals were picked up and then frozen in liquid N<sub>2</sub> under 100% N<sub>2</sub> condition. The crystals of the reconstituted [Fe]-

hydrogenase holoenzyme without substrate diffracted at 100K on beamline BM30A (French Beamline for Investigation of Proteins) at the European Synchrotron Radiation Facility (ESRF) equipped with an ADSC Q315r CCD detector. The data used for the structure determination of the form A and B crystals were obtained at beamline PXII at the Swiss Light Source (SLS) equipped with a PILATUS 6M. We processed the data with XDS and scaled with SCALA from the CCP4 suite.

The phase problem of the reconstituted [Fe]-hydrogenase from *M. aeolicus* without substrate was solved by molecular replacement with PHASER (120) by using the 2-naphthylisocyanide-inhibited [Fe]-hydrogenase from *M. marburgensis* (PDB code: 4JJF) as template. The structures of Form A and B of [Fe]-hydrogenase complexed with methenyl-H<sub>4</sub>MPT<sup>+</sup> were also solved with PHASER using the structure of the [Fe]-hydrogenase without substrate from *M. aeolicus*. In this case, the N- and C-terminal domains were separately used as the templates because of the predicted conformational changes. The models of the reconstituted [Fe]-hydrogenase without substrate bound and Form B of [Fe]-hydrogenase with methenyl-H<sub>4</sub>MPT<sup>+</sup> were manually built with COOT (121) and refined with BUSTER (122). Considering all atoms except water as anisotropic and the hydrogens in riding position, Form A was refined by Phenix (123). The final models were confirmed using the MolProbity server (<http://molprobity.biochem.duke.edu>) (123). The hydrogens were omitted in the final deposited model.

### **(B) O<sub>2</sub>-inactivated [Fe]-hydrogenase from *M. marburgensis* (112)**

O<sub>2</sub>-inactivated crystals were cryo-protected with 30 % glycerol (v/v) in the crystallization solution in an anaerobic tent (95%N<sub>2</sub>/5%H<sub>2</sub>) by soaking for 3-5 seconds. We measured diffractions at 100 K on beamline X10SA, which is equipped with a PILATUS 6M detector at the Swiss Light Source (Villigen). XDS (124) and SCALA from the CCP4 suite (125) were used for the data were processing and scaling, respectively. The phase problem was solved by molecular replacement using PHASER (126) and the [Fe]-hydrogenase from *M. marburgensis* in complex with 2-naphthylisocyanide (PDB code: 4JJF) as template. The molecular replacement search required to use the N and C-terminal domains independently as the template because the oligomeric state was different from the template. The model was manually constructed with COOT (127) and refined by PHENIX (126). The last refinement steps were performed with hydrogens in riding position. The final model was tested using the MolProbity server

(<http://molprobity.biochem.duke.edu>) (123). The hydrogens were omitted in the final deposited model.

### **(C) Intact [Fe]-hydrogenase from *M. marburgensis* (116)**

Crystals of mHmd were flash-frozen in the anaerobic tent containing 100% N<sub>2</sub> after soaking for 3-5 seconds in 0.1 M MES pH 6.0 and 0.8 M ammonium sulfate supplemented with 30% glycerol. The diffraction experiments were performed at 100K on beamline BM30A at ESRF equipped with an ADSC Q315r CCD detector. We processed the data with XDS (124) and scaled with SCALA from the CCP4 suite (125). The structure was solved with PHASER (126) by molecular replacement using the [Fe]-hydrogenase from *M. marburgensis* bound with 2-naphthylisocyanide (PDB: 4JJF) as template. The model was manually built by COOT (128) and refined with BUSTER (129). The last refinement steps were performed with hydrogens in riding position. The final model was validated by using the MolProbity server (<http://molprobity.biochem.duke.edu>) (123). The hydrogens were omitted in the final deposited model.

## **4.2.11 Infrared spectroscopy**

### **(A) [Fe]-hydrogenase from *M. aeolicus* (98)**

The sample was prepared in two kinds of anoxic buffer: a, 50-mM MES/NaOH pH 6.0; b, 50-mM Tricine/NaOH pH 8.0, which contained 150-mg/ml (4-mM) [Fe]-hydrogenase from *M. aeolicus*. When indicated, 10-mM methenyl-H<sub>4</sub>MPT<sup>+</sup> (final concentration) was supplemented. All sample solutions were prepared under anoxic gas phase (95%N<sub>2</sub>/5%H<sub>2</sub>). All samples were filled in amber-colored 1.5-ml Eppendorf tubes and stored in liquid N<sub>2</sub>.

### **(B) O<sub>2</sub>-inactivated [Fe]-hydrogenase from *M. marburgensis* (112)**

The enzyme was dissolved in two kinds of anoxic buffer: a, 120-mM potassium phosphate pH 6.0 containing 1-mM EDTA; b, 120-mM potassium phosphate pH 7.5 containing 1-mM EDTA. The enzyme concentration in the samples was 130-μM (5-mg/ml), which additionally contained 33-μM methylene-H<sub>4</sub>MPT. In the control, the substrate was omitted. The samples in 5-ml amber vials with rubber stoppers were incubated at 40 °C for 1 h under various gas phase conditions: O<sub>2</sub>/N<sub>2</sub>/H<sub>2</sub> (0%/100%/0%), O<sub>2</sub>/N<sub>2</sub>/H<sub>2</sub> (0%/90%/10%), O<sub>2</sub>/N<sub>2</sub>/H<sub>2</sub> (20%/80%/0%) and O<sub>2</sub>/N<sub>2</sub>/H<sub>2</sub> (20%/70%/10%). After incubation, the enzyme activity was measured and then the

protein samples were concentrated to 3-5 mM by a 30-kDa filter (Millipore) under anoxic gas phase. The concentrated samples frozen and stored in liquid N<sub>2</sub>.

**The device parameters and data processing were described as below (112):**

IR data were obtained using an FTIR spectrometer (Bruker, Vertex 70V) equipped with an attenuated total reflection (ATR) optical configuration with a Si prism of 45° incident angle and 2 active reflections (Smith Detection, DuraSamplIR IITM). The resolution of the spectrum was 4 cm<sup>-1</sup>. To avoid light irradiation, the spectrometer was covered by black cloth. Five microliters of the sample solutions were put onto the effective area of a 3-mm-diameter Si prism using micro syringe (Hamilton) and concentrated by slowly evaporating the solvent under mild flow of argon gas. The hydration of the sample was checked by the relative intensities of the water OH stretching band (approximately 3,500 cm<sup>-1</sup>), comparing to the intensity of the amide II band of the protein at approximately (1550 cm<sup>-1</sup>). According to the concentration of the protein by evaporation, intensity of the IR spectrum successively increased thorough the concentration process. To obtain best spectrum of the CO bands, we selected a spectrum of a mildly hydrated sample, in which there is still enough water, which provided enough intensity of the CO bands for analysis because complete removal of water caused an unknown shift of the CO bands. A baseline correction was made on the selected spectrum to eliminate the water overtone band (2,000 cm<sup>-1</sup>). In the most case, 512 spectra were used for averaging the data. Intensities of the CO bands were normalized by the peak intensities of the amide II band of each spectrum to quantitatively compare the obtained data.

#### **4.2.12 Mössbauer spectroscopy**

The two sample conditions were designed to reproduce the conditions, in which the crystals contain the open and closed conformations. For the conditions of the open conformation in the absence of methenyl-H<sub>4</sub>MPT<sup>+</sup>, the sample contained 26-mg/ml (0.7 mM) [Fe]-hydrogenase (~ 60% enriched with <sup>57</sup>Fe), 10% w/v polyethylene glycol 3350, 50-mM tri-sodium citrate pH 4.0 and 100-mM tri-sodium citrate. For the conditions of the closed conformation in the presence of methenyl-H<sub>4</sub>MPT<sup>+</sup>, the sample contained 26-mg/ml (0.7 mM) [Fe]-hydrogenase (~60% enriched with <sup>57</sup>Fe), 10%-w/v polyethylene glycol 3350, 100-mM sodium thiocyanate and 3-mM methenyl-H<sub>4</sub>MPT<sup>+</sup>. All concentrations shown above were the final concentration in the sample solution. Under the gas phase of 95%N<sub>2</sub>/5%H<sub>2</sub>, the 0.7-ml sample solution was filled into a 0.7-

ml Mössbauer cup and the cup was placed in a 250-ml brown bottle. The bottle was then sealed with a rubber stopper. For the sample without methenyl-H<sub>4</sub>MPT<sup>+</sup>, the gas inside was not exchanged and incubated at 4 °C for 1 h and then frozen at -75 °C for 1.5 h. For the sample containing methenyl-H<sub>4</sub>MPT<sup>+</sup>, the gas inside was exchanged with 100% N<sub>2</sub> at 1.3 bar and incubated at 4 °C for 1 h and then frozen at -75 °C for 1.5 h. Finally, all samples were quickly transferred into liquid N<sub>2</sub> and stored in a Dewar filled with liquid N<sub>2</sub>. Mössbauer data were collected on an alternating constant-acceleration spectrometer. The sample temperature was maintained constant in an Oxford Instruments Variox Mössbauer cryostat. All isomer shifts are quoted relative to iron metal at 300K. The zero-field spectra were fitted by using Lorentzian line shapes (84).

#### 4.2.13 QM/MM computations

We used QM/MM computations within the ONIOM (130) framework in Gaussian09 (131) to obtain the free energies of each reaction steps in the catalytic cycle which conducted in the closed [Fe]-hydrogenase. The active center including truncated FeGP cofactor and the substrate MPT<sup>+</sup>, and Cys176 and the proton transfer relay (His14, Glu207, Thr20, Arg101 and two water molecules) was involved in the “high level” computations at the M06 (132, 133)/6-31G(d,p) level. The “low level” [computed using the universal force field (UFF)] contained the remaining portions of the truncated FeGP cofactor and substrate MPT<sup>+</sup>, and other amino acid residues not included in the “high level”. All amino acids with electrically charged subgroups were protonated according to a physiological pH, which produced an overall charge of -13 for the protein (neutral for the high-level/-13 for the low-level). The nature of all stationary points (as either minima or transition states) was confirmed by analysis of vibrational frequencies (zero for minima, one for transition states). Reported free energies include unscaled free energy contributions taken from the QM/MM computations. This part is obtained from Ref (98).

#### 4.2.14 H<sub>2</sub>O<sub>2</sub> measurement

The Amplex® Red Hydrogen Peroxide/Peroxidase Assay Kit (Thermo Fisher Scientific, Dreieich, Germany) was used to measure the concentration of H<sub>2</sub>O<sub>2</sub>. The amount of H<sub>2</sub>O<sub>2</sub> was quantified by oxidation of Amplex® Red reagent (10-acetyl-3,7-dihydroxyphenoxazine) with H<sub>2</sub>O<sub>2</sub> catalyzed by horseradish peroxidase. At each time point, the 50 µl-aliquots were withdrawn from sample solution and mixed with 50-µl



assay solution that contained 100- $\mu$ M 10-acetyl-3,7-dihydroxyphenoxazine and 0.2-U/ml horseradish peroxidase. The assay mixture was incubated at room temperature for 30 min (protected from light and  $O_2$ ). The  $H_2O_2$  concentration was calculated by the absorbance value at 560 nm with a standard curve of  $H_2O_2$  (112).

#### 4.2.15 $O_2^{\bullet-}$ measurement

The measurement is based on the method previously described (109, 134, 135). The 1-ml assay mixture contained 120-mM potassium phosphate pH 6.0, 1-mM EDTA, 26- $\mu$ M (1-mg/ml) [Fe]-hydrogenase, 26- $\mu$ M methenyl- $H_4$ MPT<sup>+</sup> or methylene- $H_4$ MPT and 0.5-mM hydroxylamine hydrochloride. The mixture was incubated at 40 °C water bath under gas phase  $N_2/O_2/H_2$  (85%/5%/10%). The 33- $\mu$ L aliquots from the mixture was mixed with 11  $\mu$ L of 7-mM  $\alpha$ -naphthylamine, 11  $\mu$ L of 19-mM sulfanilic acid and 44  $\mu$ L of anoxic water under 100%  $N_2$ . At room temperature, with 20-min incubation, the nitrite concentration was determined by measuring the absorption at 530 nm because the  $O_2^{\bullet-}$  can mediate oxidation of hydroxylamine to nitrite. For the standard curve, 2 to 8- $\mu$ M sodium nitrite solutions (final concentration) were used. In order to avoid the interference of hydroxylamine hydrochloride on inactivation/inhibition of [Fe]-hydrogenase, we also used a modified method to detect the formation of  $O_2^{\bullet-}$ . In the modified method, 0.5-mM hydroxylamine hydrochloride was not injected into the mixture. The 1-ml assay mixture contained 120-mM potassium phosphate pH 6.0, 1-mM EDTA, 26- $\mu$ M (1-mg/ml) [Fe]-hydrogenase, 26- $\mu$ M methenyl- $H_4$ MPT<sup>+</sup> or methylene- $H_4$ MPT. After the incubation, 33  $\mu$ L-sample from the mixture was mixed with 11  $\mu$ L of 19-mM sulfanilic acid, 5  $\mu$ L of 10-mM hydroxylamine hydrochloride and 39  $\mu$ L of anoxic water and 11  $\mu$ L of 7-mM  $\alpha$ -naphthylamine under 100%  $N_2$ . And then the nitrite concentration was determined described above. The lowest detection limit of  $O_2^{\bullet-}$  was 2- $\mu$ M. Since the superoxide dismutase can convert  $2O_2^{\bullet-}$  to  $H_2O_2$  and  $O_2$ , the generation of  $O_2^{\bullet-}$  was double-checked by  $H_2O_2$  determination in the presence of superoxide dismutase. In this measurement, addition of superoxide dismutase to the  $O_2$  inactivation assay did not increase the amount of the  $H_2O_2$  produced (Table. S2) (112), which is in conformity with the results of the hydroxylamine dependent  $O_2^{\bullet-}$  measurements method.

#### 4.2.16 UV-Vis spectroscopy

In the presence of 32.5- $\mu$ M methenyl- $H_4$ MPT<sup>+</sup> or methylene- $H_4$ MPT, the 1-ml assay mixtures containing 120-mM potassium phosphate pH 6.0, 1-mM EDTA and 130- $\mu$ M (5-mg/ml) [Fe]-hydrogenase was incubated at 40 °C under gas phase  $N_2/O_2/H_2$  (70%/20%/10%). The control was in the absence of methenyl- $H_4$ MPT<sup>+</sup> or methylene- $H_4$ MPT. At 0, 15, 30, 45 and 60 min time point, a 50- $\mu$ l aliquots from the mixture was measured by UV-vis spectroscopy (SPECORD® S600 UV VIS Spectrophotometer (Analytic Jena)) measurements by using 3-mm quartz cuvettes (112).

#### 4.2.17 Electron paramagnetic resonance spectroscopy

The samples were prepared under anoxic gas phase and transferred to 4-mm X-band Electron paramagnetic resonance spectroscopy (EPR) tubes and then stopped with rubber stoppers via Teflon tubing as previously described (97). The sample was frozen in liquid  $N_2$ . The samples were stored in liquid  $N_2$ . X-band cw-EPR spectra were recorded on an ELEXSYS E500 spectrometer (Bruker) equipped with an ESR 900 helium flow cryostat (Oxford Instruments, Abingdon, UK) and an ER4116DM dual-mode cavity resonator (Bruker). The data were recorded at 10 K in the conditions: 2 and 0.2-mW microwave power over a wide field range (typically 50–450 mT) with field modulation at 100 kHz and 0.75-mT amplitude. For measurement of the spin concentration, a 1-mM Cu (II) standard sample was used at 30K in a narrow field range (around  $g=2$ , with 0.2 and 0.05-mW microwave power, respectively). The spectra were compared by numerical double-integration, and a weighting factor was applied to account for different temperatures and different Aasa-Vanngard factors. We assumed that the zero-field splitting of the high-spin Fe(III),  $S=5/2$  species occurring after treatment of [Fe]-hydrogenase with  $O_2$  was small, so that at 10K, the middle Kramer's doublet that gives rise to the observed  $g=4.3$  signal is virtually 33% populated (112).

#### 4.2.18 Size-exclusion chromatography

The Size-exclusion chromatography was performed using a Superdex 200 Increase 10/300 GL column (GE Healthcare) in the anaerobic tent with gas phase 95% $N_2$ /5% $H_2$  under yellow light at 18 °C (116). The elution buffer was 25-mM potassium phosphate pH 6.5. Flow rate was 0.5 ml/min. The sample contained 200  $\mu$ l of 6-mg/ml [Fe]-hydrogenase from *M. marburgensis* or *M. jannaschii* in the absence or presence of 0.5-mM TosMIC (116).

#### 4.2.19 Ultrafiltration to determine the oligomerization state of [Fe]-hydrogenase

The experiments were done in the anaerobic tent with gas phase 95% N<sub>2</sub>/5% H<sub>2</sub> under yellow light at 18 °C (116). The sample contained 500 µl of 6-mg/ml [Fe]-hydrogenase from *M. marburgensis* or *M. jannaschii* in the absence/presence of 0.5-mM TosMIC or methenyl-H<sub>4</sub>MPT<sup>+</sup>. The 0.5-ml 100-kDa cut-off ultrafilter (Merck Millipore, Darmstadt, Germany) was centrifuged to filtrate the samples using MiniSpin Plus (Eppendorf, Hamburg, Germany) with 12,000 rpm for 10 min.

#### 4.2.20 Light-inactivation of [Fe]-hydrogenase

The 5-ml vial (white and transparent) containing 500-µl (50-mg/ml or 0.05-mg/ml) [Fe]-hydrogenase from *M. marburgensis* and *M. jannaschii* under 100% N<sub>2</sub> was incubated on ice and exposed to white cold light (3000K and Cycle size A (KL 2500 LCD, SCHOTT) (116). The light irradiation experiments were performed in a closed white foamed styrol box for protection of eyes. The light fiber tube was inserted through the hole in the lid. The distance between the vial and the light was 5 cm (116). The buffer for the samples was 10-mM MOPS/KOH pH 7.0. At 0, 15, 30, 45 and 60 min time point, 10-µl aliquots from the vials was subjected to the enzyme activity assay (116).

#### 4.2.21 Inactivation of [Fe]-hydrogenase by oxidative stress

Two kinds of oxidative stress (O<sub>2</sub> and H<sub>2</sub>O<sub>2</sub>) were tested. In the case of O<sub>2</sub>, a 100-µl [Fe]-hydrogenase from *M. marburgensis* or *M. jannaschii* in different concentrations (50 mg/ml (1.3 mM) or 0.05 mg/ml (1.3 µM)) dissolved in 25-mM potassium phosphate buffer pH 6.5 was incubated on ice under air (116). In the case of H<sub>2</sub>O<sub>2</sub>, the gas phase was 100% N<sub>2</sub> (116). At each time point, 10-µl aliquot was taken and used for the enzyme activity assay (116).

## References

1. W. Lubitz, H. Ogata, O. Rüdiger, E. Reijerse, Hydrogenases. *Chem. Rev.* **114**, 4081-4148 (2014).
2. P. M. Vignais, B. Billoud, Occurrence, classification, and biological function of hydrogenases: an overview. *Chem. Rev.* **107**, 4206-4272 (2007).
3. P. M. Vignais, B. Billoud, J. Meyer, Classification and phylogeny of hydrogenases. *FEMS Microbiol. Ecol.* **25**, 455-501 (2001).
4. S. Shima *et al.*, The crystal structure of [Fe]-hydrogenase reveals the geometry of the active site. *Science* **321**, 572-575 (2008).
5. S. Shima, R. K. Thauer, A third type of hydrogenase catalyzing H<sub>2</sub> activation. *Chem. Rec.* **7**, 37-46 (2007).
6. G. C. Hartmann, A. R. Klein, M. Linder, R. K. Thauer, Purification, properties and primary structure of H<sub>2</sub>-forming N<sup>5</sup>,N<sup>10</sup>-methylenetetrahydromethanopterin dehydrogenase from *Methanococcus thermolithotrophicus*. *Arch. Microbiol.* **165**, 187-193 (1996).
7. C. Afting, A. Hochheimer, R. K. Thauer, Function of H<sub>2</sub>-forming methylenetetrahydromethanopterin dehydrogenase from *Methanobacterium thermoautotrophicum* in coenzyme F<sub>420</sub> reduction with H<sub>2</sub>. *Arch. Microbiol.* **169**, 206-210 (1998).
8. R. K. Thauer *et al.*, Hydrogenases from methanogenic archaea, nickel, a novel cofactor, and H<sub>2</sub> storage. *Annu. Rev. Biochem.* **79**, 507-536 (2010).
9. M. Korbas *et al.*, The iron-sulfur cluster-free hydrogenase (Hmd) is a metalloenzyme with a novel iron binding motif. *J. Biol. Chem.* **281**, 30804-30813 (2006).
10. C. Zirngibl *et al.*, H<sub>2</sub>-forming methylenetetrahydromethanopterin dehydrogenase, a novel type of hydrogenase without iron-sulfur clusters in methanogenic archaea. *Eur J Biochem* **208**, 511-520 (1992).
11. H. Ogata, K. Nishikawa, W. Lubitz, Hydrogens detected by subatomic resolution protein crystallography in a [NiFe] hydrogenase. *Nature* **520**, 571-574 (2015).
12. Y. Nicolet, C. Piras, P. Legrand, C. E. Hatchikian, J. C. Fontecilla-Camps, *Desulfovibrio desulfuricans* iron hydrogenase: the structure shows unusual coordination to an active site Fe binuclear center. *Structure* **7**, 13-23 (1999).
13. A. J. Cornish, K. Gartner, H. Yang, J. W. Peters, E. L. Hegg, Mechanism of proton transfer in [FeFe]-Hydrogenase from *Clostridium pasteurianum*. *J. Biol. Chem.* **286**, 38341-38347 (2011).
14. J. A. Wright *et al.*, Protonation of [FeFe]-hydrogenase sub-site analogues: revealing mechanism using FTIR stopped-flow techniques. *Faraday Discuss.* **148**, 359-371 (2011).
15. D. W. Mulder *et al.*, EPR and FTIR analysis of the mechanism of H<sub>2</sub> activation by [FeFe]-hydrogenase HydA1 from *Chlamydomonas reinhardtii*. *J. Am. Chem. Soc.* **135**, 6921-6929 (2013).
16. G. F. Qian, Z. Y. Xiao, L. Long, X. M. Liu, Probing the electron transfer mechanism of diiron-carbonyl complexes relevant to the diiron sub-unit of [FeFe]-hydrogenase. *J. Biol. Inorg. Chem.* **19**, S758-S758 (2014).
17. S. Shima *et al.*, Evidence for acyl-iron ligation in the active site of [Fe]-hydrogenase provided by mass spectrometry and infrared spectroscopy. *Dalton Trans.* **41**, 767-771 (2012).
18. A. Volbeda *et al.*, Crystal structure of the nickel-iron hydrogenase from *Desulfovibrio Gigas*. *Nature* **373**, 580-587 (1995).
19. A. Volbeda *et al.*, Structure of the [NiFe] hydrogenase active site: evidence for biologically uncommon Fe ligands. *J. Am. Chem. Soc.* **118**, 12989-12996 (1996).

20. A. J. Pierik, W. Roseboom, R. P. Happe, K. A. Bagley, S. P. J. Albracht, Carbon monoxide and cyanide as intrinsic ligands to iron in the active site of [NiFe]-hydrogenases - NiFe(CN)<sub>2</sub>CO, biology's way to activate H<sub>2</sub>. *J. Biol. Chem.* **274**, 3331-3337 (1999).
21. R. P. Happe, W. Roseboom, A. J. Pierik, S. P. J. Albracht, K. A. Bagley, Biological activation of hydrogen. *Nature* **385**, 126-126 (1997).
22. Y. Rippers, M. Horch, P. Hildebrandt, I. Zebger, M. A. Mroginski, Revealing the absolute configuration of the CO and CN- ligands at the active site of a [NiFe] Hydrogenase. *Chemphyschem* **13**, 3852-3856 (2012).
23. R. P. Happe *et al.*, Unusual FTIR and EPR properties of the H<sub>2</sub>-activating site of the cytoplasmic NAD-reducing hydrogenase from *Ralstonia eutropha*. *FEBS Lett.* **466**, 259-263 (2000).
24. A. L. deLacey *et al.*, Infrared spectroelectrochemical characterization of the [NiFe] hydrogenase of *Desulfovibrio gigas*. *J. Am. Chem. Soc.* **119**, 7181-7189 (1997).
25. C. Greening *et al.*, Genomic and metagenomic surveys of hydrogenase distribution indicate H<sub>2</sub> is a widely utilised energy source for microbial growth and survival. *ISME J.* **10**, 761-777 (2016).
26. M. E. Pandelia, H. Ogata, W. Lubitz, Intermediates in the catalytic cycle of [NiFe] hydrogenase: functional spectroscopy of the active site. *Chemphyschem* **11**, 1127-1140 (2010).
27. M. Bruschi, G. Zampella, P. Fantucci, L. De Gioia, DFT investigations of models related to the active site of [NiFe] and [Fe] hydrogenases. *Coordin. Chem. Rev.* **249**, 1620-1640 (2005).
28. G. Davidson *et al.*, Structural examination of the nickel site in *Chromatium vinosum* hydrogenase: redox state oscillations and structural changes accompanying reductive activation and CO binding. *Biochemistry* **39**, 7468-7479 (2000).
29. L. De Gioia, P. Fantucci, B. Guigliarelli, P. Bertrand, Ni-Fe hydrogenases: a density functional theory study of active site models. *Inorg. Chem.* **38**, 2658-2662 (1999).
30. A. L. De Lacey, V. M. Fernandez, M. Rousset, R. Cammack, Activation and inactivation of hydrogenase function and the catalytic cycle: spectroelectrochemical studies. *Chem. Rev.* **107**, 4304-4330 (2007).
31. S. Dementin *et al.*, A glutamate is the essential proton transfer gate during the catalytic cycle of the [NiFe] hydrogenase. *J. Biol. Chem.* **279**, 10508-10513 (2004).
32. F. Dole *et al.*, Nature and electronic structure of the Ni-X dinuclear center of *Desulfovibrio gigas* hydrogenase. Implications for the enzymatic mechanism. *Biochemistry* **36**, 7847-7854 (1997).
33. S. Foerster *et al.*, Single crystal EPR studies of the reduced active site of [NiFe] hydrogenase from *Desulfiovibrio vulgaris* Miyazaki F. *J. Am. Chem. Soc.* **125**, 83-93 (2003).
34. P. Jayapal, M. Sundararajan, I. H. Hillier, N. A. Burton, How are the ready and unready states of nickel-iron hydrogenase activated by H<sub>2</sub>? A density functional theory study. *Phys. Chem. Chem. Phys.* **8**, 4086-4094 (2006).
35. P. Jayapal, M. Sundararajan, I. H. Hillier, N. A. Burton, QM/MM studies of Ni-Fe hydrogenases: the effect of enzyme environment on the structure and energies of the inactive and active states. *Phys. Chem. Chem. Phys.* **10**, 4249-4257 (2008).

36. M. E. Pandelia, H. Ogata, L. J. Currell, M. Flores, W. Lubitz, Probing intermediates in the activation cycle of [NiFe] hydrogenase by infrared spectroscopy: the Ni-SIr state and its light sensitivity. *J. Biol. Inorg. Chem.* **14**, 1227-1241 (2009).
37. H. L. Tai *et al.*, Photoactivation of the Ni-SIr state to the Ni-SIa state in [NiFe] hydrogenase: FT-IR study on the light reactivity of the ready Ni-SIr state and as-isolated enzyme revisited. *Phys. Chem. Chem. Phys.* **18**, 22025-22030 (2016).
38. C. Bagyinka, How does the ([NiFe]) hydrogenase enzyme work? *Int. J. Hydrog. Energy* **39**, 18521-18532 (2014).
39. C. Greco, Towards [NiFe]-hydrogenase biomimetic models that couple H<sub>2</sub> binding with functionally relevant intramolecular electron transfers: a quantum chemical study. *Dalton Trans.* **42**, 13845-13854 (2013).
40. I. Sumner, G. A. Voth, Proton transport pathways in [NiFe]-Hydrogenase. *J. Phys. Chem. B* **116**, 2917-2926 (2012).
41. D. M. A. Smith, Y. Xiong, T. P. Straatsma, K. M. Rosso, T. C. Squier, Force-Field Development and Molecular Dynamics of [NiFe] Hydrogenase. *J. Chem. Theory Comput.* **8**, 2103-2114 (2012).
42. V. H. Teixeira, C. M. Soares, A. M. Baptista, Proton pathways in a [NiFe]-hydrogenase: A theoretical study. *Proteins* **70**, 1010-1022 (2008).
43. A. Parkin, F. Sargent, The hows and whys of aerobic H<sub>2</sub> metabolism. *Curr. Opin. Chem. Biol.* **16**, 26-34 (2012).
44. S. Dementin *et al.*, Introduction of methionines in the gas channel makes [NiFe] hydrogenase aero-tolerant. *J. Am. Chem. Soc.* **131**, 10156-10164 (2009).
45. G.-F. Huang *et al.*, Improved O<sub>2</sub>-tolerance in variants of a H<sub>2</sub>-evolving [NiFe]-hydrogenase from *Klebsiella oxytoca* HP1. *FEBS Lett.* **589**, 910-918 (2015).
46. P.-P. Liebgott *et al.*, Relating diffusion along the substrate tunnel and oxygen sensitivity in hydrogenase. *Nat. Chem. Biol.* **6**, 63-70 (2010).
47. B. Friedrich, J. Fritsch, O. Lenz, Oxygen-tolerant hydrogenases in hydrogen-based technologies. *Curr. Opin. Biotechnol.* **22**, 358-364 (2011).
48. T. Goris *et al.*, A unique iron-sulfur cluster is crucial for oxygen tolerance of a [NiFe]-hydrogenase. *Nat. Chem. Biol.* **7**, 310-U387 (2011).
49. P.-P. Liebgott *et al.*, Original design of an oxygen-tolerant [NiFe] Hydrogenase: major effect of a Valine-to-Cysteine mutation near the active site. *J. Am. Chem. Soc.* **133**, 986-997 (2011).
50. P.-P. Liebgott, S. Dementin, C. Léger, M. Rousset, Towards engineering O<sub>2</sub>-tolerance in [NiFe] hydrogenases. *Energy Environ. Sci.* **4**, 33-41 (2011).
51. M. J. Lukey *et al.*, Oxygen-tolerant [NiFe]-Hydrogenases: the individual and collective importance of supernumerary Cysteines at the proximal Fe-S cluster. *J. Am. Chem. Soc.* **133**, 16881-16892 (2011).
52. M.-E. Pandelia *et al.*, Characterization of a unique [FeS] cluster in the electron transfer chain of the oxygen tolerant [NiFe] hydrogenase from *Aquifex aeolicus*. *Proc. Natl. Acad. Sci. U.S.A.* **108**, 6097-6102 (2011).
53. C. Pinske *et al.*, Efficient electron transfer from hydrogen to benzyl viologen by the [NiFe]-hydrogenases of *Escherichia coli* is dependent on the coexpression of the iron-sulfur cluster-containing small subunit. *Arch. Microbiol.* **193**, 893-903 (2011).
54. Y. Shomura, K.-S. Yoon, H. Nishihara, Y. Higuchi, Structural basis for a [4Fe-3S] cluster in the oxygen-tolerant membrane-bound [NiFe]-hydrogenase. *Nature* **479**, 253-256 (2011).

55. A. S. Bingham, P. R. Smith, J. R. Swartz, Evolution of an [FeFe] hydrogenase with decreased oxygen sensitivity. *Int. J. Hydrog. Energy* **37**, 2965-2976 (2012).
56. S. Morozov *et al.*, Tolerance to oxygen of hydrogen enzyme electrodes. *Electrochem. Commun.* **8**, 851-854 (2006).
57. J. W. Peters, W. N. Lanzilotta, B. J. Lemon, L. C. Seefeldt, X-ray crystal structure of the Fe-only hydrogenase (Cpl) from *Clostridium pasteurianum* to 1.8 angstrom resolution. *Science* **282**, 1853-1858 (1998).
58. A. S. Pereira, P. Tavares, I. Moura, J. J. G. Moura, B. H. Huynh, Mössbauer characterization of the iron-sulfur clusters in *Desulfovibrio vulgaris* hydrogenase. *Journal of the American Chemical Society* **123**, 2771-2782 (2001).
59. C. V. Popescu, E. Munck, Electronic structure of the H cluster in [Fe]-hydrogenases. *J. Am. Chem. Soc.* **121**, 7877-7884 (1999).
60. G. Berggren *et al.*, Biomimetic assembly and activation of [FeFe]-hydrogenases. *Nature* **499**, 66-69 (2013).
61. D. W. Mulder, Y. S. Guo, M. W. Ratzloff, P. W. King, Identification of a catalytic iron-hydride at the H-Cluster of [FeFe]-Hydrogenase. *J. Am. Chem. Soc.* **139**, 83-86 (2017).
62. V. Pelmeshnikov *et al.*, Reaction coordinate leading to H<sub>2</sub> production in [FeFe]-Hydrogenase identified by nuclear resonance vibrational spectroscopy and density functional theory. *J. Am. Chem. Soc.* **139**, 16894-16902 (2017).
63. G. Zampella, P. Fantucci, L. De Gioia, DFT characterization of the reaction pathways for terminal- to  $\mu$ -hydride isomerisation in synthetic models of the [FeFe]-hydrogenase active site. *ChemComm* **46**, 8824-8826 (2010).
64. D. W. Mulder *et al.*, Insights into [FeFe]-Hydrogenase structure, mechanism, and maturation. *Structure* **19**, 1038-1052 (2011).
65. A. Adamska *et al.*, Identification and characterization of the "super-reduced" state of the H-cluster in [FeFe] hydrogenase: a new building block for the catalytic cycle? *Angew. Chem. Int. Ed.* **51**, 11458-11462 (2012).
66. W. M. Gao *et al.*, Attachment of a hydrogen-bonding carboxylate side chain to an [FeFe]-Hydrogenase model complex: influence on the catalytic mechanism. *Chemistry* **16**, 2537-2546 (2010).
67. M. Albertini *et al.*, Characterization of the [FeFe]-Hydrogenase maturation protein HydF by EPR techniques: insights into the catalytic mechanism. *Top. Catal.* **58**, 708-718 (2015).
68. M. W. Ratzloff *et al.*, CO-bridged H-cluster intermediates in the catalytic mechanism of [FeFe]-Hydrogenase Cal. *J. Am. Chem. Soc.* **140**, 7623-7628 (2018).
69. J. F. Capon *et al.*, Electrochemical insights into the mechanisms of proton reduction by [Fe<sub>2</sub>(CO)<sub>6</sub>{ $\mu$ -SCH<sub>2</sub>N(R)CH<sub>2</sub>S}] complexes related to the [2Fe]<sub>H</sub> subsite of [FeFe]Hydrogenase. *Chemistry* **14**, 1954-1964 (2008).
70. H. L. Wang, X. M. Liu, Intramolecular hydrogen bonding interaction, a mechanism for the bridging linkages to exert electronic influence on diiron models of [FeFe]-hydrogenase. *Inorganica Chim. Acta* **406**, 113-118 (2013).
71. J. A. Wright, C. J. Pickett, Protonation of a subsite analogue of [FeFe]-hydrogenase: mechanism of a deceptively simple reaction revealed by time-resolved IR spectroscopy. *ChemComm* **14**, 5719-5721 (2009).
72. S. Shima, R. K. Thauer, Tetrahydromethanopterin-specific enzymes from *Methanopyrus kandleri*. *Methods Enzymol.* **331**, 317-353 (2001).
73. O. Pilak *et al.*, The crystal structure of the apoenzyme of the iron-sulphur cluster-free hydrogenase. *J. Mol. Biol.* **358**, 798-809 (2006).

74. J. Schleucher, C. Griesinger, B. Schworer, R. K. Thauer, H<sub>2</sub>-forming N<sup>5</sup>, N<sup>10</sup>-methylenetetrahydromethanopterin dehydrogenase from *Methanobacterium thermoautotrophicum* catalyzes a stereoselective hydride transfer as determined by two-dimensional NMR spectroscopy. *Biochemistry* **33**, 3986-3993 (1994).
75. A. R. Klein, V. M. Fernandez, R. K. Thauer, H<sub>2</sub>-forming N<sup>5</sup>,N<sup>10</sup>-methylenetetrahydromethanopterin dehydrogenase: mechanism of H<sub>2</sub> formation analyzed using hydrogen isotopes. *FEBS Lett.* **368**, 203-206 (1995).
76. C. Zirngibl, R. Hedderich, R. K. Thauer, N<sup>5</sup>,N<sup>10</sup>-Methylenetetrahydromethanopterin dehydrogenase from *Methanobacterium thermoautotrophicum* has hydrogenase activity. *FEBS Lett.* **261**, 112-116 (1990).
77. A. Berkessel, R. K. Thauer, On the mechanism of catalysis by a metal - free hydrogenase from Methanogenic archaea: enzymatic transformation of H<sub>2</sub> without a metal and its analogy to the chemistry of alkanes in superacidic solution. *Angew. Chem. Int. Ed.* **34**, 2247-2250 (1995).
78. M. Gensheimer, A. Brandis-Heep, S. Agarwal, R. K. Thauer, A. Greiner, Polymer/bacteria composite nanofiber non-wovens by electrospinning of living bacteria protected by hydrogel microparticles. *Macromol. Biosci.* **11**, 333-337 (2011).
79. A. K. Kaster *et al.*, More than 200 genes required for methane formation from H<sub>2</sub> and CO<sub>2</sub> and energy conservation are present in *Methanothermobacter marburgensis* and *Methanothermobacter thermautotrophicus*. *Archaea* **2011**, 1-23 (2011).
80. L. Bai *et al.*, Towards artificial methanogenesis: biosynthesis of the [Fe]-hydrogenase cofactor and characterization of the semi-synthetic hydrogenase. *Faraday Discuss.* **198**, 37-58 (2017).
81. K. Ceh *et al.*, Structural basis of the hydride transfer mechanism in F<sub>420</sub>-dependent methylenetetrahydromethanopterin dehydrogenase. *Biochemistry* **48**, 10098-100105 (2009).
82. S. Shima, U. Ermler, Structure and function of [Fe]-Hydrogenase and its iron-guanylylpyridinol (FeGP) cofactor. *Eur J Biochem* **2011**, 963-972 (2011).
83. E. J. Lyon *et al.*, Carbon monoxide as an intrinsic ligand to iron in the active site of the iron-sulfur-cluster-free hydrogenase H<sub>2</sub>-forming methylenetetrahydromethanopterin dehydrogenase as revealed by infrared spectroscopy. *J. Am. Chem. Soc.* **126**, 14239-14248 (2004).
84. S. Shima, E. J. Lyon, R. K. Thauer, B. Mienert, E. Bill, Mossbauer studies of the iron-sulfur cluster-free hydrogenase: the electronic state of the mononuclear Fe active site. *J. Am. Chem. Soc.* **127**, 10430-10435 (2005).
85. E. J. Lyon *et al.*, UV-A/blue-light inactivation of the 'metal-free' hydrogenase (Hmd) from methanogenic archaea. *Eur J Biochem* **271**, 195-204 (2004).
86. P. Acharya, E. Warkentin, U. Ermler, R. K. Thauer, S. Shima, The structure of formylmethanofuran: tetrahydromethanopterin formyltransferase in complex with its coenzymes. *J. Mol. Biol.* **357**, 870-879 (2006).
87. T. Hiromoto *et al.*, The crystal structure of C176A mutated [Fe]-hydrogenase suggests an acyl-iron ligation in the active site iron complex. *FEBS Lett.* **583**, 585-590 (2009).
88. T. Hiromoto, E. Warkentin, J. Moll, U. Ermler, S. Shima, The crystal structure of an [Fe]-hydrogenase-substrate complex reveals the framework for H<sub>2</sub> activation. *Angew. Chem. Int. Ed.* **48**, 6457-6460 (2009).

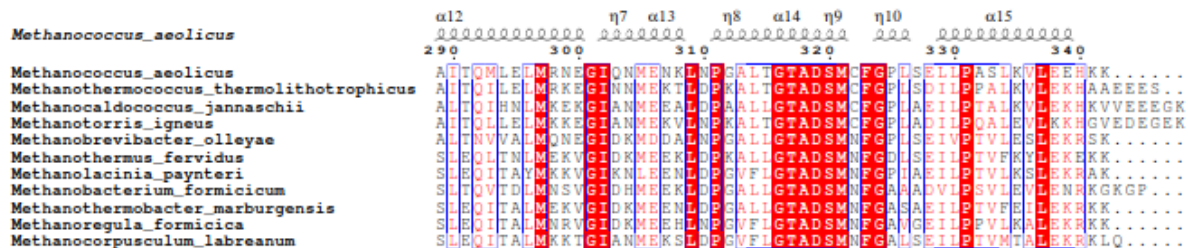
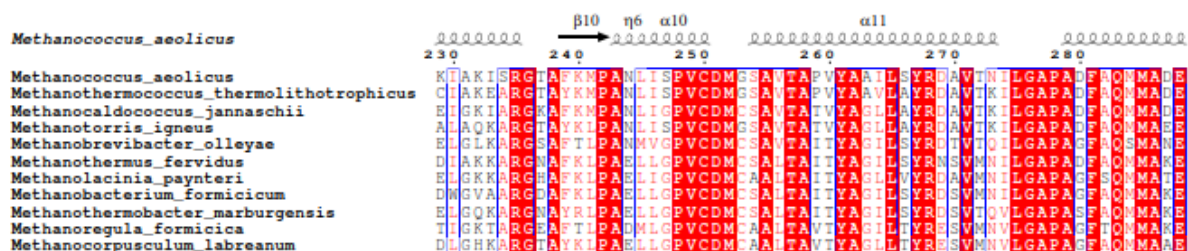
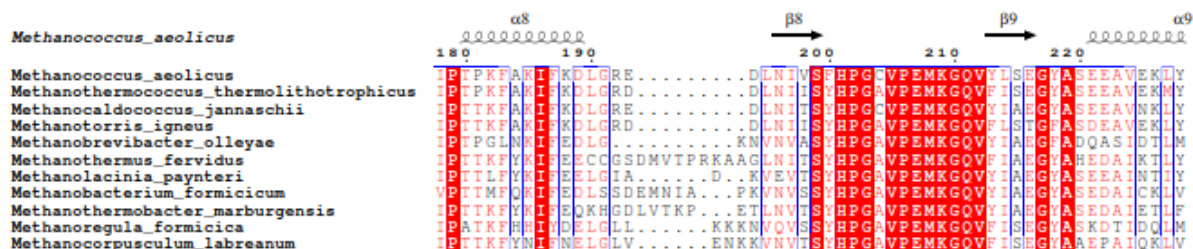
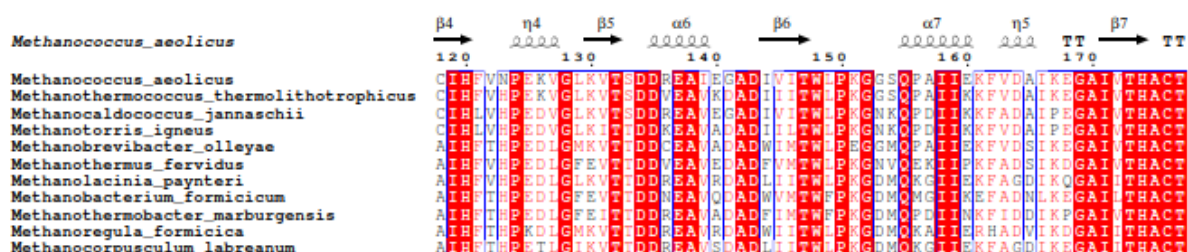
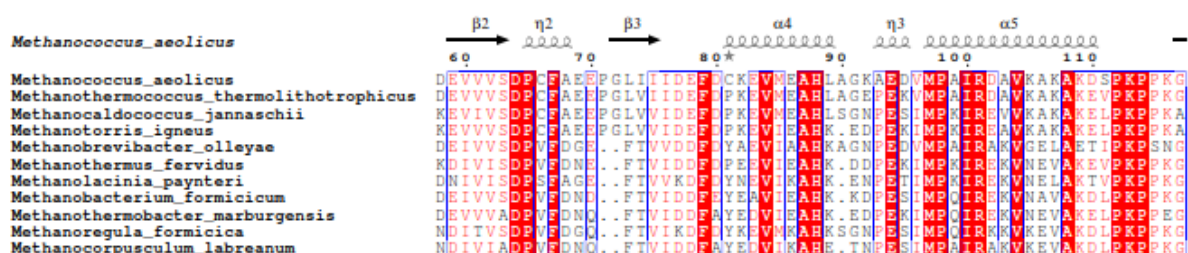
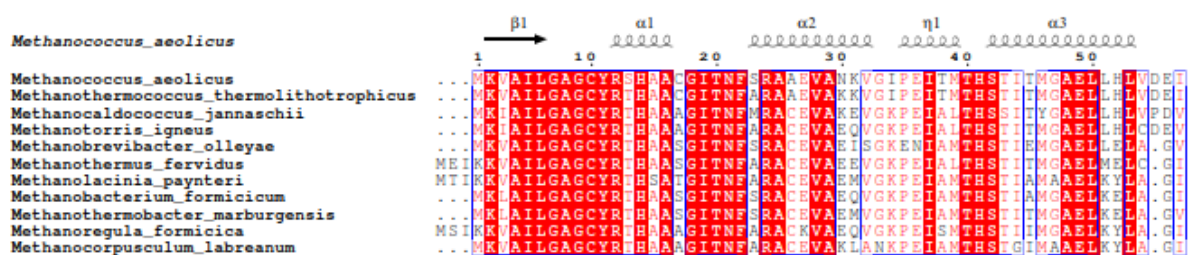


89. H. Tamura *et al.*, Crystal structures of [Fe]-hydrogenase in complex with inhibitory isocyanides: implications for the H<sub>2</sub>-activation site. *Angew. Chem. Int. Ed.* **52**, 9656-9659 (2013).
90. A. R. Klein, G. C. Hartmann, R. K. Thauer, Hydrogen isotope effects in the reactions catalyzed by H<sub>2</sub>-forming N<sup>5</sup>,N<sup>10</sup>-methylenetetrahydromethanopterin dehydrogenase from methanogenic Archaea. *Eur J Biochem* **233**, 372-376 (1995).
91. G. A. Olah, N. Hartz, G. Rasul, G. K. S. Prakash, Electrophilic substitution of methane revisited. *J. Am. Chem. Soc.* **117**, 1336-1343 (1995).
92. A. Berkessel, Activation of dihydrogen without transition metals. *Curr. Opin. Chem. Biol.* **5**, 486-490 (2001).
93. S. Vogt, E. J. Lyon, S. Shima, R. K. Thauer, The exchange activities of [Fe] hydrogenase (iron-sulfur-cluster-free hydrogenase) from methanogenic archaea in comparison with the exchange activities of [FeFe] and [NiFe] hydrogenases. *J. Biol. Inorg. Chem.* **13**, 97-106 (2008).
94. X. Yang, M. B. Hall, Monoiron hydrogenase catalysis: hydrogen activation with the formation of a dihydrogen, Fe-H<sup>δ-</sup>---H<sup>δ+</sup>-O, bond and methenyl-H<sub>4</sub>MPT<sup>+</sup> triggered hydride transfer. *J. Am. Chem. Soc.* **131**, 10901-10908 (2009).
95. A. Dey, Density functional theory calculations on the mononuclear non-heme iron active site of Hmd hydrogenase: role of the internal ligands in tuning external ligand binding and driving H<sub>2</sub> heterolysis. *J. Am. Chem. Soc.* **132**, 13892-13901 (2010).
96. E. D. Hedegård, J. Kongsted, U. Ryde, Multiscale modeling of the active site of [Fe] hydrogenase: the H<sub>2</sub> binding site in open and closed protein conformations. *Angew. Chem. Int. Ed.* **54**, 6246-6250 (2015).
97. R. Hidese, K. Ataka, E. Bill, S. Shima, Cu<sup>I</sup> and H<sub>2</sub>O<sub>2</sub> Inactivate and Fe<sup>II</sup> Inhibits [Fe]-hydrogenase at very low concentrations. *ChemBioChem* **16**, 1861-1865 (2015).
98. G. Huang *et al.*, The atomic-resolution crystal structure of activated [Fe]-hydrogenase. **In revision.**
99. D. Chen, R. Scopelliti, X. Hu, A five-coordinate iron center in the active site of [Fe]-hydrogenase: hints from a model study. *Angew. Chem. Int. Ed.* **50**, 5671-5673 (2011).
100. P. Gütllich, E. Bill, A. X. Trautwein, *Mössbauer spectroscopy and transition metal chemistry*. (Springer Verlag, Berlin Heidelberg, 2011), pp. 620.
101. Z. Rappoport, *The chemistry of phenols*. (John Wiley & Sons, 2004).
102. A. Shukla, R. P. Tewari, K. D. P. Shukla, Electronic state properties: bond length and bond angle of phenol and its some derivatives. *Int. J. Chem. Sci.* **9**, 627-636 (2011).
103. F. H. Allen *et al.*, Tables of bond lengths determined by X-ray and neutron-diffraction. Part 1. Bond lengths in organic-compounds. *J Chem Soc Perk T 2*, S1-S19 (1987).
104. S. Bartoschek *et al.*, Re-face stereospecificity of methylene-tetrahydromethanopterin dehydrogenases and methylenetetrahydrofolate dehydrogenases is predetermined by intrinsic properties of the substrate. *ChemBioChem* **2**, 530-541 (2001).
105. S. Bartoschek, G. Buurman, B. H. Geierstanger, J. Lapham, C. Griesinger, Measurement and ab initio calculation of CSA/dipole-dipole cross-correlated relaxation provide insight into the mechanism of a H<sub>2</sub>-forming dehydrogenase. *J. Am. Chem. Soc.* **125**, 13308-13309 (2003).

106. R. K. Thauer, A. R. Klein, G. C. Hartmann, Reactions with molecular hydrogen in microorganisms: evidence for a purely organic hydrogenation catalyst. *Chem. Rev.* **96**, 3031-3042 (1996).
107. S. T. Stripp *et al.*, How oxygen attacks [FeFe] hydrogenases from photosynthetic organisms. *Proc. Natl. Acad. Sci. U.S.A.* **106**, 17331-17336 (2009).
108. A. Kubas *et al.*, Mechanism of O<sub>2</sub> diffusion and reduction in FeFe hydrogenases. *Nat Chem* **9**, 88-95 (2017).
109. L. Lauterbach, O. Lenz, Catalytic production of hydrogen peroxide and water by oxygen-tolerant [NiFe]-hydrogenase during H<sub>2</sub> cycling in the presence of O<sub>2</sub>. *J. Am. Chem. Soc.* **135**, 17897-17905 (2013).
110. P. Wulff, C. C. Day, F. Sargent, F. A. Armstrong, How oxygen reacts with oxygen-tolerant respiratory [NiFe]-hydrogenases. *Proc. Natl. Acad. Sci. U.S.A.* **111**, 6606-6611 (2014).
111. Y. Shomura, K.-S. Yoon, H. Nishihara, Y. Higuchi, Structural basis for a [4Fe-3S] cluster in the oxygen-tolerant membrane-bound [NiFe]-hydrogenase. *Nature* **479**, 253-256.
112. G. Huang *et al.*, Dioxygen sensitivity of [Fe]-Hydrogenase in the presence of reducing substrates. *Angew. Chem. Int. Ed.* **57**, 4917-4920 (2018).
113. K. A. Murray, M. D. Wodrich, X. Hu, C. Corminboeuf, Toward functional type III [Fe]-hydrogenase biomimics for H<sub>2</sub> activation: insights from computation. *Chemistry* **21**, 3987-3996 (2015).
114. T. Xu *et al.*, A functional model of [Fe]-hydrogenase. *J. Am. Chem. Soc.* **138**, 3270-3273 (2016).
115. S. E. Clapham, A. Hadzovic, R. H. Morris, Mechanisms of the H<sub>2</sub>-hydrogenation and transfer hydrogenation of polar bonds catalyzed by ruthenium hydride complexes. *Coordin. Chem. Rev.* **248**, 2201-2237 (2004).
116. T. Wagner, G. Huang, U. Ermler, S. Shima, How [Fe]-hydrogenase from *Methanothermobacter* is protected against light and oxidative stress. *Angew. Chem. Int. Ed.* **57**, 15056-15059 (2018).
117. E. Krissinel, K. Henrick, Inference of macromolecular assemblies from crystalline state. *J. Mol. Biol.* **372**, 774-797 (2007).
118. Y. Shomura *et al.*, Structural basis of the redox switches in the NAD<sup>+</sup>-reducing soluble [NiFe]-hydrogenase. *Science* **357**, 928-932 (2017).
119. S. Shima, M. Schick, H. Tamura, Preparation of [Fe]-hydrogenase from methanogenic archaea. *Methods Enzymol.* **494**, 119-137 (2011).
120. A. J. McCoy *et al.*, Phaser crystallographic software. *J. Appl. Crystallogr.* **40**, 658-674 (2007).
121. P. Emsley, B. Lohkamp, W. G. Scott, K. Cowtan, Features and development of Coot. *Acta Crystallogr. D* **66**, 486-501 (2010).
122. G. Bricogne *et al.* (Cambridge, United Kingdom: Global Phasing Ltd., 2016).
123. P. D. Adams *et al.*, PHENIX: a comprehensive Python-based system for macromolecular structure solution. *Acta Crystallogr. D* **66**, 213-221 (2010).
124. W. Kabsch, XDS. *Acta Crystallogr. D* **66**, 125-132 (2010).
125. M. D. Winn *et al.*, Overview of the CCP4 suite and current developments. *Acta Crystallogr. D* **67**, 235-242 (2011).
126. P. V. Afonine *et al.*, *phenix.model\_vs\_data*: a high-level tool for the calculation of crystallographic model and data statistics. *J. Appl. Crystallogr. D* **43**, 669-676 (2010).
127. P. Emsley, K. Cowtan, Coot: model-building tools for molecular graphics. *Acta Crystallogr. D* **60**, 2126-2132 (2004).

128. ADF2017. (Software Chemistry & Materials: Theoretical Chemistry, Vrije Universiteit, Amsterdam, The Netherlands).
129. Bricogne G *et al.*, BUSTER version 2.10.1. *Cambridge, United Kingdom: Global Phasing Ltd.*, (2010).
130. L. W. Chung *et al.*, The ONIOM method and its applications. *Chem. Rev.* **115**, 5678-5796 (2015).
131. G. W. T. M. J. Frisch, J. R. Cheeseman, G. Scalmani, M. Caricato, H. P. Hratchian, X. Li, V. Barone, J. Bloino, G. Zheng, T. Vreven, J. A. Montgomery, Jr., G. A. Petersson, G. E. Scuseria, H. B. Schlegel, H. Nakatsuji, A. F. Izmaylov, R. L. Martin, J. L. Sonnenberg, J. E. Peralta, J. J. Heyd, E. Brothers, F. Ogliaro, M. Bearpark, M. A. Robb, B. Mennucci, K. N. Kudin, V. N. Staroverov, R. Kobayashi, J. Normand, A. Rendell, R. Gomperts, V. G. Zakrzewski, M. Hada, M. Ehara, K. Toyota, R. Fukuda, J. Hasegawa, M. Ishida, T. Nakajima, Y. Honda, O. Kitao and H. Nakai., Gaussian 09, Revision D.01. *Gaussian, Inc., Wallingford CT*, (2016).
132. Y. Zhao, D. G. Truhlar, The M06 suite of density functionals for main group thermochemistry, thermochemical kinetics, noncovalent interactions, excited states, and transition elements: two new functionals and systematic testing of four M06-class functionals and 12 other functionals. *Theor. Chem. Acc.* **120**, 215-241 (2008).
133. Y. Zhao, D. G. Truhlar, Density functionals with broad applicability in chemistry. *Acc. Chem. Res.* **41**, 157-167 (2008).
134. K. Schneider, H. G. Schlegel, Production of superoxide radicals by soluble hydrogenase from *Alcaligenes eutrophus* H16. *Biochem J* **193**, 99-107 (1981).
135. K. Pattichis, L. L. Louca, V. Glover, Quantitation of soluble superoxide dismutase in rat striata, based on the inhibition of nitrite formation from hydroxylammonium chloride. *Anal. Biochem.* **221**, 428-431 (1994).
136. X. Robert, P. Gouet, Deciphering key features in protein structures with the new ENDscript server. *Nucleic Acids Res.* **42**, W320-W324 (2014).

## Supplementary information



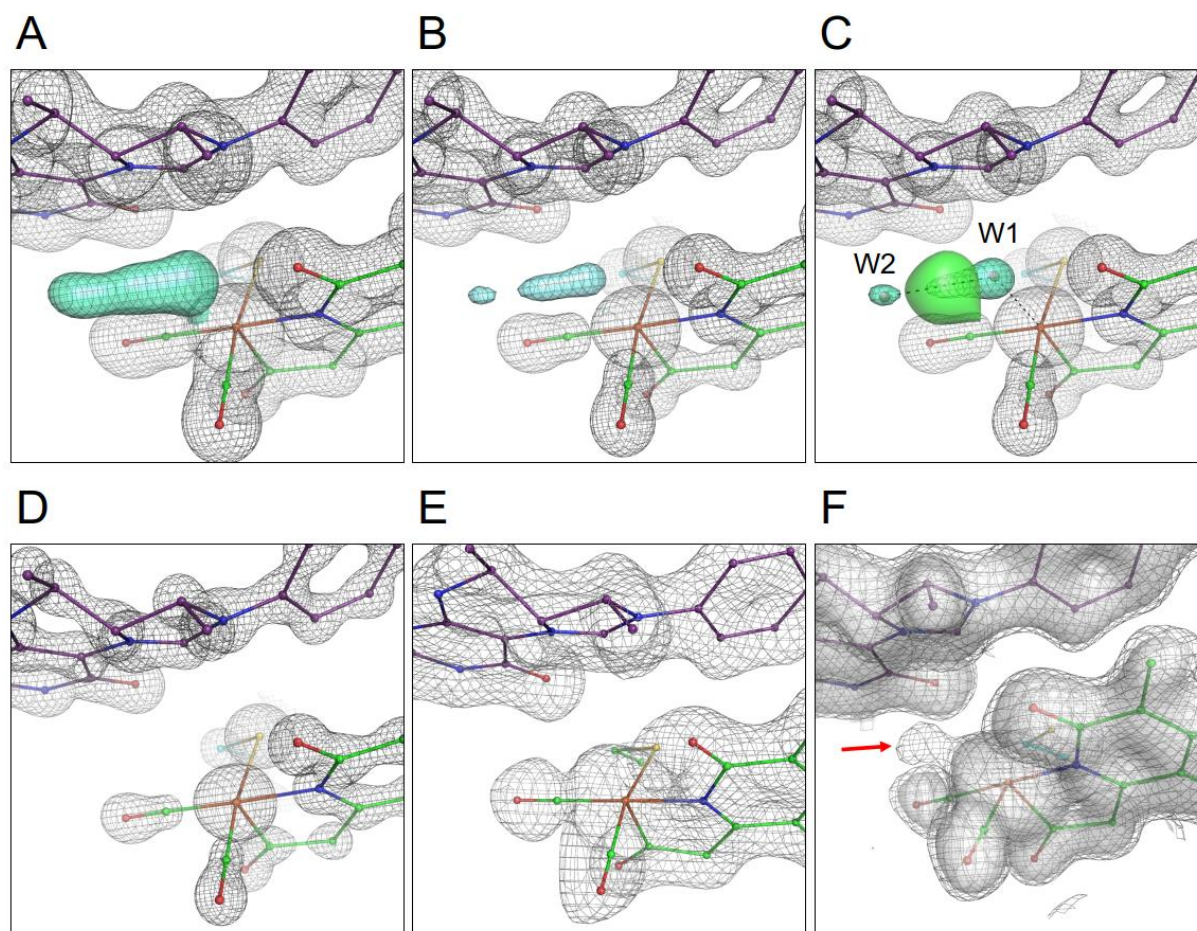
```

Methanococcus_aeolicus
Methanococcus_aeolicus          .....
Methanothermococcus_thermolithotrophicus CCCELKK...
Methanocaldococcus_jannaschii    TKCEIMSQKE.
Methanoterris_igneus             TKCEIMSQANK
Methanobrevibacter_olleyae       .....
Methanothermus_fervidus          .....
Methanolacinia_paynteri          .....
Methanobacterium_formicicum      .TCNI.....
Methanothermobacter_marburgensis  .....
Methanoregula_formicica          .....
Methanocorpusculum_labreanum     .....

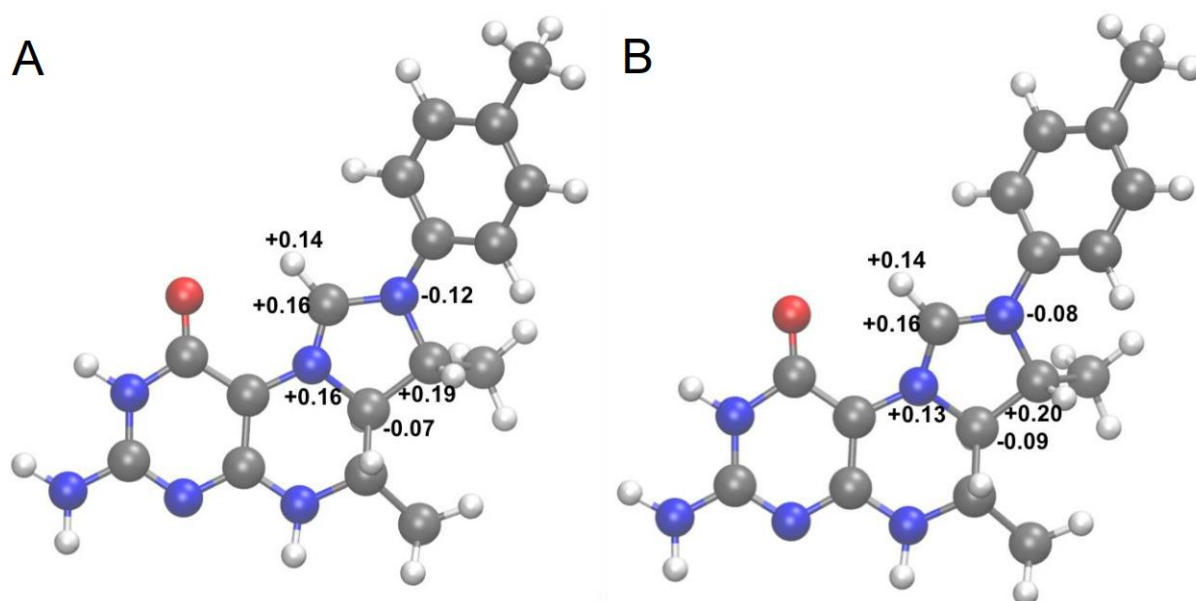
```

**Fig. S1. Alignments of protein sequences of [Fe]-hydrogenases from different organisms.** All sequences data were obtained NCBI database. Alignments was performed by Clustal Omega (<https://www.ebi.ac.uk/Tools/msa/clustalo/>). The figure was generated by ESPript 3.0 (136). The strictly conserved Met252 and Val205 were marked with black stars. This figure is obtained from Ref (98).

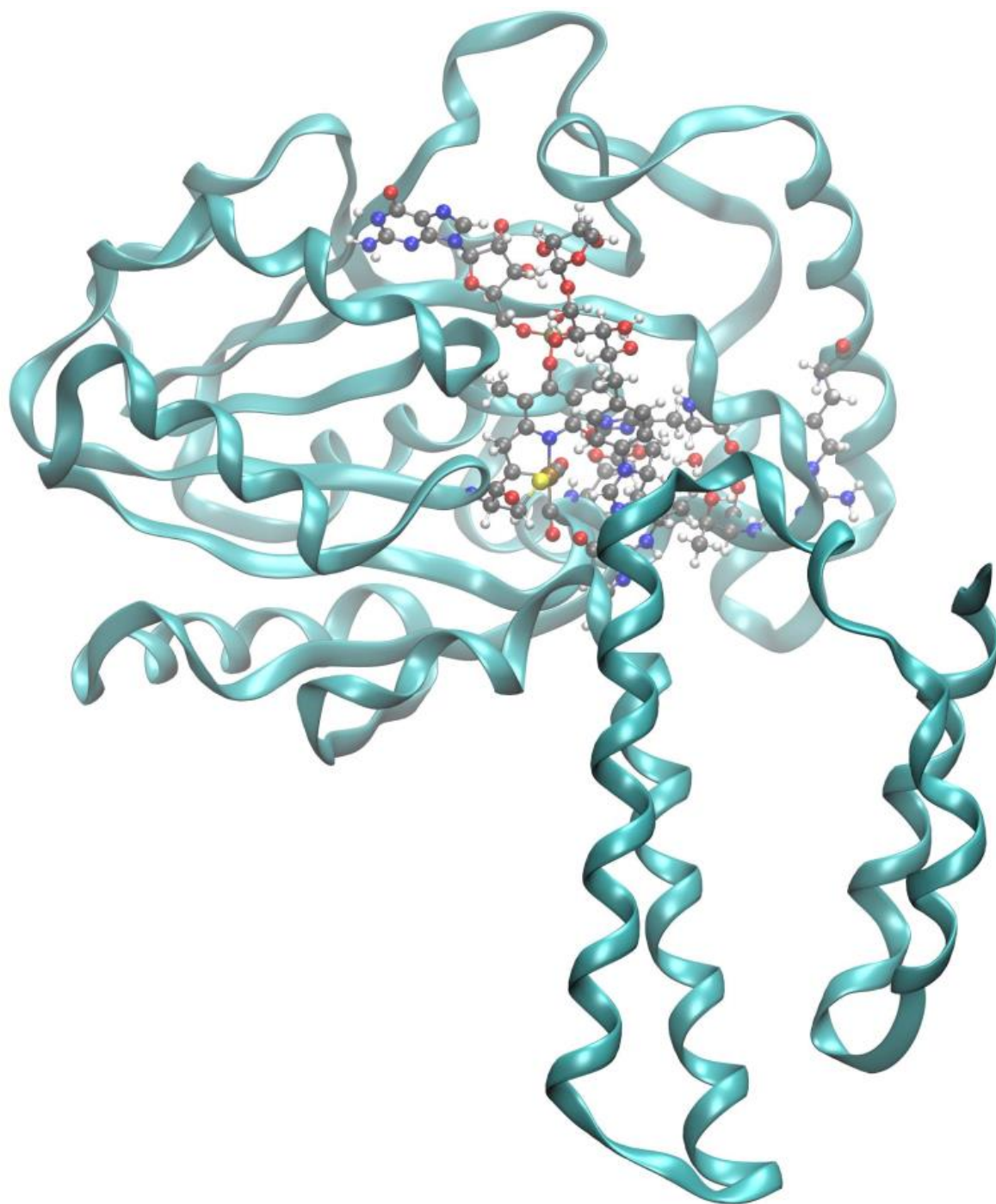




**Fig. S2. 2Fo-Fc electron-density of the binary complex (FeGP cofactor/methenyl-H<sub>4</sub>MPT<sup>+</sup>) in the closed active-form.** The contour level for closed structure Form A is 1.0  $\sigma$  in (A), 2.0  $\sigma$  in (B), 3.0  $\sigma$  in (C), 5.0  $\sigma$  in (D). The contour level for closed structure Form B is 1.0  $\sigma$  for the first monomer of the dimer in the asymmetric unit (E) and 1.0  $\sigma$  for the second monomer (F). A transparent surface corresponds to the map with a cutoff at 1.5  $\sigma$ . The extra electron density observed at 1.0  $\sigma$ , which is bound to the Fe site (shown by a red arrow in F) disappear at 1.5  $\sigma$ . This extra electron density might come from thiocyanate (200 mM in the crystallization solution). Thiocyanate did not inhibit [Fe]-hydrogenase from *M. aeolicus* at the used concentration. This figure is obtained from Ref (98).

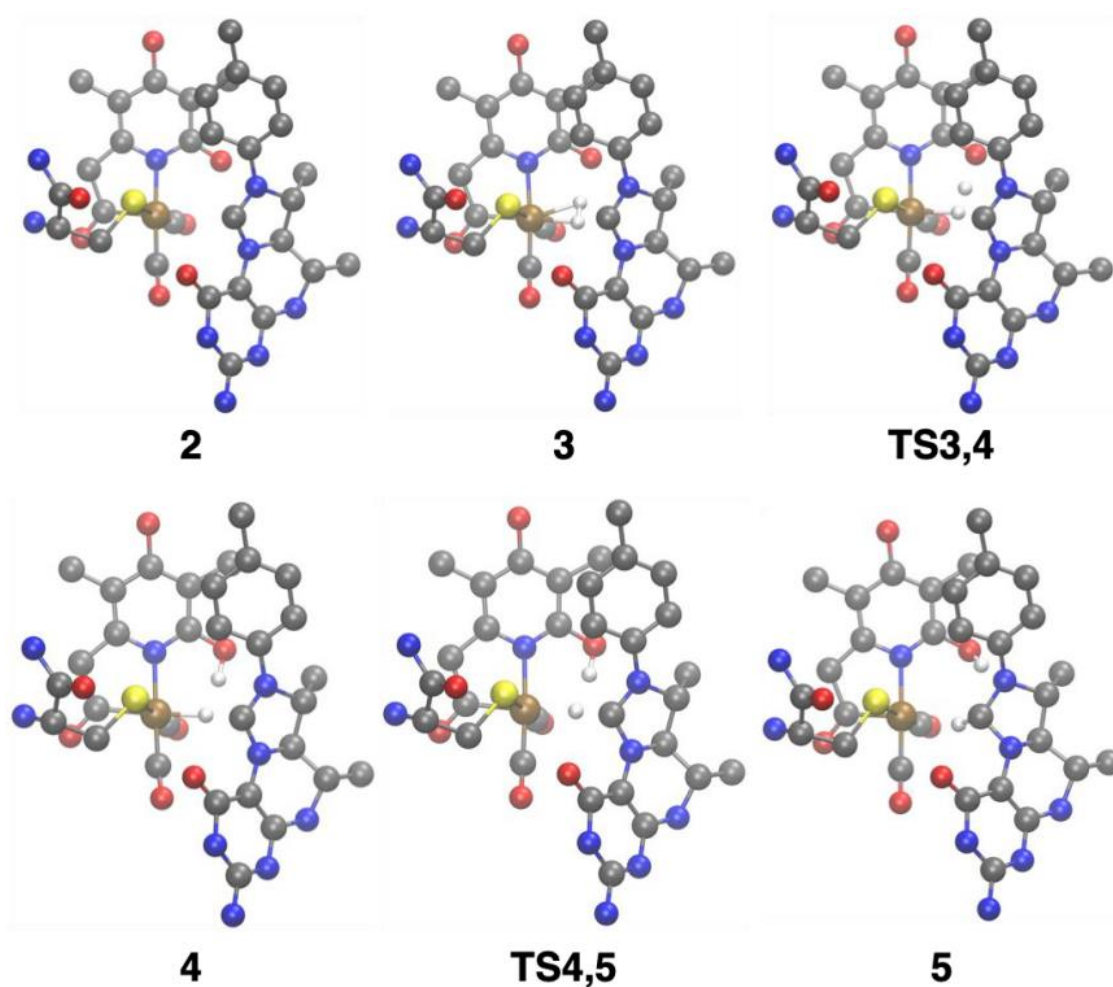


**Fig. S3. Iterative Hirshfeld atomic charges for the methenyl-H<sub>4</sub>MPT<sup>+</sup> in the closed [Fe]-hydrogenase/methenyl-H<sub>4</sub>MPT<sup>+</sup> complex. (A) In the fixed conformation. (B) The fully relaxed geometries. Charges obtained through DFT computations at the PBE0/def2-SVP level. The truncated methenyl-H<sub>4</sub>MPT<sup>+</sup> structures were shown in sticks and balls, in which carbon, nitrogen, oxygen, and hydrogen atoms were depicted in grey, blue, red and white, respectively. This figure is obtained from Ref (98).**

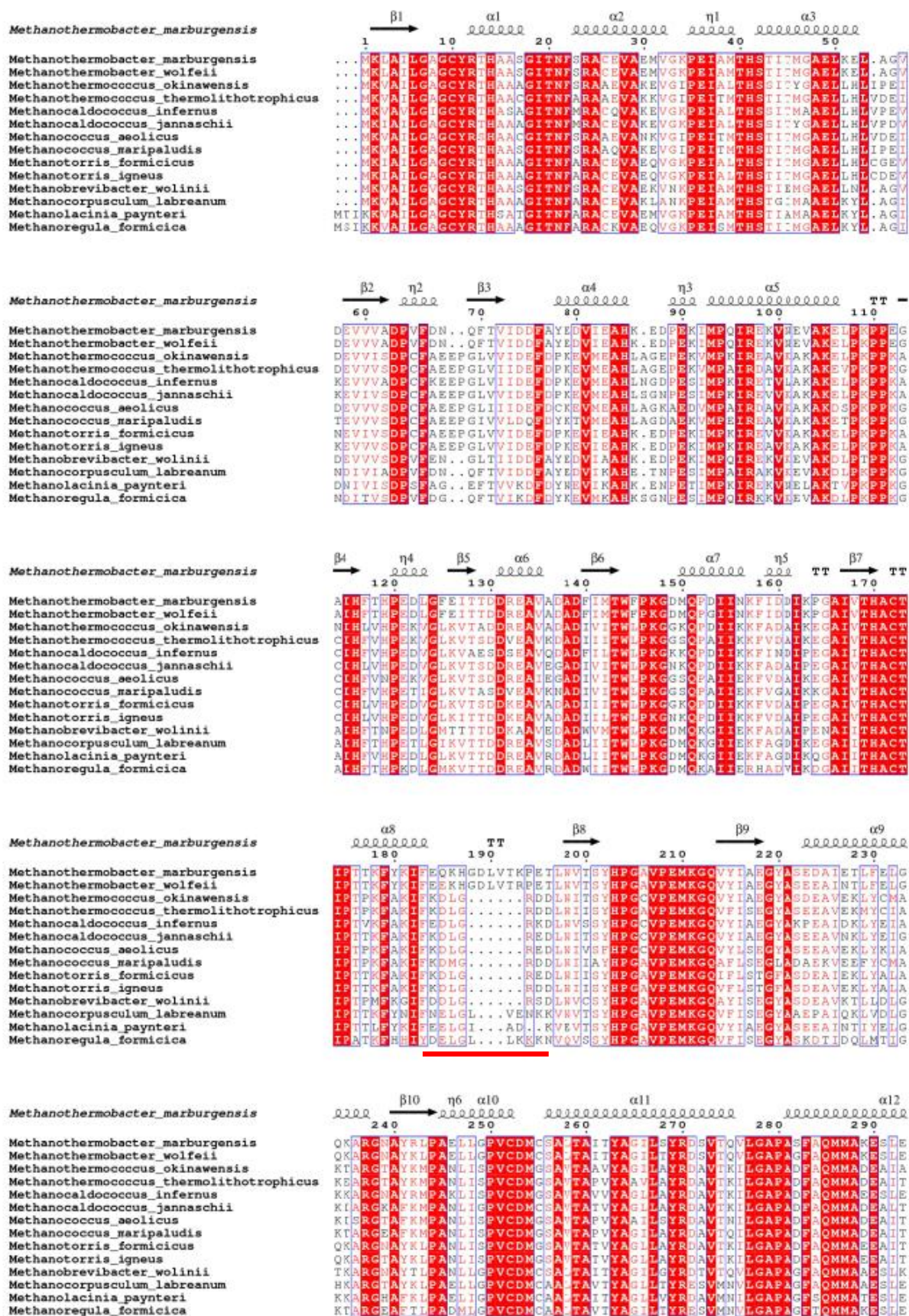


**Fig. S4. QM/MM optimized geometry of the active site of [Fe]-hydrogenase.** Cofactors, substrates, and amino acid residues related to the catalytic cycle were shown as ball and sticks. and the other part of the protein was presented in ribbon. The fixed closed geometry was used for the cofactor- and substrate-structures of relevant catalytic cycle. The atoms of carbon, nitrogen, oxygen, sulphur, phosphate, hydrogen and iron were depicted in grey, blue, red, yellow, gold, white and brown, respectively. This figure is obtained from Ref (98).





**Fig. S5. QM/MM optimized geometries of the cofactor- and substrate-structures of relevant catalytic cycle intermediates and transition states.** For clarity, only the heavy atoms and relevant hydrogen atoms are shown in this figure. The protein structure was depicted in Supplementary Fig. 6. Carbon, nitrogen, oxygen, sulphur, phosphate, hydrogen and iron atoms were colored in grey, blue, red, yellow, gold, white and brown, respectively. This figure is obtained from Ref (98).





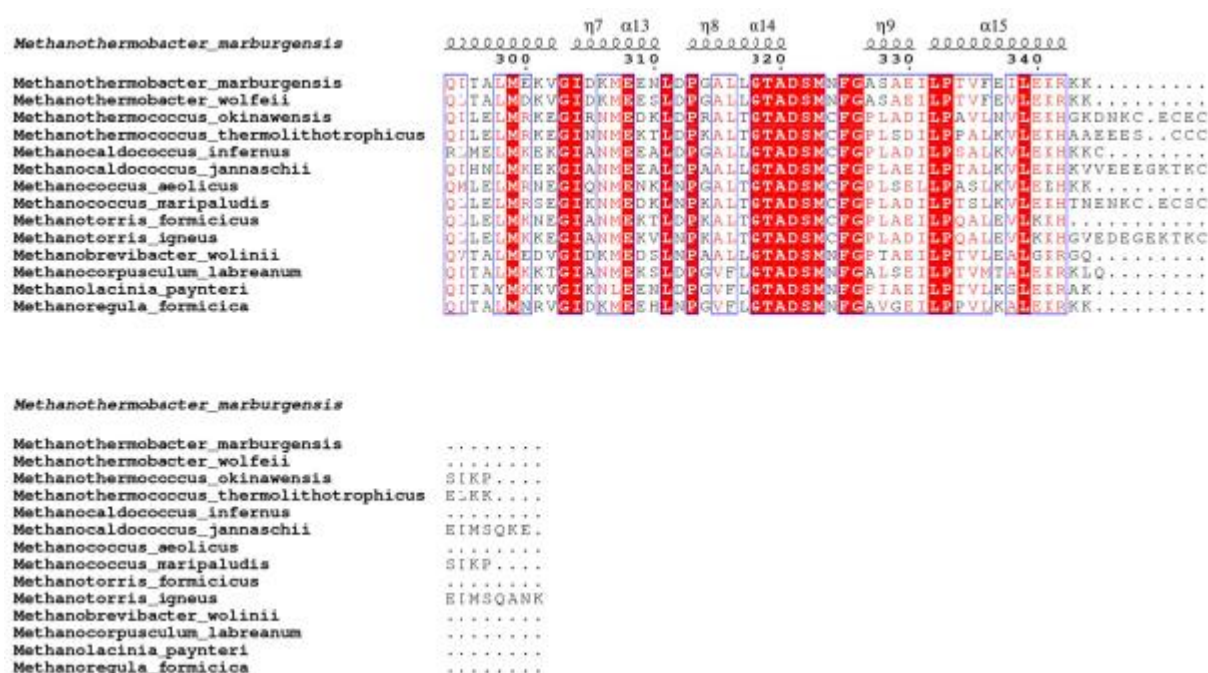


**Fig. S6. Amino acid sequences alignment of [Fe]-hydrogenase proteins from various methanogens (116).** Alignments were performed by Clustal Omega (<http://www.ebi.ac.uk/Tools/msa/clustalo/>). The figure was generated by using ESPript 3.0 (136). All sequences data were obtained NCBI database. The oligomerization loop (183-196) of [Fe]-hydrogenase from *M. marburgensis* was marked by a red line in the figure. This figure is obtained from Ref (116).

**Table. S1. Computed free energies of relevant species.** Values in hartree.

Species	M06/6-31G(d,p)//UFF QM/MM Free Energies (298K)
H <sub>2</sub>	-1.166944
2	-4185.815488
3	-4186.998128
TS3,4	-4186.998438
4	-4187.006827
TS4,5	-4186.990501
5	-4187.004461

This figure is obtained from Ref (98).

**Table. S2. Generation of H<sub>2</sub>O<sub>2</sub> from O<sub>2</sub>-inactivated [Fe]-hydrogenase (*M. marburgensis*) (112).**

Samples <sup>a</sup>	[Fe]-hydrogenase (μM)	Methylene-H <sub>4</sub> MPT (μM)	Gas phase (100%)	extra enzymes added	Residual activity (%)	H <sub>2</sub> O <sub>2</sub> produced (μM)
1	500	500	O <sub>2</sub>	None	1.2 ± 0.1	3.2 ± 0.3
2	None	500	O <sub>2</sub>	None	Not applicable	< 0.01
3	500	None	O <sub>2</sub>	None	93.3 ± 0.1	< 0.01
4	500	500	N <sub>2</sub>	None	97.8 ± 3.5	< 0.01
5	500	500	O <sub>2</sub>	Catalase <sup>b</sup>	1.4 ± 0.5	0.01 ± 0.03
6	500	500	O <sub>2</sub>	SOD <sup>c</sup>	1.2 ± 0.4	3.0 ± 0.4

<sup>a</sup> The sample contained 120-mM potassium phosphate pH 6.0, 1-mM EDTA, and it was incubated at 40 °C for 10 min. <sup>b</sup> Catalase: 2 mg (2000-5000 U/mg)/ml is the final concentration in samples. <sup>c</sup> SOD: Superoxide dismutase, 1.4 mg (3000 U/mg)/ml is the final concentration in samples.

This figure is obtained from Ref (112).

## Acknowledgements

From 26 to 30 years old, this 4-years PhD study is of importance for life. There are too many people and things for me to express sincere thankfulness. The first one is my dear supervisor – Dr. Seigo Shima, in 2015, you gave me the chance to taste the wonderful flavor of scientific research in Max Planck Institute for Terrestrial Microbiology. I still clearly remember that you personally taught me how to purify protein anaerobically, how to perform activity assay, how to make figures, how to write manuscripts, how to do research... That is my great fortune that I can directly enjoy such kind, nice and great education from you, which will benefit me in my whole life. At this moment, my excitement is indescribable. It is my great honor that I can receive suggestion, help and education from Prof. Dr. Rudolf K. Thauer – the world famous scientist in biochemistry. From you, I can know what the scientific charm is.

It is my great luck that I can study and do research with you – Dr. Liping Bai, an excellent PhD student and postdoc, and now as a research group leader in Biogas Institute of Ministry of Agriculture (Chengdu, China). You provided me many helps during my experiments in the lab and my life in Marburg. Until now, I still clearly remember that on 07.09.2015, you came to Frankfurt to pick up me in the very early morning. On the train, you gave me the food for breakfast that was prepared from Marburg. For me, this moment of touching is beyond everything, bearing in mind for my whole life. Just like that summer, at the Lakeside Cafe in Xiamen University, you introduced me about the research life in the laboratory. So far, I still cannot forget the beauty and sweetness of that moment.

It is my great luck that I can study and do research with you – Dr. Tristan Wagner, an excellent postdoc, and now as a research group leader in Max Planck Institute for Marine Microbiology (Bremen, Germany). You personally taught me lots of knowledge and skills about X-ray crystallization and took me to Synchrotron, which is not only as the great helps for my PhD project but also opens a window of structure biochemistry for me. I admire your profound knowledge, superb technology, especially the pursuit of science. You make a good example for me, how to be an excellent PhD student, an excellent postdoctoral and an excellent group leader.

It is my great luck that I can study and do research with you – Jürgen Koch, an excellent technical assistant. You kindly taught how to do fermentation, how to use the ÄKTA pure chromatography system... With your nice help, I can perform my experiments smoothly. With free and nice talking, making my lab life happier.

I would like to give lot of thanks to Prof. Dr. Rudolf K. Thauer, Prof. Dr. Johann Heider and Prof. Dr. Lars-Oliver Essen, as members of my TAC meetings; you give me many useful and kind suggestions on my PhD study. I would like to give lot of thanks again to Dr. Seigo Shima, Prof. Dr. Johann Heider, Prof. Dr. Lars-Oliver Essen and Prof. Dr. Hans-Ulrich Mösch to be members of my thesis referees; you give me many scientific advices on my thesis. Thanks a lot.

I would like to give many thanks to Prof. Dr. Xile Hu (EPFL) for the collaborations about the catalytic mechanism of [Fe]-hydrogenase and the semi-synthesized mono-Mn hydrogenase. Such collaborations give me chance to learn about chemistry and broaden my horizons. Additionally, I would like to give many thanks to Dr. Matthew D. Wodrich (EPFL) to help me perform chemical computations. I would like to give many thanks to Dr. Huijie Pan (EPFL) to help me perform the synthesis of many Mn mimic compounds and teach me some chemistry knowledge.

I would like to give many thanks to Dr. Ulrich Ermler (Max Planck Institute of Biophysics), who helps me a lot on crystallography and protein structure analysis, which make large contributions to my PhD project. With such collaborations, I can have chance to learn knowledge about bio-macromolecule structure analysis.

I would like to give many thanks to Dr. Eckhard Bill (Max Planck Institute for Chemical Energy Conversion), who helps me a lot on Mössbauer and EPR spectroscopy measurements and data analysis which is important for my O<sub>2</sub>-inactivation of [Fe]-hydrogenase and catalytic mechanism research. I would like to give many thanks to Dr. Kenichi Ataka (Freie Universität Berlin), who helps me a lot on ATR-FTIR measurements and data analysis which is important for my catalytic mechanism research. Meantime, I would like to give many thanks to Dr. Ingo Zebger (Technischen Universität Berlin) and Dr. Sven Stripp (Freie Universität Berlin) about the collaborations on iron-hydride intermediate measurements using ATR-IR and

Resonance Raman spectroscopy. Additionally, I would like to give many thanks to Dr. Christine Müller-Renno (Technische Universität Kaiserslautern) for the measurements of Nuclear resonance vibrational spectroscopy (NRVS).

I would like to give many thanks to other members of AG Shima: Dr. Tomohiro Watanabe, Sebastian Schaupp and Francisco Javier Arriaza Gallardo, for all of your helps and supports, I can enjoy the experiments and happy hours in the lab. Many thanks to Sebastian Schaupp for helps on Germany translations. Many thanks to all for the corrections of my thesis.

I would like to give many thanks to Max Planck Institute for Terrestrial Microbiology, IMPRS and Philipps-Universität Marburg, thanks for giving the chance to enjoy the study and scientific research in Germany.

In addition, I would like to give many thanks to other people in Marburg: Dr. Xiaojuan Liu, Dr. Jing Wang, Dr. Ming Chen, Dr. Wanyang Wang, Dr. Yu Chen, Dr. Bin Ni, Dr. Pengfei Liu, Dr. Liang Liang, Dr. Xiaowei Han, Dr. Jing zhu, Dr. Qicheng Bei, Dr. Jingjing Peng, Yulin Song, Liujuan Zheng, Xin Li and Kangli Guo. With all of you, I can enjoy the colorful life in Marburg.

Finally, I would like to give many thanks to China Scholarship Council (CSC) for providing me scholarship to study and live in Marburg.

Furthermore, I would like to give many thanks to my dear parents, because your love, encouragement and supports, I can have peace of mind to study in Germany.

Gangfeng Huang

08.03.2019

A.0.05

Max Planck Institute for Terrestrial Microbiology, Marburg, Germany



## Curriculum vitae

### Personal information:

**Name:** Gangfeng Huang  
**Date of Birth:** June 2, 1989  
**Place of Birth:** Shaoxing, Zhejiang, China  
**Gender:** Male  
**Address:** Max Planck Institute for Terrestrial Microbiology,  
Karl-von-Frisch-Straße10, 35043 Marburg, Germany  
**Telephone:** +49 6421 178 110  
**Fax:** +49 6421 178 199  
**E-mail:** [gangfeng.huang@mpi-marburg.mpg.de](mailto:gangfeng.huang@mpi-marburg.mpg.de)  
**Website:** <http://www.mpi-marburg.mpg.de/person/47160/43299>

### Research topics

My main research goal is to analyze the properties and catalytic mechanism of [Fe]-hydrogenase using X-ray crystallographic, biochemical and spectroscopic methods. In addition, I am working on the analysis of semi-synthetic mono-Fe and mono-Mn hydrogenases using chemical mimic compounds of [Fe]-hydrogenase cofactor.

### Education

**Ph.D student:** Max Planck Institute for Terrestrial Microbiology, Marburg, Germany, September **2015** – June **2019**.

Advisor: Dr. Seigo Shima

**Master of Science:** Department of Biochemistry and molecular biology, Xiamen University, Xiamen, China, September **2012** – June **2015**.

Advisor: Prof. Dr. Qingxi Chen and Prof. Dr. Yan Shi

**Bachelor of Science:** Department of Biotechnology, Wenzhou University, Wenzhou, China, September **2008** – June **2012**.

Advisor: Prof. Xiaowei Zhao and Prof. Maohong Zhou

